

Dissertation



**Department of Gene Therapy
Prof. Dr. Stefan Kochanek**

**Development of a novel capsid modified AAV vector platform
enabling retargeting by modular bispecific antibody binding**

**Dissertation submitted in partial fulfilment of the requirements for the degree of
„Doctor rerum naturalium” (Dr. rer. nat.) of the International Graduate School in
Molecular Medicine Ulm**

**Juliane Kuklik
Braunschweig**

2022

Current dean of the Medical Faculty: Prof. Dr. Thomas Wirth

Current chairman of the Graduate School: Prof. Dr. Bernd Knöll

Thesis Advisory Committee:

- First supervisor: Prof. Dr. Stefan Kochanek
- Second supervisor: Prof. Dr. Christian Sinzger
- Third supervisor: Dr. John Park

External reviewer: Dr. Maren Schubert

Day doctorate awarded: 29.07.2022

Results gained in my thesis have previously been published in the following publication:

Kuklik, J., Michelfelder, S., Schiele, F., Kreuz, S., Lamla, T., Müller, P., & Park, J. E. (2021). Development of a Bispecific Antibody-Based Platform for Retargeting of Capsid Modified AAV Vectors. *International journal of molecular sciences*, 22(15), 8355. <https://doi.org/10.3390/ijms22158355>. (c) The Authors. Licensed under Attribution 4.0 International (CC BY 4.0), <https://creativecommons.org/licenses/by/4.0/>

Table of contents

Table of contents	III
Index of figures.....	VII
Index of tables	IX
List of abbreviations	X
1 Introduction	1
1.1 Adeno-associated Virus type 2	1
1.1.1 AAV genome.....	1
1.1.2 Capsid structure of AAV2	4
1.1.3 Infection cycle of AAV2	4
1.1.4 Production of recombinant AAV.....	6
1.1.5 The need and design of AAV2 capsid modifications for cell-specific targeting... 7	
1.2 Antibodies.....	10
1.2.1 The structure of IgG antibodies	10
1.3 Design and production of bispecific antibodies	11
1.4 Combination of bispecific antibodies with AAV capsid modification for cell type specific targeting.....	15
1.5 Target Receptors.....	16
1.5.1 Fibroblast activation protein.....	16
1.5.2 Programmed death-ligand 1.....	17
1.6 Aim of the project.....	18
2 Materials and methods	20
2.1 Materials and devices	20
2.2 Molecular Methods.....	38
2.2.1 Plasmids.....	38
2.2.2 Mesoscale Discovery ELISA.....	39
2.2.3 Western Blot.....	40

2.2.4	AAV heparin column binding assay.....	41
2.2.5	qPCR.....	41
2.3	Production and quality control of rAAVs.....	43
2.3.1	Production and harvest of rAAV vectors	43
2.3.2	rAAV PEG precipitation	44
2.3.3	rAAV iodixanol purification	45
2.3.4	ddPCR.....	46
2.3.5	AAV2 Titration ELISA	47
2.3.6	Electron microscopy	48
2.4	Production and Quality control of bispecific antibodies	48
2.4.1	Antibody production.....	48
2.4.2	Antibody purification via MabSelect™ SuRe.....	49
2.4.3	Fab-arm exchange.....	49
2.4.4	Cation exchange chromatography via Äkta Avant.....	49
2.4.5	SDS-PAGE	50
2.4.6	Size-exclusion chromatography via Äkta Avant.....	51
2.4.7	HPLC	51
2.4.8	Endotoxin test.....	51
2.4.9	Octet bridging assay	51
2.5	Cell biology methods.....	52
2.5.1	Flow cytometry.....	52
2.5.2	Antibody internalization assay	53
2.5.3	<i>In vitro</i> retargeting assay	53
2.5.4	Firefly luciferase assay	55
2.6	<i>In vivo</i> methods and tissue analysis.....	55
2.6.1	Pharmacokinetic	55
2.6.2	Tumor xenograft model establishment.....	56

2.6.3	<i>In vivo</i> retargeting assay	57
2.6.4	Tissue homogenization for BCA and Luciferase assays	59
2.6.5	BCA assay of tissue lysates	59
2.6.6	Luciferase assay of tissue lysates	59
2.6.7	Tissue homogenization and DNA extraction	59
2.6.8	Histochemistry and immunohistochemistry	60
2.7	Statistics.....	60
3	Results	62
3.1	Design, production, and characterization of AAV2 capsid variants with novel epitope insertion domains	62
3.2	2E3 epitope viral capsid modifications influence transduction properties and HSPG binding compared to AAV2	66
3.3	Design and production of bispecific antibodies engaging 2E3 epitopes and human FAP cell surface receptors	69
3.4	<i>In vitro</i> targeting of FAP by AAV-antibody complexes	73
3.5	Bispecific antibody-mediated targeting is highly epitope- and independent of heparin interaction	80
3.6	Viral uptake is dependent on bispecific antibody binding	83
3.7	Targeting of PD-L1 by modular bispecific antibody exchange	85
3.8	Development of a murine xenograft HT1080 huFAP tumor model and processing of reagents for <i>in vivo</i> experiments.....	88
3.9	Targeting of rAAV-2E3.v6 reveals tissue detargeting but no tumor targeting ...	91
4	Discussion	98
4.1	Impact of capsid design of rAAV-2E3 viral variants on production and transduction properties.....	98
4.2	Design and production of bispecific antibodies	100
4.3	Establishment of a highly specific retargeting mechanism based on bispecific antibodies binding rAAV-2E3 viral variants and FAP receptors	101

4.4	Modular Fab-arm exchange enabled rAAV-2E3.v6 retargeting of PD-L1 receptors.....	105
4.5	The developed retargeting mechanism is not directly conferrable to <i>in vivo</i> models	106
4.6	Conclusion.....	109
5	Summary	112
6	References	113
7	Appendix	135
8	Acknowledgements	137
9	Declaration	139

Index of figures

Figure 1: Illustration of a wild-type AAV2 genome.	3
Figure 2: Illustration of the three-vector system required to produce helper virus-free rAAVs in HEK 293 cells.	7
Figure 3: Approaches of AAV capsid diversification.	10
Figure 4: Overview of the bispecific antibody design used in this study.	14
Figure 5: Development of a targeting platform of capsid modified AAV vectors by bispecific antibody binding	19
Figure 6: Ribbon drawing of the VP3 subunit with indicated capsid modifications.	63
Figure 7: Characterization of novel rAAV-2E3 viral variants	66
Figure 8: 2E3 epitope AAV2 capsid modification alters infectivity and heparin column binding compared to AAV2	68
Figure 9: Quality control of knob-into-hole bispecific antibodies	70
Figure 10: Bispecific antibodies show functional binding of FAP and 2E3 epitopes.	71
Figure 11: Octet HTX bio-layer interferometry proved simultaneously binding of 2E3 epitopes and recombinant proteins.	72
Figure 12: FAP receptors internalize independently of mono- or bispecific antibody binding.	73
Figure 13: Establishment of a FAP targeting mechanism based on the complexation of rAAV-2E3 with bispecific antibodies	75
Figure 14: Reproduction of bispecific antibody-mediated rAAV-2E3.v6 retargeting to HEK 293 hu-FAP cells	76
Figure 15: Reproduction of bispecific antibody-mediated rAAV-2E3.v6 retargeting to HEK 293 hu-FAP cells	77
Figure 16: Retargeting of rAAV-2E3.v6 is dependent on the epitope binding and ratio of KiH-antibody per viral genome.	79
Figure 17: Bispecific antibody rAAV-2E3.v6 retargeting is influenced by competitors and neutralizing antibodies but not heparin	82
Figure 18: Comparison of viral internalization and transgene expression kinetics of rAAV-2E3.v6 and AAV2	85
Figure 19: ‘Fab-arm exchange’ enabled the production of KiH-2E3-PD-L1 and modular targeting of PD-L1 with rAAV-2E3.v6.	87
Figure 20: Establishment of an HT1080 huFAP xenograft model.	88

Figure 21: Cargo alterations did not influence antibody binding of viral capsids	90
Figure 22: HT1080 huFAP firefly luciferase expression after AAV2 and rAAV-2E3.v6 transduction <i>in vitro</i>	91
Figure 23: Comprehensive overview of <i>in vivo</i> study data	93
Figure 24: Whole-body bioluminescence imaging of firefly luciferase expression.....	94
Figure 25: Detection of AAV genomes and luciferase activity in homogenized tissues	96
Figure 26: HT1080 huFAP tumor tissues showed strong FAP expression but low vascularization.....	97
Figure 27: Supplemental uncropped full-size images	136

Index of tables

Table 1: List of abbreviations and full forms	X
Table 2: List of abbreviations of essential amino acids.....	XII
Table 3: Devices	20
Table 4: Chemicals and agents	22
Table 5: Cell culture chemicals and medium	27
Table 6: Consumables	28
Table 7: Kits	31
Table 8: Antibodies	32
Table 9: TaqMan™ primer-probe	33
Table 10: Plasmids	34
Table 11: Cell lines and culture medium compositions	35
Table 12: Software and online tools	37
Table 13: Buffers used for ELISA.....	39
Table 14: Antibodies used for ELISA assays.....	40
Table 15: cDNA qPCR reagent mixture for one well of a 96-well plate	42
Table 16: gDNA qPCR reagent mixture for one well of a 96-well plate	43
Table 17: qPCR cycling protocol	43
Table 18: rAAV extraction lysis buffer.....	44
Table 19: PEG-8000 medium.....	45
Table 20: rAAV resuspension buffer.....	45
Table 21: Iodixanol solutions	46
Table 22: rAAV storage buffer.....	46
Table 23: Composition of ddPCR master mix for a 96-well plate	47
Table 24: ddPCR program.....	47
Table 25: transient transfection of 1.0 L HEK293E6 via 293fectin™	48
Table 26: Running and elution Buffer compositions for cation exchange chromatography	50
Table 27: Octet analysis of KIH bispecific antibody binding	52
Table 28: Formalin-Fixed Paraffin-Embedded tissue protocol	57
Table 29: Grouping and dosing of HT1080 huFAP mouse xenograft models.....	58
Table 30: Design of AAV2 capsid variants by 2E3 epitope insertion.....	62
Table 31: Pharmacokinetic parameters of bispecific antibodies	89
Table 32: Yield of AAV variants with Fluc expression plasmid	90

List of abbreviations

Table 1: List of abbreviations and full forms

Abbreviation	Full form
μ	micro
AAP	assembly-activating protein
AAV	adeno-associated virus
ATCC	american tissue culture collection
bp	base pair
BSA	bovine serum albumin
CD	cluster of differentiation
CDR	complementary determining region
CEX	cation-exchange chromatography
CH	constant heavy chain
CL	constant light chain
CLIC	clathrin-independent carriers
C_{max}	maximal concentration
ct	cycle threshold
CV	column volumes
ddH ₂ O	double-distilled water
ddPCR	droplet digital PCR
DEPC	diethylpyrocarbonate
dist	distribution
DMEM	dulbecco modified eagle's medium
ds	double-strand
ELISA	Enzyme-linked immunosorbent assay
FAM	fluorescein amidite
FAP	fibroblast activation protein
Fc	fragment, crystallizable
FLUC	firefly luciferase
g	gram
GEEC	gpi-anchored-protein-e endosomal compartment
GPF	green fluorescent protein

h	hour
HC	heavy chain
HPMA	N-(2-Hydroxypropyl) methacrylamide
HRP	horseradish peroxidase
HSPG	heparin sulfate-proteoglycan
hu	human
Ig	immunoglobulin
Ins	insertion
ITR	inverted-terminal repeats
IVIS	<i>in vivo</i> imaging system
kDa	kilodalton
L	liter
LC	light chain
M	molar
m	milli
MAAP	membrane-associated accessory protein
max	maximal
MFI	median fluorescence intensity
mRNA	messenger ribonucleic acid
min	minute
MRT	mean residence time
NEAA	non-essential amino acids solution
ORF	open reading frame
PCR	polymerase chain reaction
PCSK9	proprotein convertase subtilisin/Kexin type 9
PD-1	programmed cell death protein 1
PD-L1	programmed death-ligand 1
PEG	polyethylenglycol
pH	potential of hydrogen
PLA2	phospholipase 2
qPCR	quantitative polymerase chain reaction
rAAV	recombinant adeno-associated virus

RBE	rep-binding element
RLU	relative light units
RNA	ribonucleic acid
RT	room temperature
s	second
sc	self-complementary
SDS PAGE	sodium dodecyl sulfate-polyacrylamide gel electrophoresis
SEC	size-exclusion chromatography
ss	single-stranded
Sub	substitution
T _{1/2}	time of half-life
T _{max}	time of maximal concentration
TRS	terminal resolution site
VA RNA	viral associated ribonucleic acid
VG	viral genome
VH	variable heavy chain
VL	variable light chain
VP	viral protein
wt	wild type

Table 2: List of abbreviations of essential amino acids

Abbreviation	Three letter code	Amino acid
A	ala	Alanine
C	cys	Cysteine
D	asp	Aspartic acid
E	glu	Glutamic acid
F	phe	Phenylalanine
G	gly	Glycine
H	his	Histidine
I	ile	Isoleucine
K	lys	Lysine
L	leu	Leucine
M	met	Methionine

N	asn	Asparagine
P	pro	Proline
Q	gln	Glutamine
R	arg	Arginine
S	ser	Serine
T	thr	Threonine
W	trp	Tryptophan
Y	tyr	Tyrosine
V	val	Valine

1 Introduction

1.1 Adeno-associated Virus type 2

Adeno-associated virus (AAV) was first found in 1965 by (Atchison et al. 1965 and Hoggan et al. 1966) within Adenovirus preparations. AAV belongs to the *parvoviridae* family, and its replication cycle depends on co-infection with ‘helper viruses’ such as Adenovirus (Atchison et al. 1965), Herpes simplex virus (Georg-Fries et al. 1984), Vaccinia virus (Schlehofer et al. 1986), or Human Papillomavirus (Walz et al. 1997) that provide necessary proteins for effective transcription, replication, and packaging (Mitchell et al. 2010). Several human and non-human AAV serotypes have been isolated and described but the first isolated serotype 2 remains to be best characterized. AAV2 shows up to 80% high seroprevalence in humans (Erles et al. 1999) but AAVs are not related to any human disease and therefore classified as non-pathogenic (Berns and Linden 1995). Due to this good safety profile and a long-term gene expression, AAV became popular for gene therapy approaches celebrating success by the FDA approved therapies LUXTURNA (FDA approved 2017) or ZOLGENSMA (FDA approval 2019) (Carter 2004; Daya and Berns 2008; Michelfelder and Trepel 2009; Kotterman et al. 2015).

1.1.1 AAV genome

AAVs have a linear single stranded DNA genome of 4.7 kb (Srivastava et al. 1983). Sense and antisense DNA strands are packaged into the capsid with equal likelihood (Rose et al. 1969). The wild type genome (Figure 1) consists of several open reading frames flanked with 145 bp inverted terminal repeats (ITR) which are important for stability, replication, integration, and packaging of the viral genome (Hermonat et al. 1984; Tratschin et al. 1984a; Kotin et al. 1990; Daya and Berns 2008; Kotterman et al. 2015; Sonntag et al. 2010; Ogden et al. 2019). The ITR sequence consists of a 125 bp palindromic sequence that forms a T-shaped hairpin structure and an unpaired 20 bp D-sequence. The double-strand comprises the so-called sequences Rep-binding elements (RBE and RBE’) and a terminal resolution site (TRS), that is crucial for replication (Lusby et al. 1980; Daya and Berns 2008).

The first open reading frame of AAV2 contains the *rep* genes coding for the non-structural proteins Rep78, Rep68, Rep52, and Rep40. The large Rep78 and Rep68 sequences are under the control of the p5 promoter and derive from alternative splicing. The two smaller sequences are under the control of the p19 promoter and are also the product of alternative

splicing. All Rep proteins act as DNA helicases with ATPase-activity and the two large Rep proteins show site-specific endonuclease- and DNA binding activity at the RBE site (Im and Muzyczka 1990; Berns and Giraud 1996; Daya and Berns 2008). Therefore, Rep proteins function in the replication of the viral genome, regulation of gene expression, packaging, and site-specific integration into the host genome (Gonçalves 2005).

The second ORF of AAV2 encodes the structural *cap* genes. The p40 promoter runs the transcription of a single mRNA, that results in the translation of three viral proteins VP1, VP2, and VP3 of 90, 72, and 60 kDa respectively. mRNA splicing results in a coding sequence for VP1 plus an mRNA coding for VP3 starting with a conventional AUG codon as well as VP2 starting with a non-conventional ACG codon. The capsid proteins form an icosahedral structure out of 60 proteins with a ratio of 1:1:10 (VP1:VP2:VP3). Furthermore, it was discovered that only VP3 is essential for capsid assembly (Buller et al. 1978; Janik et al. 1984; Becerra et al. 1985; Xie et al. 2002; Sonntag et al. 2010; Gurda et al. 2013). All VP proteins share a common C-terminus but VP1 contains additional 202 amino acids and VP2 contains additional 65 amino acids in its N-terminus. The additional sequence of VP1 encodes a phospholipase 2 (PLA2) sequence, that enables endosomal escape at a lowering pH environment (Girod et al. 2002). A nuclear-localization sequence spans over the N-terminus of all VP proteins (Hoque et al. 1999; Vihinen-Ranta et al. 2002; Grieger and Samulski 2005; Grieger et al. 2006).

The third ORF encodes the assembly-activating protein (AAP). It is located within the VP2/VP3 cap genes as an alternative reading frame. AAP supports the capsid assembly and nuclear localization of VPs (Sonntag et al. 2010, 2011; Kotterman et al. 2015; Earley et al. 2017).

Most recently a new frameshift ORF within the cap 5'-end was identified encoding the membrane-associated accessory protein (MAAP). This gene starts with a non-canonical CTG codon and creates a protein of 119 amino acids that is localized in the membrane of infected cells (Ogden et al. 2019). MAAP is involved in regulation of Adenoviral infections, AAV capsid packaging as well as secretion (Elmore et al. 2021; Galibert et al. 2021).

In 1999, a new AAV promoter p81 was postulated supposing an uncharacterized ORF of the gene X in the distal 3'-end of the *cap* ORF (Hermonat et al. 1999). X is supposed to comprise

of 155 amino acids and experimental results suggested that X contributes to viral DNA replication (Cao et al. 2014). However, codon-scanning of the whole cap sequence could not detect an ORF in the postulated region (Ogden et al. 2019) and yet the existence and characterization of the X gene remains dubious.

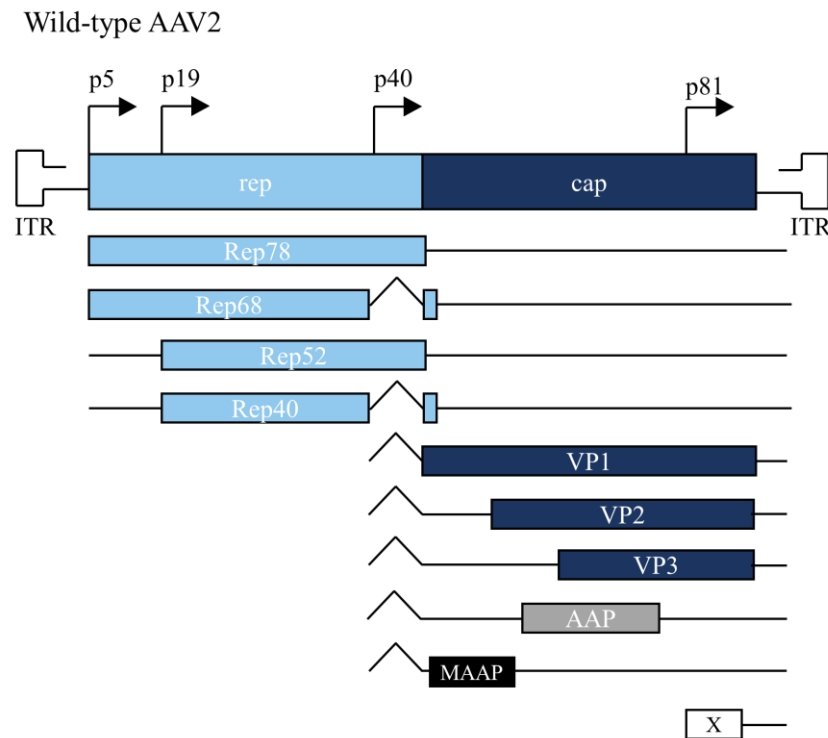


Figure 1: Illustration of a wild-type AAV2 genome. The AAV2 genome consists of two large open reading frames: *rep* (light blue), *cap* (dark blue) framed with inverted terminal repeats (ITR). The promoter p5 controls the expression of the replication proteins Rep78 and its splice variant Rep68, while p19 drives the expression of Rep52 and its splice variant Rep40. The p40 promoter runs the expression of the capsid viral proteins VP1, VP2 and, VP3 that are derived from splicing (VP1) and usage of the ACG start codon (VP2). The AAP (grey) and MAAP (black) are derived from individuals ORFs driven by p40. Another ORF called *X* (white) is supposed to exist in the 3'-end of the *cap* ORF and might be driven by p81.

1.1.2 Capsid structure of AAV2

AAVs are non-enveloped 22 nm small virions (Atchison et al. 1965; Hoggan et al. 1966). First AAV2 capsids were visualized by electron microscopy in 1966 while the atomic structure of AAV2 was resolved by X-ray crystallography in 2002 (Atchison et al. 1966; Xie et al. 2002). The capsid is composed of 60 asymmetric subunits assembled in a T=1 icosahedral symmetry. The subunits comprise a conserved core sequence of an eight-stranded antiparallel β -barrel (β A – β H) with nine interstrand variable regions (VR-I – VR-IX). These regions create specific surface structures and loops important for antibody binding or receptor interaction (Xie et al. 2002; Gurda et al. 2013). Interactions of capsid subunits form distinct surface features. VR-XI forms depressions at the 2-fold axis of symmetry, VR-VIII forms protrusions at the 3-fold axis of symmetry, and a cylindrical-pore structure is formed by VR-II at the 5-fold axis of symmetry (Govindasamy et al. 2006; Nam et al. 2007; Gurda et al. 2013). The cylindrical-pore structure is used by the Rep52 and Rep40 proteins to transfer viral genomes into empty capsids (King et al. 2001; Bleker et al. 2005).

The protrusions (VR-VIII) form a threefold spike region that presents the basic amino-acids R484, R487, K532, R585, and R588 at the viral surface (VP1 numbering). This positively charged cluster is important for first cellular attachment via electrostatic interactions with negatively charged heparin sulfate-proteoglycan (HSPG) that is expressed on target cells (Summerford and Samulski 1998; Kern et al. 2003; Zhang et al. 2013). Amino acids flanking this spike region are prone to immune recognition, therefore adjacent mutations could hide AAV capsids from the binding of neutralizing antibodies (Wobus et al. 2000; Gurda et al. 2013). The NGR sequence (511-513) forms another highly conserved binding motif that interacts with the cell surface receptor integrin α 5 β 1, which is an important co-receptor for viral internalization (Asokan et al. 2006).

1.1.3 Infection cycle of AAV2

AAV infects humans mainly via the respiratory or gastrointestinal tract (Hoggan et al. 1966). The cellular entry depends on the expression of HSPG and co-receptors such as integrin α 5 β 1, integrin α v β 5 (Summerford and Samulski 1998; Summerford et al. 1999; Asokan et al. 2006), hepatocyte growth factor receptor (Kashiwakura et al. 2005), CD9 (Kurzeder et al. 2006), fibroblast growth factor receptor-1 (Qing et al. 1999), laminin receptor (Akache et al. 2006) AAVR (Pillay et al. 2016) or GPR108 (Dudek et al. 2020).

The interaction of AAV2 with HSPG and co-receptors initiates receptor-mediated endocytosis via clathrin-coated vesicles (Bartlett et al. 1999; Duan et al. 1999). Dynein mediates the vesicular transport to the trans-Golgi network. Stimulation of HSPG and co-receptors activates intracellular signaling pathways such as Rac1 and activation of the phosphatidylinositol-3 kinase pathway, which is required for viral uptake and intracellular transport (Sanlioglu et al. 2000).

In 2012 a new AAV2 entry pathway was described, whereas the AAV2 endocytosis pathway requires the CLIC (clathrin-independent carriers)/ GEEC (GPI-anchored-protein-enriched endosomal compartment) pathway. This clathrin, caveolin, and dynamin independent AAV2 endocytosis uses the formation of clathrin-independent carriers and translocation to the Golgi-apparatus via GPI-anchored-protein-enriched endosomal compartment (Nonnenmacher and Weber 2012).

AAVs are described to escape endosomes before those mature into lysosomes (Bartlett et al. 2000). Acidification and cleavage of the capsid proteins lead to conformational changes and exposure of a phospholipase 2 domain within VP1 to support the release of the virus into the cytosol (Girod et al. 2002). Released AAVs are transported towards the nucleus by ATP-dependent molecular motors using actin and tubulin filaments (Sanlioglu et al. 2000; Seisenberger et al. 2001). The nuclear translocation of the virions is yet unclear and might be processed by a non-conventional nuclear pore localization signal in the VP2 sequence (Hoque et al. 1999). It is suggested that final viral uncoating happens in the nucleus. Subsequently, a second DNA strand is synthesized, which improves viral genome stability. The p5 and p19 promoters are activated in presence of the adenoviral E1A and a cascade for AAV gene expression is induced (Chang et al. 1989, Tratschin, et al. 1984b). However, AAV gene expression is repressed by Rep proteins without a helper virus proteins. This phenomenon may be explained by an autoregulation of Rep's own gene expression that stops viral replication and favors the pro-viral state (Muzyczka 1992). AAV2 can establish viral latency by integration into the host genome at the q-arm on chromosome 19 (AAVS1) (Samulski et al. 1991) or persists as circular extrachromosomal episomes that can provide long-term gene expression for years (Xiao et al. 1996; Schnepf et al. 2005).

1.1.4 Production of recombinant AAV

Natural replication of AAV relies on helper virus co-infections that provide essential proteins and sequences for production and release of infectious AAVs (Atchison et al. 1965; Xiao et al. 1998b). Adenoviral co-infection was the most efficient technique to produce sufficient titers of AAVs until 1998 (Samulski et al. 1998, Xiao et al. 1998b). However, clinical, and commercial research requires recombinant AAV (rAAV) production methods that are safe and prevent co-production of wt AAV or helper virus (Salveti et al. 1998; Xiao et al. 1998b and Ferrari et al. 1997).

rAAVs were designed by replacement of the two open reading frames *rep* and *cap* of the wt genome with a gene of interest under the control of the desired promoter, making the framing ITR sequences the only remaining wt sequences (*cis*-acting element) (Figure 2). *Rep*, *cap*, and helper virus sequences must be provided in *trans* for recombinant virus production. Usually, rAAVs are produced by transfection of HEK 293 cells with a three-plasmid system encoding: 1) the gene of interest flanked with ITRs, 2) the AAV *rep* and *cap* genes, and 3) the adenoviral helper genes encoding E2A, E4, and VA RNA. HEK 293 cells provide the residual adenoviral helper genes E1A and E1B. The E1A is important to initiate upregulation of AAV *rep*, *cap*, and adenoviral helper genes (Chang et al. 1989, Tratschin, et al. 1984b). E1B together with E4 encoded 34K ORF 6 supports nuclear export of viral mRNA and its accumulation in the cytoplasm (Samulski and Shenk 1988). The DNA binding E2A protein is involved in translation and the non-coding VA RNA regulates translation (West et al. 1987; Xiao et al. 1998b; Janik et al. 1989). The produced rAAV is replication-deficient, wt free, helper virus-free, and can be produced in high titers (Graham et al. 1977; Samulski et al. 1989; Matsushita et al. 1998; Xiao et al. 1998b). rAAV particles lack the ability to integrate into the genome and persist as high-molecular-weight concatamers extrachromosomally in non-dividing cells (Xiao et al. 1996). Nevertheless, random background integration into the genome can be detected with the frequency being dependent on the target tissue (Nakai et al. 2000; McCarty et al. 2004; Kaepfel et al. 2013).

The AAV genome naturally consists of a single-stranded (ss) genome and therefore gene expression of infected tissues can be delayed by the rate-limiting step of second-strand synthesis. This slow gene expression can be circumvented by deletion of one D-sequence packaging signal within one ITR (left or right) and deletion of an adjacent TRS. Consequently, a

self-complementary (sc) DNA genome is formed with a hairpin-like structure. Self-complementary vectors show rapid gene expression with the drawback of a 50% reduced packaging capacity (Fu et al. 2003; McCarty et al. 2003; Zhong et al. 2004; McCarty 2008; Duque et al. 2009).

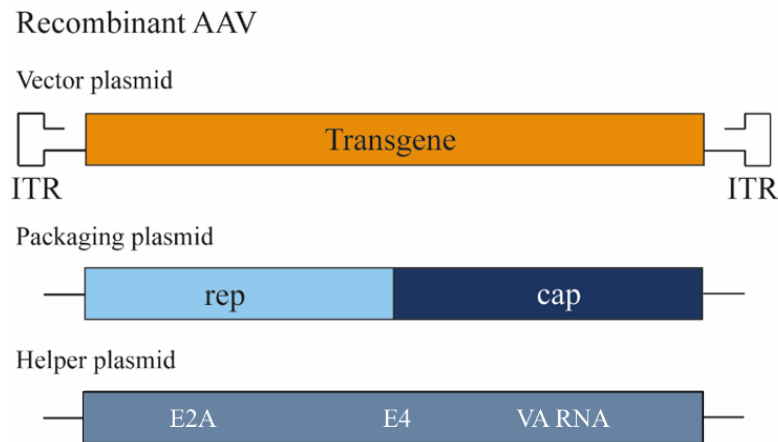


Figure 2: Illustration of the three-vector system required to produce helper virus-free rAAVs in HEK 293 cells. The *cis*-element vector plasmid consists of the wild-type AAV-derived inverted terminal repeats (ITR) framing the transgene (orange) under the control of a selected promoter. The packaging plasmid (*trans*-element) contains the AAV wild-type sequences *rep* (expressing necessary replication proteins, light blue) and *cap* (expressing all capsid proteins, dark blue). The helper plasmid (grey) encodes adenoviral E2A, E4, and VA RNA. Adenoviral E1A and E1B genes are encoded by HEK 293 cells. This vector system provides all information for activation of transcription, RNA stability and regulation of translation for a helper virus free AAV production.

1.1.5 The need and design of AAV2 capsid modifications for cell-specific targeting

AAV2 transduces a wide variety of dividing and non-dividing cells *in vitro* and *in vivo* such as muscle, liver, brain, lung, and tumor tissue due to the wide range of potential co-receptors (Xiao et al. 1996, 1997, 1998a; Fisher et al. 1997; Snyder et al. 1997; Bartlett et al. 1998; Arruda et al. 2005; Hacker et al. 2005; Palomeque et al. 2007). AAVs in general show rather inefficient transduction performance which limits the systemic application as a therapeutic (Trepel et al. 2015; Büning and Srivastava 2019). A broad systemic infection dilutes the drug resulting in non-optimal transduction of the target tissue. Furthermore, widespread capsid and transgene distribution in non-relevant tissues can cause unwanted immune system acti-

vation (e.g., T-cell activation via TLR9) (Colella et al. 2017), acute platelet decline, complement system activation, or serious adverse events such as acute hepatotoxicity (Wilson et al. 2020). Therefore, viral gene therapies need to specifically target the diseased area and cells with certain surface antigens to reduce side effects in healthy tissue (Baudino 2015).

The knowledge of the AAV capsid structure and characteristics allows the design of novel capsid variants with selective tissue targeting properties. Several methods were developed to modify AAV capsids with the overall aim of detargeting and/or retargeting (Figure 3). “Detargeting” in this context refers to the modification of capsids in a manner that ablates the natural capsid–receptor interactions. “Retargeting” describes the de-novo generation of recombinant capsids that specifically interact with the cell surface receptor(s) of interest (Kuklik et al. 2021).

A simple approach to modify produced capsids is the use of exogenous agents such as bispecific antibodies (Bartlett et al. 1999), HPMA polymers (Carlisle et al. 2008), PEGylation (Lee et al. 2005), biotinylation (Ponnazhagan et al. 2002), or coating with cationic lipids (Fein et al. 2009). The first retargeting approach used unmodified AAVs and bispecific antibodies, directly binding to the capsid and platelet-specific α IIb β 3 integrin. This enhanced cell-type selective transduction (Bartlett et al. 1998). Coverage of the capsids with those agents has the benefit of not modifying the capsid on protein level and shielding it from neutralizing antibody binding. However, this approach does not ablate the natural tropism. A combination of capsid detargeting and retargeting requires capsid modifications on protein level (Kuklik et al. 2021).

Chimeric serotypes were developed by swapping sequences of VP of different AAV serotypes. Furthermore, mosaic capsids were produced by mixing different serotype capsid proteins. Those serotypes obtain characteristics of both viral serotypes, but packaging efficiency and capsid characteristics are not predictable. Furthermore, the novel serotypes are sensitive to a broader array of neutralizing antibodies (Hauck et al. 2003; Rabinowitz et al. 2004; Gigout et al. 2005).

Directed evolution approaches *in vitro* or *in vivo* have been developed to modify AAV capsids. This approach does not require certain knowledge of target tissue or capsid characteristics (Mitchell and Samulski 2013). First, random cap mutations are produced by error-prone PCR (Maheshri et al. 2006; Bartel et al. 2012) or DNA shuffling (Stemmer 1994), and

a capsid library is produced. The selected tissue is transduced with those capsids and after tissue resection or harvest of cells, vector genomes are amplified by PCR. By this, capsids with desired characteristics are biopanned in iterative cycles until capsids with high transduction abilities have been selected (Yang et al. 2009; Gray et al. 2010; Michelfelder et al. 2011). However, this mutagenesis approach is time and cost expensive and the target receptor remains unidentified in this process.

The capsid can be modified by single amino acid alterations (Liu et al. 2013; Kim et al. 2019) or integration of short peptides or ligands that directly bind the desired receptor (Trepel et al. 2000; Ried et al. 2002; Liu et al. 2013; Eichhoff et al. 2019; Feiner et al. 2019, 2020; Kim et al. 2019). A prominent modification site of AAV2 is 587/588 located in the variable loop eight of the capsid (Xie et al. 2002). This loop tolerates up to 35 additional amino acids before the capsid assembly is hindered. As this position is important for HSPG binding, modifications can result in detargeting (Müller et al. 2003; Michelfelder et al. 2009, 2011). Such surface modifications have furthermore the potential to reduce neutralizing antibody binding (Huttner et al. 2003). Such a rational design of AAV capsid modifications enables direct and selective binding of the desired receptor but requires a de-novo time and cost-intensive capsid development for every new target.

AAV capsid modification using a myc-tag in combination with a multispecific adaptor antibody proved successful targeting of liver, pancreas, and intestine tissue *in vivo* (Kyratsous et al. 2019). This approach is advantageous, as it was proven that the same modified viral capsid could be reused to target various tissues.

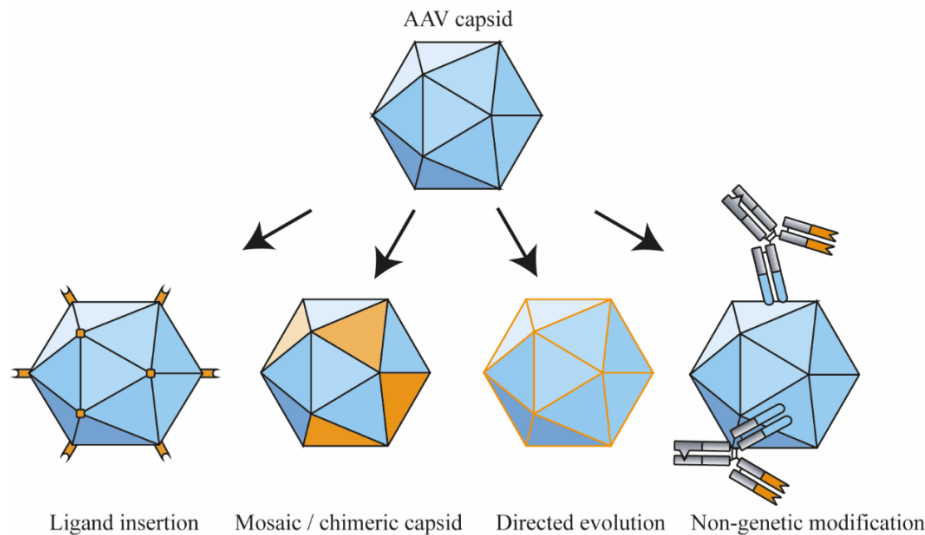


Figure 3: Approaches of AAV capsid diversification. Four main strategies to diversify the wild-type AAV capsid (blue) have been described. Modified regions and binding ligands are shown in orange. Ligands such as epitopes, peptides, nanobodies, or Darpins can directly be inserted into the capsid, leading to direct receptor binding. Novel AAV serotypes were developed by mixing subunits (chimeric AAVs) or VP proteins (mosaic) of several serotypes into one capsid. Directed evolution of capsids can be achieved in cycles of error-prone PCR amplification of capsids and transduction of selected tissues. Purified AAV capsid can be non-genetically modified by coupling to exogenous agents such as polymers, lipids, or antibodies.

1.2 Antibodies

Antibodies are so-called immunoglobulins (Ig) and are proteins playing a major role in the adaptive immune response. These proteins recognize foreign material, so-called antigens, (Pauling 1940) on the surface of viruses, bacteria, or disease-associated organisms. Immunoglobulins are produced and secreted by B-cells and show two major functions: first the specific binding of a pathogen that induced immune response (neutralization) and second the mobilization of cells and interaction with other molecules of the immune system (effector function). These two functions are structurally separated. The antigen-binding region is variable and differs between antibodies that allow the recognition of a wide diversity of antigens. The encoded region of the effector function is not variable and enables permanent interaction with the immune system (constant region) (Davies and Chacko 1993; Murphy et al. 2009).

1.2.1 The structure of IgG antibodies

Immunoglobulins are divided into five classes (IgM, IgD, IgG, IgA, and IgE) according to the isotype of the heavy chain (γ , μ , α , δ and ϵ) (Pauling 1940). All Igs share a common

structure, but the isotype determines their different effector functions (Davies and Chacko 1993; Murphy et al 2009). IgG shows an 80% prevalence and therefore is the predominant class in human serum. It has the longest half-life compared to other Igs and is commonly used for therapeutic approaches. IgG is further divided into subclasses IgG1 - IgG4, with IgG1 being the most common in western European populations (Murphy et al. 2009).

IgG antibodies have a molecular weight of around 150 kDa and are composed of two identical heavy chains (HC) of each 50 kDa and two identical light chains (LC) of each 25 kDa that form a 'Y' shaped protein. The light chains are separated into the two classes lambda and kappa with the differences in sequence and length but unknown functional differences (Davies and Chacko 1993; Murphy et al. 2009). IgG can be digested by papain and results in two so-called Fab fragments and one Fc-fragment. These identical two fragments contain N-terminal antigen-binding sites. The Fc-fragment is the stem of the protein composed only of two heavy chains that are joined with the Fab fragments via a flexible hinge region. A Fab fragment consists of parts of the heavy chain and a light chain.

The light chain is divided into two parts: the N-terminal variable domain (V_L) and the C-terminal constant domain (C_L). The heavy chain is divided into four parts C_{H3} , C_{H2} , C_{H1} , and V_H (C-terminal to N-terminal terminology). A pair of $C_{H3}:C_{H3}$ and $C_{H2}:C_{H2}$ domains form the Fc-fragment. A flexible hinge region builds two disulfide bonds between the C_{H2} and C_{H1} regions and connects two heavy chains. The C_{H1} region is connected to the C_L region via one disulfide bond. Furthermore, the fragments interact via non-covalent binding. The fragment V_L of a light chain and the V_H region of a heavy chain form the antigen-binding site (Porter 1959; Inbar et al. 1972; Davies and Chacko 1993) (Figure 4).

The domains of each heavy and light chain share a common β -barrel structure of anti-parallel β -sheets connected by one disulfide bond in each domain. C_L forms a smaller β -barrel consisting of seven antiparallel β -sheets. V_L is formed by nine β -sheets with flexible loops. Three loops of V_L and three loops of V_H form hypervariable regions stabilized by the scaffold of the β -barrel that are responsible for antigen binding and are called complementary determining regions (CDR1, CDR2, and CDR3) (Murphy et al. 2009).

1.3 Design and production of bispecific antibodies

Naturally occurring antibodies comprise two identical antigen-binding sites except for IgG4. This immunoglobulin has an unstable hinge region that enables random Fab arm exchanges

and results in a bivalent molecule (Kolfshoten et al. 2007). Bispecific IgG molecules contain two different antigen-binding sides and are of high interest, as they can be used as adaptors between effector and target. They enable the combination of effector mechanisms with a disease-related-target structure and have been used to recruit effector molecules, cells, or viral vectors (Spriell et al. 2000; Nyakatura et al. 2016; Brinkmann and Kontermann 2017).

The first artificial bispecific antibody, an $F(ab')_2$ format, has been developed in 1961 by (Nisonoff and Rivers 1961). The development of novel monoclonal antibody production technologies (hybridoma technology) accelerated the design and production of antibodies in general, while the generation of hybrid hybridomas allowed for the production of bispecific antibodies with defined specificities (Köhler and Milstein 1975; Milstein and Cuello 1983). Later, recombinant antibody production systems enabled custom-designed mono- and bispecific antibodies productions with defined sequence, structure, composition, minimized toxicity, and optimized functional properties. Various bispecific antibody formats were developed with the main discrimination by the presence or absence of the Fc domain that mainly influences the size, purification strategy, stability, and effector functions (Spriell et al. 2000; Kontermann 2005; Brinkmann and Kontermann 2017).

Novel bispecific antibody formats such as tandem scFv, Diabodies, or dual-affinity retargeting proteins contain only the variable regions of V_H and V_L connected via polypeptide linkers (Mallender and Voss 1994; Johnson et al. 2010). These formats are of small size and therefore may allow for increased tissue penetration. The formats furthermore enable the production of single-chain antibodies with simplified production and purification protocols (Huston et al. 1991). The absence of the Fc domain abrogates any effector functions (antibody-dependent cell-mediated cytotoxicity, antibody-dependent cellular phagocytosis, complement fixation, and neonatal Fc receptor-mediated recycling) but decreases stability and serum half-life (Johnson et al. 2010; Brinkmann and Kontermann 2017). Diverse Fc-mutations have been described to modulate the Fc-mediated interactions (Wang et al. 2018), such as the IgG1 mutations L234A and L235A that are known to reduce $Fc\gamma R$ and C1q binding (Xu et al. 2000).

The production of recombinant bispecific antibodies in an IgG format requires cell transfection with four different peptide chains (two different heavy chains and two corresponding

light chains). The pairing of unmodified sequences can result in 16 different peptide combinations, of which only one pairing results in the desired functional bispecific antibody (Schaefer et al. 2015; Brinkmann and Kontermann 2017). This pairing problem can be overcome by genetic engineering of the heavy chains. To force a correct assembly a strategy called knobs-into-holes (KiH) has been developed. The KiH method makes use of modified C_{H3} domains resulting in asymmetric Fc regions (Ridgway et al. 1996). One amino acid within the C_{H3} region is replaced by a larger one to build a ‘knob’- C_{H3} variant. This ‘knob’ inserts into a ‘hole’- C_{H3} variant, in which large amino acid was replaced by a small one. Several Fc-heterodimerization approaches have been developed using different mutations in the C_{H3} region. Assembly of bispecific antibodies with KiH mutations abolishes the risk of false heavy chain pairing and results in four different peptide combinations due to wrong light chain pairing. The original KiH model was further improved and yet several different mutational sites for knob and hole generation are described (Ridgway et al. 1996; Atwell et al. 1997; Merchant et al. 1998; Davis et al. 2010; Gunasekaran et al. 2010; Moore et al. 2011; Strop et al. 2012; Choi et al. 2013; Kreudenstein et al. 2013; Labrijn et al. 2013; Moretti et al. 2013; Leaver-Fay et al. 2016).

In this study, the natural IgG4 process of Fab-arm exchange was modified into a process called ‘controlled Fab-arm exchange’ to generate stable bispecific IgG1 (Labrijn et al. 2009, 2013). The mutation F405L is used to generate knobs and K409L is used to generate holes within the C_{H3} region. A schematic presentation of the bispecific antibody design is shown in Figure 4. This method enables a simple formation of bispecific antibodies with minimal sequence mutation of the original antibody structure. A bispecific antibody with the correct pairing of heavy and light chains is produced via the production of half-antibodies carrying the knob or hole mutation. Purified half-antibodies are mixed in equimolar amounts under mild reducing conditions that reduce heavy chain disulfide bonds and enable efficient pairing of matching knob and hole IgG antibody fragments. This method claimed > 90 % yield of bispecific antibodies, which is the thermodynamically preferred product (Goulet et al. 2018). Additionally, the C_{H2} point mutations L234A and L235A were inserted to decrease Fc-effector functions (Wang et al. 2018).

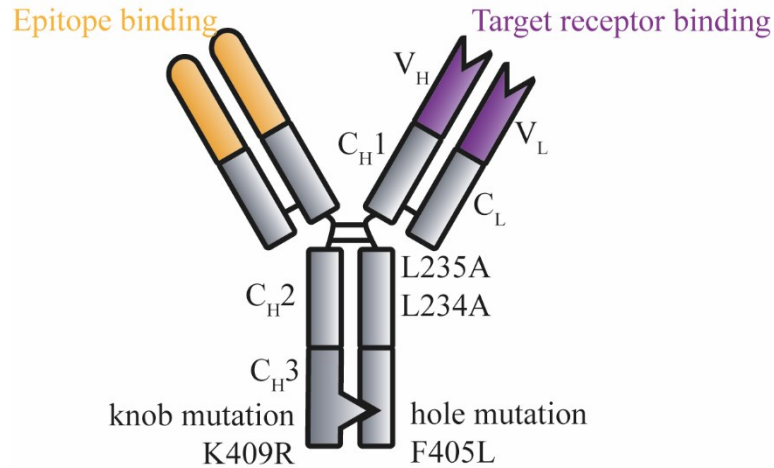


Figure 4: Overview of the bispecific antibody design used in this study. Bispecific antibodies used in this study are composed of a knob mutation K409R within the constant heavy chain 3 (C_H3) region of the epitope (orange) binding arm and a corresponding hole mutation F405L of the target receptor (violet) binding arm. The C_H2 region contains two point mutations L234A and L235A in both arms to abrogate Fc-effector functions. Antibodies were produced with their corresponding light chain (C_L) kappa or lambda and differ in their variable regions of heavy (V_H) and light (V_L) chains.

1.4 Combination of bispecific antibodies with AAV capsid modification for cell type specific targeting

A rational capsid modification by insertion of small epitopes combined with bispecific antibodies may result in AAV tropism destruction with the benefit of antibody-mediated receptor targeting. This approach is attractive as it is a modular and flexible approach regarding target selection. Exchange of one arm of the adaptor antibody would allow targeting of different receptors based on the same modified AAV variant (Kuklik et al. 2021). However, this capsid modification requires a peptide sequence that is short and keeps capsid assembly unaffected while the peptide must form a linear antigen that enables antibody binding.

The epitope chosen in this study to modify AAV2 capsids was previously analyzed by (Schiele 2013), who described and characterized the antigen of a novel antibody binding the protein proprotein convertase subtilisin/kexin type 9 (PCSK9). The PCSK9 binding antibody was derived from hybridoma cells. Peptide microarray screening was used to precisely identify the antigen sequence. The antibody binds a linear epitope of PCSK9 near the epidermal growth factor-like repeat A domain ranging from Ile161 to Glu170 (ITPPRYRADE). Antigen binding is mediated by all CDRs of the light chain as well as CDR2 and 3 of the heavy chain. Most important for antibody: epitope binding is Tyr166, which forms hydrogen bonds with Asp50 and Trp52 of the heavy chains CDR2. ITPPRYRADE (KD = 4.96 nM) showed slight loss of affinity when shortened to TPPRYRADE (KD = 22.1 nM) (Schiele 2013).

The full length and shortened epitope called '2E3' was used in this study to rationally design new AAV2 capsid variants. The corresponding antibody was modified into a bispecific format that was combined with cell surface receptor binding antibodies.

1.5 Target Receptors

1.5.1 Fibroblast activation protein

The integral membrane-bound glycoprotein fibroblast activation protein (FAP) is highly conserved between humans and mice and shows serine protease -, post-proline dipeptidyl peptidase- and endopeptidase enzymatic activity (Mathew et al. 1995; Park et al. 1999; Busek et al. 2018). Upregulated FAP expression can be found in fetal mesenchymal tissue, during wound healing and migration of bone marrow mesenchymal stem cells. Healthy adult tissue lacks FAP expression (Rettig et al. 1988; Garin-Chesa et al. 1990; Park et al. 1999; Chung et al. 2014; Busek et al. 2018). Further disease conditions are associated with upregulated FAP expression such as arthritis (Bauer et al. 2006; Milner et al. 2006), atherosclerotic plaques (Stein et al. 2021), liver cirrhosis (Levy et al. 1999), and idiopathic pulmonary fibrosis (Acharya et al. 2006). FAP is also expressed in reactive stromal fibroblasts of epithelial neoplasms, in malignant mesenchymal cells, and in bone and soft tissue sarcomas (Rettig et al. 1988; Garin-Chesa et al. 1990).

Epithelial cancers are often associated with changes in the surrounding stroma. The tumor stroma is a heterogeneous mix of blood vessels, tumor stromal fibroblasts, lymphoid and phagocytic cells, peptide mediators, and proteolytic enzymes that altogether alter the normal extracellular matrix (Garin-Chesa et al. 1990). Especially primary and metastatic tumors contain reactive stromal fibroblasts with high FAP expression, and it was found that stroma could make up to 90% of the mass of solid epithelial tumors. As the FAP expressing stromal cells promote blood vessel formation, FAP has high accessibility by antibodies. Furthermore, stromal cells show higher genetic stability that allows the targeting of an unaltered epitope (Rettig et al. 1988; Welt et al. 1994; Busek et al. 2018). FAP internalization was described upon antibody binding and numerous FAP binding antibodies are available, such as MO33, MO36, and BIBH1 (sibrozumab) (Brocks et al. 2001; Mersmann et al. 2001; Hofheinz et al. 2003; Scott et al. 2003; Tahtis et al. 2003; Fischer et al. 2012). Internalized FAP can be found in endosomes indicating internalization by endocytosis (Baum et al. 2008; Fischer et al. 2012). It was previously shown that immunoliposomes of an average size of 90 nm coupled with scFv anti-FAP antibody fragments were able to be internalized by cells (Baum et al. 2008).

Due to the increased expression of FAP in the tumor stroma and disease tissue, it's the absence in healthy adult tissue, internalization ability upon antibody binding, and availability of antibodies, the receptor was chosen as a promising target for the viral gene therapy approach in this study (Kuklik et al. 2021).

1.5.2 Programmed death-ligand 1

The 33 kDa programmed death-ligand 1 (PD-L1) is a type I transmembrane protein of the immunoglobulin superfamily principally bound by the programmed cell death protein 1 (PD-1). PD-1 is mainly expressed on T- and B- cells. The PD-1 and PD-L1 interaction therefore controls the peripheral and central immune response (Dong et al. 1999; Freeman et al. 2000; Ahmadzadeh et al. 2009). PD-L1 mRNA expression was described in several tissues such as heart, skeletal muscle, placenta, and lung tissues and low-level expression in the thymus, spleen, kidney, and liver (Dong et al. 1999). The further expression can be induced in monocytes and keratinocytes by interferon-gamma stimulation that resembles inflammation (Freeman et al. 2000). Many tumor types express PD-L1 (Ghebeh et al. 2006; Patel and Kurzrock 2015) as well as cancer-associated fibroblasts within the tumor stroma (Cheng et al. 2018; Li et al. 2019) resulting in PD-1:PD-L1 interaction and therefore destruction of immune responses by inhibition of the activation and expansion of T-cells (Freeman et al. 2000; Burr et al. 2017; Mezzadra et al. 2017). Many antibodies binding PD-L1 have been developed and approved such as avelumab (Collins and Gulley 2018). The interaction of avelumab and PD-L1 has been extensively validated in various (pre-)clinical studies (Collins and Gulley 2018) and the internalization of PD-L1 upon interaction with avelumab as well as further ligands or antibodies have been described earlier (Contreras-Sandoval et al. 2014; Li et al. 2018; Gurung et al. 2020; Jin et al. 2020). Although the exact internalization pathway of PD-L1 is unknown yet, it was reported that avelumab internalization was reduced in absence of Fc γ receptors on human blood cells (Jin et al. 2020) and that glycolisation of PD-L1 is important to induce internalization (Li et al. 2018)

As both biomarkers, FAP and PD-L1, are widely expressed on tumors and within the tumor microenvironment, the described modular targeting approach of this study has the potential to be applicable for a significant portion of human cancers (Kuklik et al. 2021).

1.6 Aim of the project

Most capsid modification approaches develop new AAV variants for every new target, which requires time and cost-intensive design, screening, and production of every single capsid. Rational design of a new AAV capsid with silenced tropism in combination with bispecific adapters would allow using one engineered AAV as a targeting base. Two receptors expressed in the tumor microenvironment were used to show proof-of-concept targeting. To achieve this aim, this study focused on three major steps: AAV capsid modification, bispecific adaptor production and establishment of a modular targeting mechanism (Figure 5).

The full length and shortened epitope called '2E3' was used to rationally design new AAV2 capsid variants. Modification sites were chosen rationally based on the capsid structure and published interactions domains with the natural AAV2 receptors HSPG or integrin $\alpha 5\beta 1$. These modifications aim to silence the broad tropism of AAV2 and simultaneously provide an epitope for antibody binding. 2E3 has never been used before for AAV capsid modifications and consequently, novel AAV2 capsid variants were designed with novel characteristics.

A bispecific antibody was used as an adapter between the inserted epitope within the viral capsid and the target cell surface receptor. FAP and PD-L1 are both disease-relevant membrane proteins that are upregulated in tumor stroma or cancer tissue. Antibodies were previously described to bind and induce internalization of both receptors. Receptor binding antibodies were cloned into a bispecific format and combined with an 2E3 binding antibody. This allowed the simultaneous targeting of receptor and capsid modified AAV2 based on the same antibody backbone. Neither FAP nor PD-L1 have been described as AAV gene therapy targets before.

A novel retargeting mechanism was developed by combination of capsid modified AAV2 with bispecific antibodies and tumor cell lines expressing the desired target receptor *in vitro*. The exchange of the bispecific receptor targeting antibody should prove the advantage of the modular targeting system that is based on the same AAV backbone. Additionally, the system should be challenged *in vivo* to observe viral detargeting in a complex organism and simultaneously retargeting towards tumor tissue.

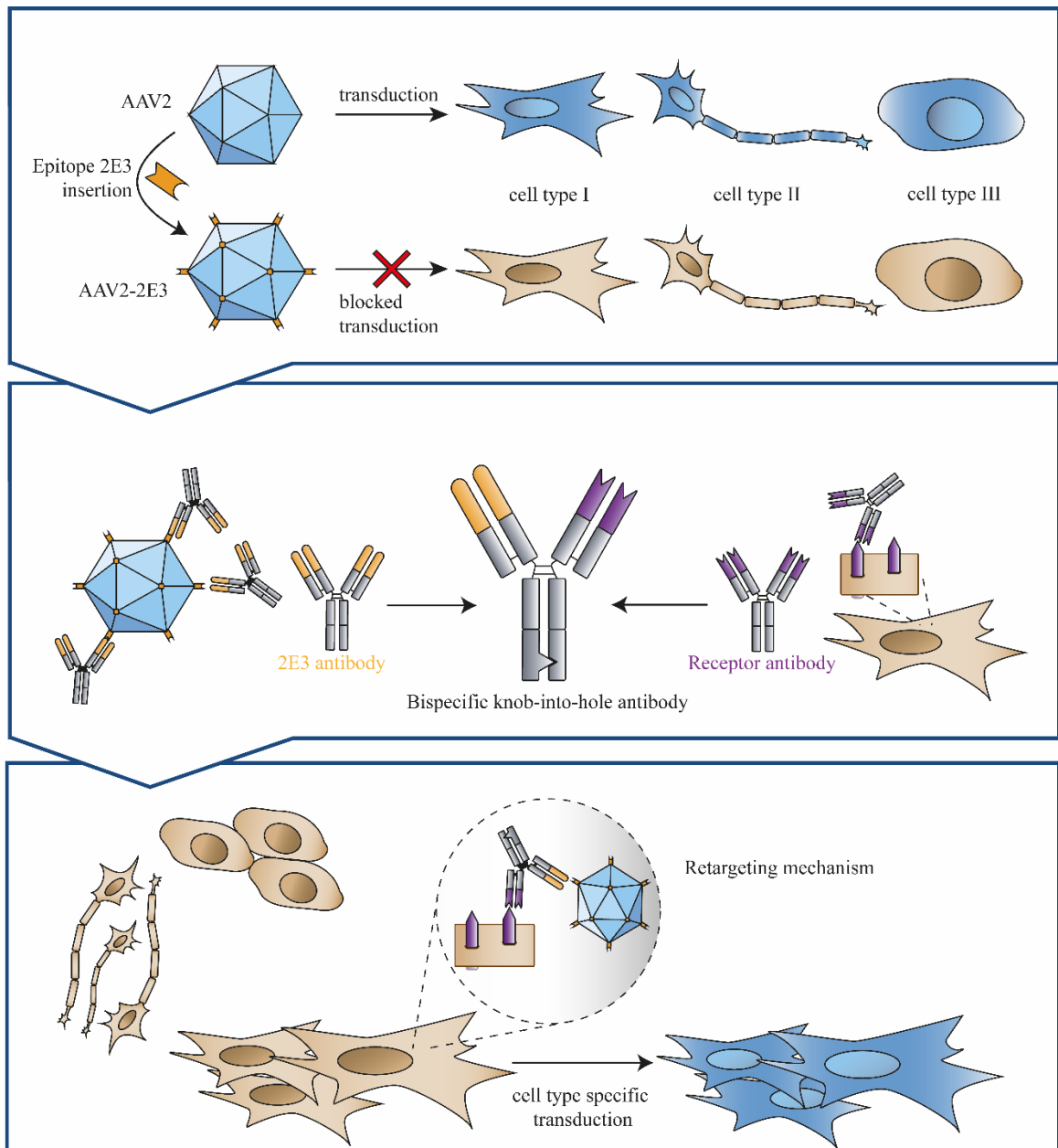


Figure 5: Development of a targeting platform of capsid modified AAV vectors by bispecific antibody binding Modified from (Kuklik et al. 2021). CC BY 4.0, <https://creativecommons.org/licenses/by/4.0/>. Capsid modified AAV vector variants were developed by insertion of a short epitope 2E3 (orange) into the viral capsid (AAV-2E3). This destroyed the broad AAV2 infectivity (transduced cells shown in blue, non-transduced cells are shown in beige). Next, a bispecific knob-into-hole antibody was produced that bound both, the 2E3 epitope modified viral capsids and the target cell surface receptor (violet). Finally, pre-incubation of AAV-2E3 with the bispecific antibody resulted in an AAV:antibody complex, targeting the desired cell surface receptor, and consequently selective transduction of receptor-positive cells. The exchange of one arm of the bispecific antibody enabled the targeting of other receptors based on the same targeting platform.

2 Materials and methods

2.1 Materials and devices

Table 3: Devices

Device	Manufacturer
1290 Infinity II LC System	Agilent Technologies, Santa Clara, CA, USA
ÄKTAavant™ 25	Cytiva, Marlborough, MA, USA
Axio Imager 2	Zeiss SMT, Oberkochen, Germany
Axioscan 7	Zeiss SMT, Oberkochen, Germany
Biochrom™ NanoVue Plus	Thermo Fisher Scientific Waltham, MA, USA
BOND RX Fully Automated Research Stainer	Leica Biosystems, Wetz- lar, Germany
Countess II FL Automated Cell Counter	Thermo Fisher Scientific Waltham, MA, USA
Endosafe -PTS™	Charles River, Wilming- ton, MA, USA
EVOS FL Cell Imaging System	Thermo Fisher Scientific Waltham, MA, USA
Gyrolab® xPand	Gyros Protein Technolo- gies AB, Uppsala, Sweden
iBlot 2 Dry Blotting System	Invitrogen™, Carlsbad, CA, USA
Image Quant LAS 4000	Cytiva, Marlborough, MA, USA
Incucyte S3	Sartorius, Göttingen, Ger- many
Infinite® M200 PRO Multimode Microplate Reader	Tecan Group Ltd, Männ- edorf, Switzerland

iQue® Screener PLUS	Sartorius, Göttingen, Germany
IVIS® SpectrumCT	PerkinElmer®, Waltham, MA, USA
Mastercycler® X50	Eppendorf, Hamburg, Germany
SECTOR Imager 6000	MSD® Rockville, MD, USA
Octet HTX	FortéBio, Fremont, CA, USA
Opera Phenix High-Content Screening System	PerkinElmer®, Waltham, MA, USA
Precellys Evolution Homogenizer	Bertin Technologies SAS, Montigny-le-Bretonneux, France
PX1™ PCR Plate Sealer	Bio-Rad, Hercules, CA, USA
QuantStudio™ 6 Flex Real-Time PCR System	Thermo Fisher Scientific Waltham, MA, USA
QXDx AutoDG ddPCR System	Bio-Rad, Hercules, CA, USA
Sorvall Discovery 90SE and Fixed Angle Rotor Type 70 Ti	Thermo Fisher Scientific Waltham, MA, USA, and Beckman Coulter
Transmission electron microscope EM 912	Zeiss SMT, Oberkochen, Germany

Table 4: Chemicals and agents

Chemical / Agent	Manufacturer	Application
2×HBS	Thermo Fisher Scientific Waltham, MA, USA	Calcium chloride transfection
2-MEA	Sigma-Aldrich, St. Louis, MO, USA	Fab-exchange
3% Hydrogen peroxide solution	Sigma-Aldrich, St. Louis, MO, USA	Histology
4% Paraformaldehyde (PFA) Solution In PBS	Boster, Pleasanton, CA, USA	Tissue fixation
293fectin™ Transfection Reagent	Thermo Fisher Scientific Waltham, MA, USA	Antibody production
β-Mercapthoethanol	Sigma-Aldrich, St. Louis, MO, USA	Tissue homogenization
Acetic acid 100%	Carl Roth, Karlsruhe, Germany	Buffer solution
AdvanceBio SEC 300A Proteinstandard	Agilent Technologies, Santa Clara, CA, USA	HPLC
AdvanceBio SEC 8300A	Agilent Technologies, Santa Clara, CA, USA	HPLC
Alexa Fluor™ 647 NHS Ester	Thermo Fisher Scientific Waltham, MA, USA	Pharmacokinetic
BOND Polymer Refine Detection	Leica Biosystems, Wetzlar, Germany	Histology
CKMix-Tissue homogenizing tubes	Bertin Technologies, Montigny-le-Bretonneux, France	Tissue homogenization

Ethanolamine	Sigma-Aldrich, St. Louis, MO, USA-Aldrich	Fab-arm exchange
Ethanol Rotipuran®	Carl Roth, Karlsruhe, Germany	DNA extraction
Blocker A	MSD® Rockville, MD, USA	ELISA assay
BSA	Merck Millipore, Burlington, MA, USA	Blocking buffers
BSA Conjugated Digoxin	Biozol, Eching, Germany, Eching, Germany	Octet assay
Chloroform Isoamyl Alcohol	Sigma-Aldrich, St. Louis, MO, USA-Aldrich	DNA tissue purification
ddPCR™ Supermix for Probes	Bio-Rad, Hercules, CA, USA	ddPCR
Dehydroisoandrosterone 3-acetate 97%	Sigma-Aldrich, St. Louis, MO, USA-Aldrich	Cell culture medium
DEPC water	Thermo Fisher Scientific Waltham, MA, USA	qPCR
EZ-Link™ Sulfo-NHS-LC-Biotin	Thermo Fisher Scientific Waltham, MA, USA	Pharmacokinetic
Glycerol	Sigma-Aldrich, St. Louis, MO, USA-Aldrich	rAAV purification
Gyrolab Bioaffy 1000	Gyrolab Protein Technologies	Pharmacokinetic

Halt™ Protease Inhibitor Cocktail, EDTA-Free (100×)	Thermo Fisher Scientific Waltham, MA, USA	rAAV extraction
Hydrochloric acid	Sigma-Aldrich, St. Louis, MO, USA-Aldrich	Buffer solution
IncuCyte® FabFluor pH Red Antibody Labeling reagent	Sartorius, Göttingen, Germany	Antibody internalization
InstantBlue™ Protein Stain	Thermo Fisher Scientific, Waltham, MA, USA	SDS PAGE
Trypan Blue Stain	Thermo Fisher Scientific Waltham, MA, USA	Countess™ Automated Cell Counter
Isopropanol	Sigma-Aldrich, St. Louis, MO, USA-Aldrich	Tissue fixation
Iodixanol	Sigma-Aldrich, St. Louis, MO, USA-Aldrich	rAAV purification
Magnesium chloride solution 1 M	Sigma-Aldrich, St. Louis, MO, USA-Aldrich	rAAV extraction
NuPAGE Bis-Tris Gels	Thermo Fisher Scientific Waltham, MA, USA	SDS PAGE
NuPAGE™ MES SDS Running Buffer (20×)	Thermo Fisher Scientific Waltham, MA, USA	SDS PAGE
NuPAGE™ Sample Reducing Agent (10×)	Invitrogen™, Carlsbad, CA, USA	SDS PAGE

OptiPrep™ Density Gradient Medium	Sigma-Aldrich, St. Louis, MO, USA-Aldrich	rAAV purification
Paraffin	Sigma-Aldrich, St. Louis, MO, USA-Aldrich	Tissue fixation
Phenol-Chloroform	Sigma-Aldrich, St. Louis, MO, USA-Aldrich	DNA tissue purification
Phosphotungstic acid	Sigma-Aldrich, St. Louis, MO, USA-Aldrich	Electron microscopy
Pierce™ LDS Sample Buffer, Non-Reducing	Thermo Fisher Scientific Waltham, MA, USA	SDS PAGE
Poly(ethylene glycol) BioUltra	Sigma-Aldrich, St. Louis, MO, USA-Aldrich	rAAV purification
Potassium Chloride BioUltra 1M	Sigma-Aldrich, St. Louis, MO, USA-Aldrich	rAAV purification
Primary Antibody Diluent	Leica Biosystems, Wetzlar, Germany	Histology
QuantiFast Probe PCR Master Mix 2×	Qiagen, Hilden, Germany	qPCR
Read Buffer T (4×)	MSD® Rockville, MD, USA	ELISA Assay
Rexxip AN	Gyros Protein Technologies AB, Uppsala, Sweden	Pharmacokinetic

Rexxip F	Gyros Protein Technologies AB, Uppsala, Sweden	Pharmacokinetic
RLT buffer	Qiagen, Hilden, Germany	Tissue homogenization
Salt Active Nuclease	SERVA Electrophoresis GmbH, Heidelberg, Germany	rAAV extraction
SeeBlue™ Plus2 Pre-stained Protein Standard	Invitrogen™, Carlsbad, CA, USA	SDS PAGE
Skim milk powder	Sigma-Aldrich, St. Louis, MO, USA-Aldrich	Blocking buffer
Sodium acetate	Sigma-Aldrich, St. Louis, MO, USA-Aldrich	Buffer composition
Sodium chloride	Sigma-Aldrich, St. Louis, MO, USA-Aldrich	Buffer composition
Sodium hydrogen carbonate	Sigma-Aldrich, St. Louis, MO, USA-Aldrich	Buffer composition
Sodium hydroxide	Sigma-Aldrich, St. Louis, MO, USA-Aldrich	Buffer composition
TaqMan™ Universal PCR Master Mix	Thermo Fisher Scientific Waltham, MA, USA	qPCR
Tris Lysis Buffer	MSD® Rockville, MD, USA	Tissue lysis
Tris, Pufferan® ≥99,9 %, p.a.	Carl Carl Roth, Karlsruhe, Germany	Buffer composition

TWEEN® 20	Sigma-Aldrich, St. Louis, MO, USA-Aldrich	Wash buffer
UltraPure™ 0.5M EDTA, pH 8.0	Thermo Fisher Scientific Waltham, MA, USA	rAAV extraction
VivoGlo™ D-luciferin substrate	Promega, Madison, WI, USA	IVIS
Xylol	Sigma-Aldrich, St. Louis, MO, USA-Aldrich	Tissue fixation

Table 5: Cell culture chemicals and medium

Chemical /Medium	Manufacturer	Application
Calcium chloride	Sigma-Aldrich, St. Louis, MO, USA-Aldrich	Calcium chloride transfection
Corning, Inc, Corning, NY, USA Nu-Serum™ I/IV Growth Medium Supplements	Thermo Fisher Scientific Waltham, MA, USA	Cell culture medium
Dulbecco's Modified Eagle's Medium (DMEM) 30-2002™	ATCC, Manassas, VA, USA	Cell culture medium
Gibco™ DMEM, high glucose, GlutaMAX™ Supplement	Thermo Fisher Scientific Waltham, MA, USA	Cell culture medium
Gibco™ F17 Expression Medium	Thermo Fisher Scientific Waltham, MA, USA	Cell culture medium
Gibco™ Fetal Bovine Serum	Thermo Fisher Scientific Waltham, MA, USA	Cell culture medium
Gibco™ Geneticin	Thermo Fisher Scientific Waltham, MA, USA	Cell culture medium

Gibco™ GlutaMAX™ Supplement	Thermo Fisher Scientific Waltham, MA, USA	Cell culture medium
Gibco™ Ham's F-12	Thermo Fisher Scientific Waltham, MA, USA	Cell culture medium
Gibco™ MEM NEAA (100x)	Thermo Fisher Scientific Waltham, MA, USA	Cell culture medium
Gibco™ Opti-MEM™	Thermo Fisher Scientific Waltham, MA, USA	Cell culture medium
Gibco™ PBS, pH 7.4	Thermo Fisher Scientific Waltham, MA, USA	Cell culture medium
Gibco™ Pluronic™ F-68 Non-ionic Surfactant (100x)	Thermo Fisher Scientific Waltham, MA, USA	rAAV extraction, Anti-body production
Gibco™ RPMI 1640	Thermo Fisher Scientific Waltham, MA, USA	Cell culture medium
Gibco™ Sodium Pyruvate (100mM)	Thermo Fisher Scientific Waltham, MA, USA	Cell culture medium
HyClone™ Fetal Bovine Serum characterized	Thermo Fisher Scientific Waltham, MA, USA	Cell culture medium
Insulin solution from bovine pancreas	Merck Millipore, Burlington, MA, USA	Cell culture medium
TrypLE™ Express Enzyme (1x)	Thermo Fisher Scientific Waltham, MA, USA	Cell culture medium
Tryptone N1	Sigma-Aldrich, St. Louis, MO, USA-Aldrich	40 % Feeding solution

Table 6: Consumables

Consumables	Manufacturer
96-well transparent v-bottom	Biozym, Hessian Oldendorf, Germany
Amicon Ultra-15 centrifugal filters	Sigma-Aldrich, St. Louis, MO, USA-Aldrich

Biosensor / Streptavidin (SA) Tray	Molecular Devices, LLC, San Jose, CA, USA
CELLdisc™ 16 layer	Greiner Bio-One GmbH, Frickenhausen Germany
ddPCR™ 96-Well Plates	Bio-Rad, Hercules, CA, USA
ddPCR™ Droplet Reader Oil	Bio-Rad, Hercules, CA, USA
ddPCR™ Supermix for Probes (No dUTP)	Bio-Rad, Hercules, CA, USA
DG8™ Cartridges for QX200™ Droplet Generator	Bio-Rad, Hercules, CA, USA
DG8™ Gaskets for QX200™ Droplet Generator	Bio-Rad, Hercules, CA, USA
Droplet Generation Oil for Probes	Bio-Rad, Hercules, CA, USA
Erlenmeyer cell culture flasks 3L	Sigma-Aldrich, St. Louis, MO, USA-Aldrich
HiTrap® MabSelect SuRe 5 mL	Cytiva, Marlborough, MA, USA
Hi Trap® SP FF 1 ml	Cytiva, Marlborough, MA, USA
HiLoad® 26/600 Superdex® 200 pg	Cytiva, Marlborough, MA, USA
iBlot™ 2 Transfer Stacks	Invitrogen™, Carlsbad, CA, USA
MicroAmp™ EnduraPlate™ Optical 384-Well Clear Reaction Plate	Thermo Fisher Scientific Waltham, MA, USA
MicroAmp™ Optical Adhesive Film	Thermo Fisher Scientific Waltham, MA, USA
Micro Bio-Spin® Columns	Bio-Rad, Hercules, CA, USA

Minivette® POCT	Sarstedt, Inc., Newton, NA, USA
MULTI-ARRAY 96 Plate Pack, SECTOR Plate	MSD® Rockville, MD, USA
OptiPlate-96, White Opaque 96-well Microplate	PerkinElmer®, Waltham, MA, USA®
OptiPlate-384, White Opaque 384-well Microplate	PerkinElmer®, Waltham, MA, USA®
PCR Plate Heat Seal, foil, pierceable	Bio-Rad, Hercules, CA, USA
Phase lock Gel tubes	Quanta Biosciences, Gaithersburg, MD, USA
PTS20 LAL Test Cartridge	Charles River, Wilmington, MA, USA
Quick-Seal Ultracentrifugation Tubes	Beckman Coulter Life Sci- ences Life Sciences Divi- sion Headquarters, Indian- apolis, IN, USA
QXDx AutoDG Consumable Pack	Bio-Rad, Hercules, CA, USA
Snap Ring vials	Sigma-Aldrich, St. Louis, MO, USA-Aldrich
Sterile Ultrafree-MC and CL Centrifugal Filter Units	Merck Millipore, Burling- ton, MA, USA
T-175 Tissue culture flask	Corning, Inc, Corning, NY, USA
Tilted bottom TW384 Microplates	FortéBio, Fremont, CA, USA
Ultrafree-CL, GV 0,22 µm, steril	Sigma-Aldrich, St. Louis, MO, USA-Aldrich
ViewPlate™- 96 F TC	PerkinElmer®, Waltham, MA, USA®

Table 7: Kits

Kit	Manufacturer
AAV2 Titration ELISA	Progen, Heidelberg, Germany
AllPrep DNA/RNA 96 Kit	Qiagen, Hilden, Germany
Bright-Glo™ Luciferase Assay System	Promega, Madison, WI, USA
Luciferase Assay System	Promega, Madison, WI, USA
Pierce™ BCA Protein Assay Kit	Thermo Fisher Scientific Waltham, MA, USA
QIAfilter Plasmid Midi Kit (25)	Qiagen, Hilden, Germany
QuantiFast Probe PCR Kit	Qiagen, Hilden, Germany
SuperScript™ IV VILO™ Master Mix with ezDNase™ Enzyme	Thermo Fisher Scientific Waltham, MA, USA
ViralXpress™ Nucleic Acid Extraction Kit	Merck Millipore, Burlington, MA, USA

Table 8: Antibodies

Antibody	Type	Manufacturer /Origin
Anti-2E3	huIgG1	(Schiele 2013)
Anti-AAV2 A20	muIgG3, monoclonal	Progen, Heidelberg, Germany
anti-AAV VP1/VP2/VP3, B1	muIgG1 monoclonal	Progen, Heidelberg, Germany
anti-Digoxigenin	huIgG1	(Bramlage et al. 2009)
Anti-human antibody Goat SULFO-TAG	polyclonal	MSD® Rockville, Md, USA
Anti-mouse antibody Goat SULFO-TAG	polyclonal	MSD® Rockville, Md, USA
APC anti-human IgG Fc	polyclonal	Biolegend®, San Diego, CA, USA
BIBH1	huIgG1	Boehringer Ingelheim Pharma KG, Biberach Riß, Germany
CD31 Polyclonal Antibody	Rabbit polyclonal	Invitrogen™, Carlsbad, CA, USA
Cleaved Caspase-3	Rabbit monoclonal	Cell Signaling, Danvers, Massachusetts, USA
goat anti-mouse IgG1 (H+L) HRP	Goat IgG1	Invitrogen™, Carlsbad, CA, USA
Goat anti-Human IgG F(ab') ₂ :HRP	Goat IgG1	Bio-Rad, Hercules, CA, USA
Goat anti-Human IgG (H+L) Secondary Antibody (Pre-ad- sorbed)	Goat IgG polyclonal	Novus Biologicals, Little- ton, CO, USA
Goat Anti-Human IgG, Monkey ads-UNLB	Goat IgG polyclonal	SouthernBiotech, Birming- ham, AL, USA
human FcR Blocking Reagent	polyclonal	Miltenyi Biotec, Bergisch Gladbach, Germany

MO33	huIgG1	(Brocks et al. 2001)
MO36	huIgG1	(Brocks et al. 2001)
Recombinant Anti-Fibroblast activation protein, alpha antibody	Rabbit IgG monoclonal	Abcam, Cambridge, UK
Rituximab	Chimeric IgG1	Sigma-Aldrich, St. Louis, MO, USA-Aldrich

Table 9: TaqMan™ primer-probe

Name	Forward primer	Reverse primer	Probe	Reporter Dye
CMV	CCAAGTAC GCCCCCTA TTGAC	CTGCCAAGT AG- GAAAGTCCC ATAAG	CCGCCTGG- CATTATG	FAM
GFP	GAGCG- CAC- CATCTTCTT CAAG	TGTCGCCCT CGAACTTCA C	ACGACGG- CAACTACA	FAM
FLUC	GAG- GAGCCTTC AGGAT- TACAA- GATT	GCTTTT- GGCGAA- GAAGGA- GAATAG	CAGCAGCG- CACTTTG	FAM
Human RNA polymerase II subunit A	Hs00172187_m1			FAM

All TaqMan™ primer-probe oligos were purchased from Thermo Fisher Scientific Waltham, MA, USA.

Table 10: Plasmids

Construct number	Name	Application
#472	pHelper	rAAV production
#652	pFB_scAAV2_CMV_GFP	
#2242	pAAV-rAAV-2E3.v2	
#2243	pAAV-rAAV-2E3.v3	
#2244	pAAV-rAAV-2E3.v4	
#2245	pAAV-rAAV-2E3.v5	
#2246	pAAV-rAAV-2E3.v6	
#R177	pAAV-CMV-Fluc	
K1263	anti-DIG-hum_VK	Antibody production
K1931	MO33-lambda_pcDNA3	
K1942	MO36-kappa_pcDNA3	
K2279	anti-DIG-hum_VK_WO2011003780_Seq_5#pcDNA3	
K2355	chi_2E3_VH_huIgG1_pOptivec	
K2356	chi_2E3_VL_hukappa_pcDNA3	
K3332	Chi2E3-huIgGI-KO-knob_pOptivec	
K3335	MO33-huIgGI-KO-hole_pOptivec	
K3337	MO36-huIgGI-KO-hole_pOptivec	
K3339	PD-L1-huIgGI-KO-hole_pOptivec	
K3341	Dig-huIgGI-KO-hole_pOptivec	
K3342	PD-L1-LC lambda	

Table 11: Cell lines and culture medium compositions

Cell line	Provider	Medium	Supplements
4T1	ATCC, Manassas, VA, USA® CRL-2539™	Gibco™ RPMI 1640	10.0% Gibco™ Fetal Bovine Serum
B16-F10	ATCC, Manassas, VA, USA® CRL-6475™	Gibco™ DMEM, high glucose, GlutaMAX™ Supplement	10.0% Gibco™ Fetal Bovine Serum
bEND.3	ATCC, Manassas, VA, USA® CRL-2299™	Gibco™ DMEM, high glucose, GlutaMAX™ Supplement	10.0% Gibco™ Fetal Bovine Serum
CT26-CL25	ATCC, Manassas, VA, USA® CRL-2638™	Gibco™ RPMI 1640	10.0% HyClone™ Fetal Bovine Serum 400.0 µg/mL Gibco™ Geneticin 1×Gibco™ MEM NEAA (100×)
FL8-3B	ATCC, Manassas, VA, USA® CRL-2390™	Gibco™ Ham's F-12 Nutrient Mix	10.0 % Gibco™ Fetal Bovine Serum
HEK 293	Invitrogen™, Carlsbad, CA, USA	Gibco™ DMEM, high glucose, GlutaMAX™ Supplement	10.0 % Gibco™ Fetal Bovine Serum
HEK 293H	Invitrogen™, Carlsbad, CA, USA	Gibco™ DMEM, high glucose, GlutaMAX™ Supplement	10.0 % Gibco™ Fetal Bovine Serum

HEK 293-E6	National Research Council (NRC) of Canada	Gibco™ F17 Expression Medium	1× Gibco™ GlutaMAX™ Supplement 0.1× Gibco™ Pluronic™ F-68 Non-ionic Surfactant (100×) 0.25 µg/mL Gibco™ Geneticin
HT1080	ATCC, Manassas, VA, USA® CCL-121™	Gibco™ RPMI 1640	10.0 % Gibco™ Fetal Bovine Serum
HT1080 huFAP/muFAP	(Park et al. 1999)	Gibco™ RPMI 1640	10.0 % Gibco™ Fetal Bovine Serum 1× Gibco™ MEM NEAA (100×) 300 µg/mL Gibco™ Geneticin
MC-38	NIH/NCI	DMEM + High Glucose	10.0% FBS 1× Sodium Pyruvate 1× MEM NEEA 5.0 mL 1M HEPES 1× GlutaMAX-I 500 µg/mL Gibco™ Geneticin
NIH3T3	ATCC, Manassas, VA, USA® CL-173™	Gibco™ DMEM, high glucose, GlutaMAX™ Supplement	10.0 % Gibco™ Fetal Bovine Serum

Renca	ATCC, Manassas, VA, USA® CRL-2947™	Gibco™ RPMI 1640	10.0% Gibco™ Fetal Bovine Serum 1× Gibco™ MEM NEAA (100×) 1.0 mM Sodium Pyruvate
Tramp C2	ATCC, Manassas, VA, USA® CRL-2731™	Gibco™ DMEM, high glucose, GlutaMAX™ Supplement	5.0% Gibco™ Fetal Bovine Serum 5.0% Nu-Serum™ I/IV 10.0 nM Dehydroisoandrosterone 0.005 mg/mL Insulin solution from bovine pancreas

Table 12: Software and online tools

Software	Manufacturer	Application
FlowJo 10.7.1	FlowJo, LLC, Ashland, OR, USA	Flow cytometry analysis
GraphPad Prism 9.0	GraphPad Software, San Diego, CA, USA	Statistics
Incucyte®2019B Rev2	Sartorius, Göttingen, Germany	Antibody internalization
Living Image software version 4.7.3	PerkinElmer®, Waltham, MA, USA	IVIS
Microsoft Office Suite 2016	Microsoft, Redmond, WA, USA	Text, Tables, Calculations
QuantStudio™ Real Time-PCR Software v1.3	Thermo Fisher Scientific Waltham, MA, USA	qPCR
ZEN slidescan software	Zeiss SMT, Oberkochen, Germany	Microscopy

2.2 Molecular Methods

2.2.1 Plasmids

An overview of all plasmids is provided in Table 10. All plasmids were validated by sequencing (Eurofins Genomics Europe Sequencing GmbH, Konstanz, Germany).

AAV expression constructs

AAV expression plasmids contain a CMV promoter followed by a Kozak sequence, a reporter gene (GFP or Fireflyluciferase), and an SV40 polyA signal. This expression sequence is flanked by AAV2 ITRs. Depending on the used ITR sequence, self-complementary (pFBsc-CMV-eGFP) or single-stranded (pAAV-CMV-Fluc) viral genomes were produced (Kuklik et al. 2021).

AAV capsid constructs

Different variations of the PCKS9 epitope ITPPRYRADE were used to modify the AAV2 cap gene (Table 30). Those sequences were synthesized by GeneArt (Thermo Fisher Scientific Waltham, MA, USA) and cloned into a plasmid AAV helper construct p-AAV-RC (Agilent Technologies, Santa Clara, CA, USA) via restriction digestion, ligation, and cloning in DH5 α cells (Kuklik et al. 2021).

Antibody constructs

The 2E3-antibody sequence was described by (Schiele 2013), anti-FAP antibodies MO33 and MO36 were described by (Brocks et al. 2001), the anti-PD-L1 (avelumab) sequence was accessible from DrugBank (DrugBank Accession Number: DB11945, <https://go.drugbank.com>), the anti-digoxigenin antibody sequence was described previously (Bramlage et al. 2009). Sequences were synthesized by GeneArt (Thermo Fisher Scientific Waltham, MA, USA) and cloned into their respective vectors by restriction digestion, ligation, and cloning in chemically competent *E.coli* DH5 α cells (Thermo Fisher Scientific Waltham, MA, USA). All heavy chain antibody sequences contain a CMV promoter followed by a Kozak sequence and signal sequences was cloned into the backbone of a human IgG antibody of a pOptivec vector. Light chain sequences are designed accordingly and cloned into a pcDNA3 vector.

Knob-into-hole antibodies contain Fc- mutations K409R (knob) and F405L (hole) as described in (Labrijn et al. 2013) and further knock-out mutations L234A and L235A to decrease effector functions through the Fc region (Wang et al. 2018, Kuklik et al. 2021).

2.2.2 Mesoscale Discovery ELISA

MSD is a highly sensitive variant of ELISA, that detects protein samples via SULFO-TAG labeled antibodies, which emit light after electrochemical stimulation (Eklund et al., 2017; Poorbaugh et al., 2018). The method was used to analyze the interaction of antibodies with immobilized AAV particles. All required MSD buffers are listed in Table 13. The viral variants were diluted in 1× PBS and were immobilized on an MSD standard plate with a concentration of 5×10^8 VG/well at 4°C overnight. The plate was washed three times with 300 μ L/well wash buffer and then blocked with 150 μ L/well blocking solution A for 1 h at RT, followed by three washing steps. The first antibody was diluted in detection reagent in the desired dilution (Table 14) and 25 μ L/well were added to each well. The secondary antibody was diluted in detection reagent (25 μ L/well) following incubation with 150 μ L/well with 2× read buffer. The electrochemical signal was directly measured using the SECTOR® Imager 6000 (MSD® Rockville, MD, USA). The original data were analyzed by subtraction of the background signal from the sample signal followed by normalization to control signals (Kuklik et al. 2021).

Table 13: Buffers used for ELISA

Buffer name	Composition
Wash buffer	Gibco™ PBS 1× 0.05% Tween 20
Blocking solution	Gibco™ PBS 1× 3% Blocker A
Detection reagent	Gibco™ PBS 1× 1% Blocker A
Read Buffer	1:2 dilution MSD Read Buffer (4×) in ddH ₂ O

Table 14: Antibodies used for ELISA assays

Antibody type	Antibody name	Dilutions range
Primary	Anti-AAV2 A20	1:200
	Anti-Digoxigenin IgG	
	KiH-2E3-Digoxigenin	
	Anti-2E3 IgG	1:1000
	KiH-2E3-MO33	1:10,0000
	KiH-2E3-MO36	1:100,0000
	KiH-2E3-PD-L1	
Secondary	Anti Mouse Antibody Goat SULFO-TAG Labeled	1:1000
	Anti Human Antibody Goat SULFO-TAG Labeled	

2.2.3 Western Blot

AAV particles (1×10^{10} VG per lane) were reduced in 10 μ L ddH₂O containing 1 \times NuPAGE™ Sample Reducing Agent (Invitrogen™, Carlsbad, CA, USA) and 1 \times Pierce™ LDS Sample Buffer, Non-Reducing (Thermo Fisher Scientific Waltham, MA, USA) for 5 min at 95°C. Samples were applied to a NuPAGE Bis-Tris Gel (Thermo Fisher Scientific Waltham, MA, USA) in 1 \times NuPAGE™ MES SDS Running Buffer (Thermo Fisher Scientific Waltham, MA, USA). The gel run was performed for 1 h at 120 V. Separated proteins were blotted to a membrane using the iBlot 2 Dry Blotting System (Invitrogen™, Carlsbad, CA, USA) and iBlot™ 2 Transfer Stacks (Invitrogen™, Carlsbad, CA, USA). Membrane blocking was performed using 5.0 % skim milk in PBS-T (0.1% Tween in PBS) for 1 h at RT following one washing step. The membrane was incubated with primary antibody (B1 monoclonal mouse anti VP1, VP2, VP3, Progen, Heidelberg, Germany) diluted 1:250 or anti-2E3 IgG1 human diluted 1:250 in 1.0% skim milk PBS-T for 1 h at RT. To detect B1, the secondary antibody goat anti-mouse IgG1 (H+L) HRP (Invitrogen™, Carlsbad, CA, USA) was used diluted 1:1000 and to detect anti-2E3 IgG the secondary antibody Goat anti-Human IgG F(ab')₂:HRP (Bio-Rad, Hercules, CA, USA) was used in 1.0% skim milk PBS-T for 1

h at RT. The SuperSignal™ West Pico PLUS Chemiluminescent Substrate (Thermo Scientific™) was used to detect chemiluminescent signals using the Image Quant LAS 4000 device (Cytiva, Marlborough, MA, USA) (Kuklik et al. 2021).

2.2.4 AAV heparin column binding assay

The ability of AAV2 and rAAV-2E3 viral capsids to interact with Heparin-Agarose (Sigma-Aldrich, St. Louis, MO, USA) was analyzed by using an adapted protocol of (Opie et al. 2003). Micro Bio-Spin® Columns (Bio-Rad, Hercules, CA, USA) were blocked with 100% FCS overnight at 4°C, packaged with 500 µL Heparin-Agarose each and were washed with AAV buffer (1× PBS, 1 mM MgCl₂, 2.5 mM KCl, 10% Glycerol, 0.001% Pluronic, pH 7.4) thrice. Viral particles (5×10^{10} VG) were diluted in 600 µL AAV buffer, of which 100 µL were stored as ‘Load’ and 500 µL were loaded to prepared closed columns following 15 min incubation at RT. Closure tips were removed and columns spun down for 1 min at RT for 1200 rpm. The flow-through was collected in 2 mL tubes. Columns were washed 5 times with AAV buffer and viral capsids were eluted in two steps using AAV buffer supplemented with 1M NaCl. Each fraction was collected in fresh 2 mL tubes. Viral DNA from all fractions was extracted using the ViralXpress™ Nucleic Acid Extraction Kit (Merck Millipore, Burlington, MA, USA) according to the manufacturer’s instructions. Viral genomes within each fraction were analyzed by ddPCR using a CMV primer/probe set (Table 9) according to the protocol described in chapter 2.3.4. The measured viral genomes were normalized according to the total load of VG (Kuklik et al. 2021).

2.2.5 qPCR

qPCR analysis was performed of frozen cell pellets derived from the internalization kinetic assay described in chapter 2.5.3. The AllPrep DNA/RNA 96 Kit (Qiagen, Hilden, Germany) was used to extract DNA and RNA from cell pellets according to the manufacturer’s instructions. All primer-probe sets used for qPCR are shown in Table 9. The qPCR mix was prepared in 96-well plates using the QuantiFast Probe PCR Kit (Qiagen, Hilden, Germany) for either gDNA or cDNA analysis as described below (Table 15 and Table 16). The mix was transferred in triplicates to a MicroAmp™ EnduraPlate™ Optical 384-Well Clear Reaction Plate (Thermo Fisher Scientific Waltham, MA, USA) and was sealed with a MicroAmp™ Optical Adhesive Film (Thermo Fisher Scientific Waltham, MA, USA). Fluorescence amplified signals were analyzed using the QuantStudio™ 6 Flex Real-Time PCR System

(Thermo Fisher Scientific Waltham, MA, USA) with cycling conditions as indicated in Table 17. Data analysis was done using QuantStudio™ Real Time-PCR Software v1.3 (Thermo Fisher Scientific Waltham, MA, USA).

Analysis of mRNA expression levels

The concentration of mRNA was measured using Biochrom™ NanoVue Plus (Thermo Fisher Scientific Waltham, MA, USA) and 800 ng of each sample were transcribed into cDNA using SuperScript™ IV VILO™ Master Mix with ezDNase™ Enzyme (Thermo Fisher Scientific Waltham, MA, USA). cDNA data were normalized to housekeeping gene expression of human RNA polymerase II subunit A (delta ct). The sample showing the highest viral mRNA expression was used as a reference sample to calculate delta delta ct values. Finally, the relative fold gene expression delta delta ct was calculated by two to the power of negative delta delta ct.

Table 15: cDNA qPCR reagent mixture for one well of a 96-well plate

Reagent	Volume
Nuclease-free H ₂ O	10.0 µL
2× QuantiFast Probe PCR Master Mix	20.0 µL
20× Primer-Probe-Mix	2.0 µL
Template cDNA	8.0 µl

Analysis of gDNA levels

gDNA samples were compared to a standard dilution of the AAV transfer plasmid (pFB_scAAV2_CMV_GFP or pAAV-CMV-Fluc with 1×10^9 - 1.28×10^4 copies per 384-well). The master mix was prepared as indicated in Table 16. The total amount of gDNA copies was calculated from the signal of the standard dilution of the corresponding plasmid.

Table 16: gDNA qPCR reagent mixture for one well of a 96-well plate

Reagent	Volume
Nuclease-free H ₂ O	2.0 μ L
2 \times QuantiFast Probe PCR Master Mix	20.0 μ L
20 \times Primer-Probe-Mix	2.0 μ L
Template gDNA or standard plasmid	16.0 μ L

Table 17: qPCR cycling protocol

Step	Time [s]	Temperature [°C]	cycles
PCR initial activation step	180	95	0
Denaturation	3	95	35
Annealing and extension	130	60	

2.3 Production and quality control of rAAVs

The production and quality control of rAAVs was performed with the kind support of Dr. Thorsten Lamla and Dr. Benjamin Strobel of the Drug Discovery Sciences Department at Boehringer Ingelheim KG.

2.3.1 Production and harvest of rAAV vectors

AAVs were produced in HEK-293H cells. HEK cells were developed by transformation with sheared adenovirus type 5 DNA (Graham et al.1977), that provide E1 in *trans*. Frozen HEK-293H cells (60 \times 10⁶ cells/vial) (Thermo Fisher Scientific Waltham, MA, USA) were instantly seeded in a 16-layer CELLdisc™ (Greiner Bio-One GmbH, Frickenhausen Germany) containing 1.0 L respective culture medium (Table 11). Cells were transfected using calcium chloride 72 h after seeding. A three-plasmid-based production protocol (AAV helper free system; Agilent Technologies, Santa Clara, CA, USA) was used comprising of the plasmids pHelper, pAAV-recombinant vector, and a cargo plasmid. Plasmid DNA (690 μ g each) was mixed with calcium chloride (mixture A), added dropwise to 2 \times HBS (Thermo Fisher Scientific Waltham, MA, USA) (mixture B). Mix B was incubated for 20 min at RT and added to 1.0 L of pre-warmed transfection medium (Gibco™ DMEM, high glucose, GlutaMAX™ Supplement supplemented with 5% Gibco™ Fetal Bovine Serum). The cell culture medium was removed from cells and replaced with the transfection medium. After 5 h the transfection

medium was removed, and cells were cultured in a medium containing 5% FBS for three days.

Cells were harvested by removing 500 mL of cell culture medium and supplementation of the remaining medium with 7.0 mL EDTA 0.5 M (Invitrogen™, Carlsbad, CA, USA) until cells detached. Cells were collected and spun down for 15 min at 4°C at 800×g. rAAVs were extracted using lysis buffer according to Table 18 with freshly added HALT™ Protease Inhibitor Cocktail (Thermo Fisher Scientific Waltham, MA, USA). Cells were lysed by three freeze/thaw cycles in liquid nitrogen and 37°C water bath iterations following PEG precipitation of rAAVs.

Table 18: rAAV extraction lysis buffer

Component	Concentration
Tris	50.0 mM
Sodium chloride	1.0 M
Magnesium chloride	10.0 mM
Pluronic	0.001%
adjust pH to 8.5	
HALT™ Protease Inhibitor Cocktail	1:100

2.3.2 rAAV PEG precipitation

Cell lysates were treated with salt active nuclease (SERVA Electrophoresis GmbH, Heidelberg, Germany) for 1 h at 37°C at 100 rpm to remove cellular and plasmid DNA. The tubes were spun down at 2,500×g for 15 min at RT and the supernatant was transferred into fresh falcon tubes. The harvested supernatant was supplemented with ¼ volume PEG-8000 medium (Table 19) and incubated for 3 h on ice following centrifugation for 30 min at 4°C at 2,500×g. The supernatant was carefully removed. The pellet was resuspended in 14.5 mL resuspension buffer (Table 20) for at least 16 h at 4°C at 25 rpm following iodixanol purification.

Table 19: PEG-8000 medium

Components	Concentration
PEG	40%
NaCl	800 mM
Pluronic	0.0001%
Diluted in ddH ₂ O	

Table 20: rAAV resuspension buffer

Component	Concentration
Tris	50 mM
NaCl	1.0 M
Pluronic	0.001%
Diluted in ddH ₂ O	

2.3.3 rAAV iodixanol purification

To purify rAAV from proteins, DNA, and empty capsids, iodixanol gradient ultracentrifugation was performed. Four solutions with decreasing iodixanol concentrations (54%, 40%, 25%, and 15%) were prepared according to Table 21. Resuspended rAAVs were transferred into Quick-Seal tubes (Beckman Coulter Life Sciences Division Headquarters, Indianapolis, IN, USA) and sub layered with 9.0 mL 15% iodixanol solution, 6.0 mL 25% iodixanol solution, 5.0 mL 40% iodixanol solution, and 5.0 mL 50% iodixanol solution. Tubes are sealed and ultracentrifugation was performed for 1.15 h at 69,100 rpm using Sorvall Discovery 90SE (Thermo Fisher Scientific Waltham, MA, USA) in a fixed angle rotor Type 70 Ti (Beckman Coulter Life Sciences Division Headquarters, Indianapolis, IN, USA). Fractioning of rAAVs was performed by punctation of the bottom of the tube. The first 4 mL of the lowest layer was discarded and the following 3.5 mL were collected. Buffer exchange of this fraction was performed using Amicon Ultra-15 100 kDa tubes (Sigma-Aldrich, St. Louis, MO, USA-Aldrich) that were centrifugated at 1000×g in iterations and constant refill with storage buffer (Table 22). Finally, rAAVs were concentrated to 2 mL volume and sterile filtered. rAAVs are stored at -80°C.

Table 21: Iodixanol solutions

Component	54% Iodixanol solution	40% Iodixanol solution	25% Iodixanol solution	15% Iodixanol solution
60% Iodixanol in ddH₂O	500 mL	480 mL	480 mL	500 mL
10× PBS	48.26 mL	48.0 mL	48.0 mL	50.0 mL
1000 mM MgCl₂	0.50 mL	0.48 mL	0.48 mL	0.50 mL
1000 mM KCl	1.25 mL	1.19 mL	1.19 mL	1.25 mL
NaCl	-	-	-	1M
10% Pluronic	0.05 mL	0.048 mL	0.048 mL	0.05 mL
ddH₂O	-	Add to 480 mL	Add to 480 mL	Add to 500 mL

Table 22: rAAV storage buffer

Component	Concentration
10× PBS	1×
MgCl ₂	1.0 mM
KCl	2.5 mM
Glycerol	10%
Pluronic	0.001%

2.3.4 ddPCR

The ddPCR technique allows the measurement of the smallest amounts of DNA concentrations without a standard (Hindson et al. 2011). Viral genomes were purified using the ViralXpress™ Nucleic Acid Extraction Kit (Merck Millipore, Burlington, MA, USA) according to the manufacturer's instructions. The samples were diluted in DEPC-treated water ranging from 1:10⁴ up to 1:10¹¹ VG/mL in a 96-well plate. Viral genomes were mixed with 1× ddPCR™ Supermix for Probes (Bio-Rad, Hercules, CA, USA) and 1× Primer-Probe-Mix for detection of CMV sequences according to Table 23. The QXDx AutoDG ddPCR

System (Bio-Rad, Hercules, CA, USA) was used to create droplets in a 96-well plate that was sealed with pierceable PCR plate heat foil by using PX1™ PCR Plate Sealer (Bio-Rad, Hercules, CA, USA). The sealed plate was transferred into the Mastercycler® X50 (Eppendorf, Hamburg, Germany) and a PCR was performed according to (Table 24). The droplets were analyzed for positive fluorescence signals using the QX200™ droplet reader (Bio-Rad, Hercules, CA, USA) (Kuklik et al. 2021).

Table 23: Composition of ddPCR master mix for a 96-well plate

Master mix	Volume
2x ddPCR™ Supermix for Probes (No dUTP)	10.0 µL
20x Primer-Probe-Mix	1.0 µL
Template DNA	9.0 µL
Total volume	20.0 µL

Table 24: ddPCR program

Step	Temperature	Time
1	95°C	10:00 min
2	95°C	00:30 min
3	60°C	01:00 min
4	98°C	10:00 min
5	10°C	hold

2.3.5 AAV2 Titration ELISA

The AAV2 Titration ELISA (Progen, Heidelberg, Germany) was used to quantify assembled AAV2 capsids according to the manufacturer's instructions. After inhibition of the substrate reaction, absorbance was measured by Infinite® M200 PRO Multimode Microplate Reader (Tecan Group Ltd, Männedorf, Switzerland).

2.3.6 Electron microscopy

Negative staining of rAAV capsids and electron microscopy was performed in the laboratory of Dr. Colbatzky the department of Development NCE NDS. Virus suspensions (10.0 μ L) were incubated on a pre-cleaned grid for 60 s and residual fluid was removed by filter paper. Immobilized rAAVs were negatively stained by incubation with 10 μ L of 2% phosphotungstic acid (Sigma-Aldrich, St. Louis, MO, USA) in ddH₂O (pH 7.0) for 60 s. Samples were analyzed using the transmission electron microscope EM 912 (Zeiss SMT, Oberkochen, Germany) (Kuklik et al. 2021).

2.4 Production and Quality control of bispecific antibodies

2.4.1 Antibody production

HEK 293-6E suspension cells, licensed from the National Research Council (NRC) of Canada and described previously (Durocher et al. 2002), were incubated at 37°C and 5.0% CO₂ at 120 rpm. The culture was passaged every three days to 0.2 $\times 10^6$ cells/mL in a 250 mL culture medium (Table 11) in a 1.0 L Erlenmeyer cell culture flask (Thermo Fisher Scientific Waltham, MA, USA). One day before transfection, HEK 293-E6 cells were passaged to a concentration of 0.45 $\times 10^6$ viable cells/mL in their respective medium without geneticin. Transient transfection of cells was performed with 293fectin™ Transfection Reagent (Thermo Fisher Scientific Waltham, MA, USA) according to Table 25. Per 1.0 mL volume of cell culture, 1.0 μ g of DNA and 1.0 μ L of 293fectin™ were used. Mixture A was produced containing DNA and Opti-MEM™ (Thermo Fisher Scientific Waltham, MA, USA) and mixture B containing 293fectin™ and Opti-MEM™. A and B were gently mixed resulting in mix C that was incubated at RT for 20 min before being added into the culture flask. After 24 h cells were fed with 40% Tryptone N1 resulting in 1% final concentration and were cultured for 4 days or until cellular viability dropped below 50%. Knob-into-holes antibodies were produced as ‘half antibodies’ in separated flasks containing only heavy and respective light chains (Kuklik et al. 2021).

Table 25: transient transfection of 1.0 L HEK293E6 via 293fectin™

Mixture A	Mixture B	Mixture C
1000 μ g DNA 54.0 mL Opti-MEM™	1000 μ L 293fectin™ 54.0 mL Opti-MEM™	A mix of A and B incubated for 20 min at RT

2.4.2 Antibody purification via MabSelect™ SuRe

IgG antibodies are bound by protein A via the C_H2-C_H3 domain (Deisenhofer 1981, Graille et al. 2000). This interaction is used to purify antibodies with protein A coupled beads. The purification of antibodies was performed via Äkta Avant™ 25 (Cytiva, Marlborough, MA, USA) and HiTrap™ MabSelect™ SuRe 5.0 mL (Cytiva, Marlborough, MA, USA). Antibody-producing cells were spun down and discarded. The antibody-containing supernatant was sterile filtered and directly used for antibody purification. The column was washed with 1 × PBS, followed by the load of the cellular supernatant. Subsequently, antibodies were eluted with 0.1 M Glycine buffer in ddH₂O (pH 3.0). Buffer neutralization was performed with 1/10 volume of neutralization buffer 1M Tris-HCl in ddH₂O (pH 9.0). Buffer exchange to 1 × PBS and concentration of antibodies was performed using Amicon® Ultra-30 Centrifugal Filter Units (30 kDa) (Sigma-Aldrich, St. Louis, MO, USA-Aldrich). The concentration of antibodies was measured via Biochrom™ NanoVue Plus (Thermo Fisher Scientific Waltham, MA, USA) and the quantity was verified via SDS PAGE (Kuklik et al. 2021).

2.4.3 Fab-arm exchange

Bispecific antibodies were produced according to (Labrijn et al. 2013). Mabselect purified knob and holes antibodies were incubated in equimolar amounts in 25 mM 2-MEA (Sigma-Aldrich, St. Louis, MO, USA) in PBS for 5 min at RT under rotation and following 5 h at 25°C without agitation. The buffer was exchanged via Amicon® Ultra-30 Centrifugal Filter Units (30 kDa) (Sigma-Aldrich, St. Louis, MO, USA-Aldrich) to the desired storage buffer (PBS). Bispecific antibodies were stored at 4°C overnight for reoxidation of disulfide bonds. The final antibody concentration was measured via Biochrom™ NanoVue Plus (Thermo Fisher Scientific Waltham, MA, USA) and the quantity was verified via SDS PAGE.

2.4.4 Cation exchange chromatography via Äkta Avant

Bispecific antibodies produced via Fab-arm exchange were purified via cation exchange chromatography. This step was performed to clear bispecific antibodies from unpaired knob and hole fragments. The cation exchange chromatography was performed in sodium acetate running buffer and elution was performed by a gradual increase of NaCl concentration (Table 26). KiH samples were buffer exchanged to running buffer, sterile filtered, and applied to the Hi Trap SP FF 1 mL column (Cytiva, Marlborough, MA, USA). Fractions were collected and single peaks were pooled. The pools were buffer exchanged to PBS. The protein

size and purity were analyzed by SDS-PAGE, the samples were sterile filtrated by centrifugation using Sterile Ultrafree-MC and CL Centrifugal Filter Units (Merck Millipore, Burlington, MA, USA) and the protein concentration was measured.

Table 26: Running and elution Buffer compositions for cation exchange chromatography

Buffer type	Buffer composition	Gradient
Running Buffer	50 mM Sodium acetate pH 5.0 with acetic acid ddH ₂ O sterile filtered	-
Elution Buffer	50 mM Sodiumacetate 1 M NaCl pH 5.0 with acetic acid ddH ₂ O sterile filtered	5% gradient 15 CV 5% step 8 CV 10% gradient 15 CV 10% step 8 CV 20% gradient 15 CV 20% step 8 CV 40% gradient 5 CV 100% step 5 CV

2.4.5 SDS-PAGE

The antibody (-fragments) were visualized and quantified by SDS PAGE and InstantBlue™ Protein Stain (Thermo Fisher Scientific, Waltham, MA, USA). 2.5 µg of each antibody production was prepared under reducing and non-reducing conditions and was analyzed by SDS-PAGE. Non-reduced samples were mixed with Pierce™ LDS Sample Buffer Non-Reducing (Thermo Fisher Scientific Waltham, MA, USA) and added to a 4-12% NuPAGE Bis-Tris Gel (Thermo Fisher Scientific Waltham, MA, USA). Reduced samples were mixed with Pierce™ LDS Sample Buffer Non-Reducing (Thermo Fisher Scientific Waltham, MA, USA) containing 1×NuPAGE™ Sample Reducing Agent (Invitrogen™, Carlsbad, CA, USA). Samples were boiled at 99°C for 5 min before being loading to the gel. The SeeBlue™ Plus 2 Pre-stained Protein Standard (Invitrogen™, Carlsbad, CA, USA) was used as a marker. The chamber was filled with 1× NuPAGE™ MES SDS Running Buffer (Thermo Fisher Scientific Waltham, MA, USA) diluted in H₂O. The gel was run at 200 V for 35 min,

removed from the plastic cartridge, and stained for 2 h with InstantBlue™ Protein Stain (Thermo Fisher Scientific, Waltham, MA, USA) followed by ddH₂O washing steps until residual staining solution was removed from the gel.

2.4.6 Size-exclusion chromatography via Äkta Avant

Bispecific antibodies were separated by size via SEC in PBS Buffer using Äkta Avant™ 25 (Cytiva, Marlborough, MA, USA) using the HiLoad® 26/600 Superdex® column (Cytiva, Marlborough, MA, USA). 150 kDa antibodies main fractions were collected, concentrated and quality controlled by SDS PAGE.

2.4.7 HPLC

The purity of antibody productions was analyzed by HPLC using the 1290 Infinity II LC System (Agilent Technologies, Santa Clara, CA, USA) and the AdvanceBio SEC 8300A (Agilent Technologies, Santa Clara, CA, USA). 1× PBS was used as running buffer at a flow rate of 0.7 mL/min for 4 CV. AdvanceBio SEC 300A Proteinstandard (Agilent Technologies, Santa Clara, CA, USA) was used at each HPLC run and Rituximab (Sigma-Aldrich, St. Louis, MO, USA-Aldrich) was used as a reference antibody. 30 µl per run of each sample was transferred into 0.5 snap ring vials (Sigma-Aldrich, St. Louis, MO, USA Aldrich). The vials were spun down carefully at 4,000 rpm for 5 min to remove air bubbles. The UV emission at 280 nm and light scattering 90° signal was measured.

2.4.8 Endotoxin test

Purified antibodies and AAVs were tested endotoxin-free using the PTS20 LAL Test Cartridges and the Endosafe -PTS™ system (Charles River, Wilmington, MA, USA) according to the manufacturer's manual. The endotoxin level should be < 5.0 EU/ml for cell culture experiments and < 1.0 EU/ml for animal experiments.

2.4.9 Octet bridging assay

The binding of the 2E3 target, as well as the FAP recombinant proteins by bispecific antibodies, was analyzed by biolayer-interferometry using Octet HTX (FortéBio, Fremont, CA, USA). Streptavidin Biosensor tips (Molecular Devices, LLC, San Jose, CA, USA) were hydrated in 1×PBS in a 96-Well plate 20 min before measurement. A tilted bottom TW384 Microplate (FortéBio, Fremont, CA, USA) was used to prepare samples with a concentration of 10.0 µg/mL in PBS at a total volume of 50.0 µL per well. The interferometry of protein

interaction was measured within repetitive steps of association and dissociation (Table 27). First, the biotin-2E3 peptide (Biotin-ITPPRYRADE, EMC Microcollections, Tübingen, Germany) was incubated with streptavidin tips. Second, peptide-labeled tips were incubated with bispecific antibodies. Finally, the protein complex was incubated with recombinant FAP (Enzo Biochem, Inc., Farmingdale, NY, USA). The binding of KiH-2E3-Digoxigenin was analyzed equivalently but in PBS buffer supplemented with 0.05% Tween 20 to reduce background signals and BSA-conjugated digoxigenin (Biozol, Eching, Germany) (Kuklik et al. 2021).

Table 27: Octet analysis of KIH bispecific antibody binding

Step	Sample	Detection	Time (s)
1	PBS	Baseline	60
2	Biotin-Peptide	Association	210
3	PBS	Dissociation	60
4	KiH-bispecific antibody	Association	120
5	PBS	Dissociation	60
6	Recombinant Protein	Association	120
7	PBS	Dissociation	60

2.5 Cell biology methods

2.5.1 Flow cytometry

Cell surface receptor expression was analyzed by antibody staining and flow cytometry analysis. 5.0×10^5 cells/stain were detached with Accutase (Invitrogen™, Carlsbad, CA, USA) and collected in a round-bottom 96-well plate in buffer (1× PBS and 1.0% FBS). Human Fc- receptors were blocked with 1.0% human FcR Blocking Reagent (Miltenyi Biotec, Bergisch Gladbach, Germany) in the buffer for 10 min on ice. Cells were washed three times in buffer after each antibody incubation. Cells were incubated with 0.5 µg primary antibody for 30 min on ice followed by incubation with 0.5 µg secondary antibody APC anti-human IgG Fc (BioLegend®, San Diego, CA, USA) for 30 min on ice. APC positive cells were analyzed by iQue® Screener PLUS (Sartorius, Göttingen, Germany) and FlowJo 10.7.1 software (FlowJo, LLC, Ashland, OR, USA). GFP expression of cells transduced with rAAVs was measured by the iQue® Screener PLUS (Sartorius, Göttingen, Germany) (Kuklik et al. 2021).

2.5.2 Antibody internalization assay

The internalization of antibodies upon cell line interaction was analyzed using the IncuCyte® FabFluor pH Red Antibody Labeling reagent (Sartorius, Göttingen, Germany) rehydrated with ddH₂O to 0.5 mg/mL. Antibodies (4 µg/mL) were mixed with labeling reagent in a ratio of 1:3 and incubated for 15 min at RT in the appropriate cell culture medium. Cells were seeded 4 h before assay starts at a density of 10,000 per well in a ViewPlate-96 Black (PerkinElmer®, Waltham, MA, USA®) in 50 µL appropriate cell culture medium per well. The cell culture medium was removed and replaced with a medium containing the labeled antibodies, followed directly by analysis with the IncuCyte® S3live-cell analysis system using the 10× objective in the channel “phase” and “red” every 15 min for 5 hours. The Incucyte®2019B Rev2 Software (Sartorius, Göttingen, Germany) was used for image analysis (Kuklik et al. 2021).

2.5.3 *In vitro* retargeting assay

Bispecific antibody-mediated rAAV-2E3 targeting was established *in vitro* using cells expressing FAP or PD-L1 (HT1080 (ATCC, Manassas, VA, USA), HT1080 huFAP and HT1080 muFAP (Park et al. 1999), HEK 293 (ATCC, Manassas, VA, USA) and HEK 293 huFAP. One day before transduction 5000 cells were plated into a ViewPlate-96 Black (PerkinElmer®, Waltham, MA, USA®). The bispecific antibody was diluted in serial 1/3 dilution steps starting with 15.0 ng/µL equally to 1.0 nMol/L in 15 µL Buffer (1×PBS, 1.0% FCS) per well. AAV particles were diluted (50,000 VG/cell, 15,000 VG/cell and 5000 VG/cell) in 15 µL Buffer (1×PBS, 1.0% FCS) per well. Antibody dilutions and AAV dilutions were mixed in a V-bottom 96-well plate, quickly spun down following incubation for 1 h at 37°C. 20.0 µL of pre-incubated AAV and antibody were transferred to each well of cells following incubation in a wet chamber for three days without medium change. Depending on packaged transgenes, GFP expression was measured by flow cytometry using the iQue® Screener PLUS (Sartorius, Göttingen, Germany) or firefly luciferase expression was measured using Infinite® M200 PRO Multimode Microplate Reader (Tecan Group Ltd, Männedorf, Switzerland).

After the *in vitro* retargeting mechanism was established, a simplified transduction protocol was used. Cells were plated at 5,000 cells/well in a ViewPlate-96 Black (PerkinElmer®, Waltham, MA, USA®). 10 nMol/L bispecific antibodies were diluted in 15.0 µL Buffer

(1×PBS, 1.0% FCS) for transduction of one 96-well. 50,000 AAV particles per cell were diluted in 15.0 µL Buffer (1×PBS, 1.0% FCS) per 96-well. Antibody- and AAV dilutions were mixed in a V-bottom 96-well plate quickly spun down following incubation for 1 h at 37°C. 20.0 µL of pre-incubated AAV and antibody were transferred to each well of cells following incubation in a wet chamber for three days without medium change (Kuklik et al 2021).

Retargeting kinetic

The *in vitro* retargeting kinetic of rAAV-2E3.v6 complexed with KiH-2E3-MO33, KiH-2E3-MO36, or isotype control in comparison to AAV2 was performed using HT1080 huFAP cells. Cells were plated at a density of 30,000 cells per well in a 24-well plate 24 h before transduction. The *in vitro* retargeting protocol was adapted according to the number of cells. Two wells were prepared for one-time point and qPCR analysis, while a third well was used for flow cytometry analysis of GFP expression at each time point. Cells were cooled down on ice for 1 h before transduction. The complex of rAAV-2E3.v6:KiH-2E3-MO36 or AAV2 was transferred to pre-cooled cells and incubated for 1 h, time point 0. After 1 h, 6 h, 24 h, 48 h, and 72 h samples were collected by removing the medium following three PBS washing steps. Cells were detached with TrypLE™ Express Enzyme (Gibco™) and transferred into reaction tubes. Two wells were pooled for qPCR analysis, cells were spun down, the supernatant was removed and the pellet was stored at -80°C for later analysis. The third well was used to measure the cell amount using Countess II FL Automated Cell Counter (Thermo Fisher Scientific Waltham, MA, USA) and GFP expression levels.

Competition assays

Competition of rAAV-2E3.v6:KiH-2E3-MO33 or rAAV-2E3.v6:KiH-2E3-MO36 receptor binding was performed using the human FAP binding antibody BIBH1 antibody (Boehringer Ingelheim Pharma KG, Biberach Riß, Germany). Soluble epitopes 2E3 (ITPPRYRADK-Biotin-Aca) and 2E3 mutant epitope (ITPPRARYDK-Biotin-Aca) (EMC microcollections GmbH, Tübingen, Germany) were used to compete with 2E3-epitope bispecific antibody binding. Heparin-sodium (Sigma-Aldrich, St. Louis, MO, USA-Aldrich) was used to compete with AAV capsid-HPSG interactions. Purified human intravenous immunoglobulins (Baxter Innovations GmbH) were used to analyze neutralizing effects of human anti-AAV antibodies. Competitors were diluted in PBS containing 1.0% FCS in 15 µL per 96-well.

AAV particles and bispecific antibody dilutions were prepared as described and the competitor was added. 30.0 μ L of the pre-incubation was added to the cells following incubation in a wet chamber for three days (Kuklik et al. 2021).

2.5.4 Firefly luciferase assay

Transduction of cells via AAV2 or rAAV-2E3.v6:KiH-2E3 was performed as described in chapter 2.5.3. Firefly luciferase expression was measured after 72 h using the Bright-Glo™ Luciferase Assay System (Promega, Madison, WI, USA) according to the manufacturer's instructions. To reduce background signals, supernatants of lysed cells were transferred into the white OptiPlate-96 (PerkinElmer®, Waltham, MA, USA) and the luminescence signal was measured using Infinite® M200 PRO Multimode Microplate Reader (Tecan Group Ltd, Männedorf, Switzerland).

2.6 *In vivo* methods and tissue analysis

2.6.1 Pharmacokinetic

Antibody pharmacokinetics was analyzed in the department of drug discovery sciences in the laboratory of Dr. Wolfgang Rist by Dr. Lars Dittus and Eva Griesser by LI-DDS- 9 and LI T3/ LI 22 / LI 6. Each antibody analysis was performed using a group of 4 female mice (C57BL/6NRj) with a dosing of 10 mg/kg sample by intravenous application. Blood was collected using a Minivette® POCT (Sarstedt, Inc., Newton, NA, USA) via punctation of the vena saphena at 10 time points after dosing (0.03; 0.5; 2.0; 8.0; 24.0; 48.0; 96.0; 192.0; 240.0; 336.0 h). Blood was sampled in K₂EDTA anticoagulant-treated tubes. Samples were centrifuged at 15,000 \times g at 4°C following plasma collection.

Antibody concentrations from plasma samples were determined using a semi-automated ligand binding assay platform Gyroslab® xPand (Gyros Protein Technologies AB, Uppsala, Sweden). The samples were diluted at 1:3000 in REXXIP AN buffer (Gyros Protein Technologies AB, Uppsala, Sweden). The analyte was immobilized on streptavidin-coated Cs Gyroslab Bioaffy 1000 (Gyros Protein Technologies AB, Uppsala, Sweden) using a biotin-tagged (EZ-Link™ Sulfo-NHS-LC-Biotin, Thermo Fisher Scientific Waltham, MA, USA) antibody raised against human IgG1 (Novus Biologicals, Littleton, CO, USA) (100 μ g/mL in PBS supplemented with 0.01% Tween 20) and recording the fluorescence of a fluorophore-labeled (Alexa Fluor™ 647 NHS Ester, Thermo Fisher Scientific Waltham, MA, USA) anti-human IgG1 antibody (SouthernBiotech, Birmingham, AL, USA) used at 20 nM

in Rexas F buffer (Gyros Protein Technologies AB, Uppsala, Sweden). Biotinylation and fluorophore-conjugation of the unlabeled antibodies were performed for 1 h at RT after mixing 1.67 μM antibody with 16.7 μM label reagent, and 0.1 M Sodium hydrogen carbonate (Sigma-Aldrich, St. Louis, MO, USA) all dissolved in PBS. The Gyroslab® xPand was operated using a manufacturer's method 1000-3W-001-A.

For quantification of the analytes, calibration curves were generated in a matrix collected from untreated animals. Matrix concentrations used for the calibration curves were adjusted according to the minimal required dilution of the samples (0.033% plasma). Response signals from unknown samples were matched against the calibration curves to derive the corresponding analyte concentration. The results were accepted as valid if assay internal spike-in QC recovery was $70\% < x < 130\%$ (assay run under non-GxP conditions). Concentrations in plasma were calculated by multiplying the results with the assay dilution factor.

2.6.2 Tumor xenograft model establishment

The cell lines HT1080 (no FAP expression) and Ht1080 huFAP were sent to Charles River, Discovery Research Services Germany GmbH, Tübingen, Germany), which established a tumor xenograft model using female NSG nude mice (*Crt1:NMRI-Foxn1nu*) at the age 5-7 weeks. Cells were expanded and tested pathogen-free. The model was established by injection of three different concentrations of cells per animal per group (1.0×10^6 ; 3.3×10^6 and 1.0×10^7 cells/animal). Cells were injected into the flank of each animal. Every group consisted of five animals. The body weight was recorded and tumor volume was measured by caliper every two to three days until day 42 or until tumors exceeded the volume of 2,000 mm^3 . At the end of the study, animals were sacrificed, two tumors were sampled of each group and Formalin-Fixed Paraffin-Embedded tissues were prepared according to Table 28. Fixed tissues were used for immunohistochemistry staining of FAP.

Table 28: Formalin-Fixed Paraffin-Embedded tissue protocol

Station	Solution	Time	Temperature
1	4% PFA	24 h	RT
2	70% Ethanol	30 s	35°C
3	70% Ethanol	30 s	35°C
4	80% Ethanol	60 s	35°C
5	80% Ethanol	60 s	35°C
6	100 % Ethanol	30 s	35°C
7	100 % Ethanol	30 s	35°C
8	Isopropanol	90 s	35°C
9	Xylol	60 s	35°C
10	Xylol	90 s	35°C
11	Paraffin	60 s	60°C
12	Paraffin	60 s	60°C
13	Paraffin	60 s	60°C
14	Paraffin	120 s	60°C

2.6.3 *In vivo* retargeting assay

The *in vivo* retargeting study has been performed at Charles River Discovery Research Services North Carolina, USA. Eight weeks old JAX female NSG mice (NOD.Cg-*Prkdc^{scid}* *Il2rg^{tm1Wjl}*/SzJ, The Jackson Laboratory) received a subcutaneous injection of 1.0×10^6 cells HT1080 huFAP into the right flank. Tumors were grown to an average size of 30 – 60 mm³ until the treatment was started. Animals were divided into four groups according to Table 29. Viral variants packaged with firefly luciferase and bispecific antibodies were produced in sufficient amounts, Endotoxin units were proven to be < 1 EU per injection, and viral variants, and antibodies were concentrated. Bispecific antibodies (0.18 mg/ animal) and viral variants (2.0×10^{12} VG/animal) were mixed and incubated at 37°C for one hour. 100 μ L of the mix was injected into the tail vein of animals. The ratios have been calculated based on *in vitro* transduction data.

The body weight, tumor volume, and luciferase expression were monitored twice every week until the study's end. *In vivo* bioluminescence imaging was performed on days 1, 4, 7, 10,

14, 18, and 19 on sedated animals in a light-tight chamber in an IVIS® SpectrumCT (PerkinElmer®, Waltham, MA, USA) with a sensitive CCD camera cooled at -90°C. Sterile-filtered VivoGlo™ D-Luciferin substrate (Promega, Madison, WI, USA) dissolved in PBS (150 mg/kg) was injected intraperitoneally. Mice were placed in an anesthesia induction chamber containing 2.5 - 3.5% isoflurane in oxygen and stage heating to maintain body temperature. 10 min after substrate injection dorsolateral images of animals were taken and the data were analyzed using Living Image software version 4.7.3 (PerkinElmer®, Waltham, MA, USA). The upper abdomen region was shaved from Groups 1 and 2 animals and both dorsolateral and ventral images were taken to capture the signal in the liver and tumor at high resolution at day 19. Total flux was quantified and reported as 10^6 photons per second. Mandibular blood (0.025 mL) was collected in group 1 and group 2 from all mice 0.5 h and 6 h after dosing on day 1. At the end of the study, blood was collected from all animals of groups 1 to 3. The blood samples were processed for plasma with the K₂EDTA anticoagulant, snap-frozen, and stored at -80 °C.

At the end of the study or detection of adverse reactions (>30% body weight loss, >25% body weight loss of three consecutive measurements or tumor size above 2000 mm²) animals were euthanized and organs (heart, liver, lung, and tumor) were harvested. Each organ was divided into three parts. Part one was fixed in 4% PFA, transferred in ethanol, and embedded in paraffin. The formalin-fixed paraffin-embedded tissues were analyzed for FAP expression and vascularization by immunohistochemistry. Organ parts two and three were collected in sampling tubes and snap-frozen in liquid nitrogen for qPCR and luminescence analysis.

Table 29: Grouping and dosing of HT1080 huFAP mouse xenograft models

Group	Number of animals	Bispecific antibody dosing per animal	Viral variant dosing per animal
1	6	KiH-2E3-MO36 (0.18 mg)	rAAV-2E3.v6 (2.0×10^{12} VG)
2	6	KiH-2E3-Digoxigenin (0.18 mg)	rAAV-2E3.v6 (2.0×10^{12} VG)
3	4	KiH-2E3-Digoxigenin (0.18 mg)	AAV2 (2.0×10^{12} VG)
4	4	No treatment	

2.6.4 Tissue homogenization for BCA and Luciferase assays

Murine tissues were lysed in CKMix-Tissue homogenizing tubes (Bertin Technologies, Montigny-le-Bretonneux, France) in 100 μ L MSD Tris Lysis Buffer (MSD® Rockville, MD, USA) supplemented with 1 \times Halt™ Protease Inhibitor Cocktail (Thermo Fisher Scientific Waltham, MA, USA) for 30 s at 6000 rpm using the Precellys Evolution Homogenizer (Bertin Technologies SAS, Montigny-le-Bretonneux, France), followed by addition of 900 μ L of fresh lysis buffer and a second homogenization step. Lysed tissues were incubated for 10 min on ice and centrifuged for 10 min at 4°C at 20,000 \times g. The supernatant was collected in fresh tubes and stored at -80°C.

2.6.5 BCA assay of tissue lysates

The protein concentration was measured using the Pierce™ BCA Protein Assay Kit (Thermo Fisher Scientific Waltham, MA, USA) according to the manufacturer's instructions. The absorbance was measured using Infinite® M200 PRO Multimode Microplate Reader (Tecan Group Ltd, Männedorf, Switzerland). Based on the BSA standard the protein concentration of the tissue lysates was calculated.

2.6.6 Luciferase assay of tissue lysates

Luciferase expression of lysed tissues was measured using the Luciferase Assay System (Promega, Madison, WI, USA). 10.0 μ L of cell lysate were transferred in triplicates in a white OptiPlate-384 (PerkinElmer®, Waltham, MA, USA®) mixed with 50 μ L of luciferase assay reagent and incubated for 5 min at RT. The luciferase signal was measured using Infinite® M200 PRO Multimode Microplate Reader (Tecan Group Ltd, Männedorf, Switzerland). The RLU per mg protein was calculated using the BCA assay data. Finally, RLU Background signals were subtracted from RLU per mg protein.

2.6.7 Tissue homogenization and DNA extraction

Snap frozen mice tissues were mixed with 900 μ L RLT buffer (Qiagen, Hilden, Germany) supplemented with 1.0% β -Mercapthoethanol (Sigma-Aldrich, St. Louis, MO, USA) and homogenized at 6000 rpm for 30 s using Precellys Evolution Homogenizer (Bertin Technologies SAS, Montigny-le-Bretonneux, France). Samples were centrifuged at maximal speed for three minutes. The supernatant was transferred into Phase Lock Gel™ tubes (Quanta Biosciences, Gaithersburg, MD, USA), mixed with 350 μ L Chloroform Isoamyl Alcohol (Sigma-Aldrich, St. Louis, MO, USA) and centrifuged at 16,000 \times g for 5 min. This step was

repeated with an additional 350 μ L Chloroform Isoamyl Alcohol (Sigma-Aldrich, St. Louis, MO, USA). The mix was incubated for 3 min at RT and centrifuged at 12,000 \times g for 5 min. The upper phase was collected in a deep well plate. DNA was extracted using the AllPrep 96 DNA/RNA Kit (Qiagen, Hilden, Germany) according to the manufacturer's instructions. The DNA concentration was measured by Biochrom™ NanoVue Plus (Thermo Fisher Scientific Waltham, MA, USA) and used for the qPCR analysis of AAV genomes as described in chapter 2.2.5.

2.6.8 Histochemistry and immunohistochemistry

Histochemistry and immunohistochemistry were performed in the group of Dr. Birgit Stierstorfer in the department of Target Discovery Sciences. Three-micron tissue sections of formalin-fixed paraffin-embedded tumor samples were de-waxed with xylene (Sigma-Aldrich, St. Louis, MO, USA-Aldrich), rehydrated in a graded ethanol series, and blocked with 3.0% hydrogen peroxide (Sigma-Aldrich, St. Louis, MO, USA-Aldrich). Slides were either stained with hematoxylin and eosin as previously described (Mulisch and Welsch 2015) or via immunohistochemistry. For this, antigen retrieval was performed for all primary antibodies by heating the sections in Tris-EDTA buffer (95°C; pH 9.0) for 20 min. Sections were incubated with the following primary antibody Recombinant Anti-Fibroblast activation protein (Abcam, Cambridge, UK) (1:200), Cleaved Caspase-3 Antibody (Cell signaling, Danvers, Massachusetts, USA) (1:200) or CD31 Polyclonal Antibody (Invitrogen™, Carlsbad, CA, USA) (1:50). Antibodies were diluted with Leica Biosystems Primary Antibody Diluent (Leica Biosystems, Wetzlar, Germany) and incubated for 1 h at room temperature. Bond Polymer Refine Detection (Leica Biosystems, Wetzlar, Germany) was used for detection (3,3' Diaminobenzidine as chromogen, DAB) and counterstaining (hematoxylin). Staining was performed on the automated Leica Biosystems IHC Bond-RX™ platform (Leica Biosystems, Wetzlar, Germany). Microscopy was conducted with a Zeiss SMT Axio Imager 2 microscope and images were created using an Axio Scan scanner and ZEN slidescan software (Zeiss SMT, Oberkochen, Germany).

2.7 Statistics

Statistical calculations were performed with GraphPad Prism software version 9.0 (GraphPad Software, San Diego, CA, USA). Data were presented as mean \pm standard deviation and statistical analysis was performed by either one-way ANOVA, Uncorrected Dunn's test, or Mann Whitney test. Data in Figure 8C are presented as mean \pm standard error of

mean and statistical analysis was performed by one-way ANOVA and Uncorrected Fisher's LSD. p -values are denoted as follows: * $p < 0.05$, ** $p < 0.01$, *** $p < 0.001$ and **** $p > 0.0001$; ns = non-significant (Kuklik et al. 2021).

3 Results

3.1 Design, production, and characterization of AAV2 capsid variants with novel epitope insertion domains

Novel AAV2 capsid variants were designed based on the PCSK9 derived epitope sequence ‘2E3’ to ablate natural transduction and concurrently insert a new epitope for antibody binding. A panel of ‘pure’ 2E3 sequences or extended with Gly-Ser linkers were inserted into AAV2 capsid sites crucial for HSPG - or integrin $\alpha 5\beta 1$ binding (Table 30, Figure 6). To modify the conserved NGR sequence (511-513, VP1 numbering) we substituted the near domain 491 to 501 or 510 – 514 with a 16 amino acid long GS-linker framed epitope 2E3, which resulted in the new viral variants rAAV-2E3.v2 and rAAV-2E3.v3. The positions R585 and R588 in loop VIII of VP3 were chosen for modification as these amino acids are on the one hand known as binding sites for HSPG and on the other hand has the loop been described to allow ligand insertions (Ponnazhagan et al. 2002; Xie et al. 2002; Gurda et al. 2013; Münch et al. 2015; Eichhoff et al. 2019). The loop was modified with 2E3 epitopes with GS-linker (rAAV-2E3.v4) and without GS-linker (rAAV-2E3.v5). The position 581 to 589 was substituted with GS-linker 2E3 (rAAV-2E3.v6). The five novel rAAV-2E3 capsid designs and AAV2 were produced in HEK 293-H cells packaged with a cargo plasmid that expressed GFP under the CMV promoter (Kuklik et al. 2021).

Table 30: Design of AAV2 capsid variants by 2E3 epitope insertion (Kuklik et al. 2021)

Modification and amino acid position	Original sequence/insertion	Novel rAAV
Sub 491-501-GS4	VSKT GGGG TPPRYRAD GGGG SWTG	rAAV-2E3.v2
Sub510-514-GS4	YHL GGGG TPPRYRAD GGGG DSL	rAAV-2E3.v3
Ins588-GS4	TNLQRGNR GGGG TPPRYRAD GGGG QAA	rAAV-2E3.v4
Ins588	TNLQRGNR GTPPRYRAD QAA	rAAV-2E3.v5
Sub581- 589-GS4	T GGGG ITPPRYRAD GGGG QAA	rAAV-2E3.v6

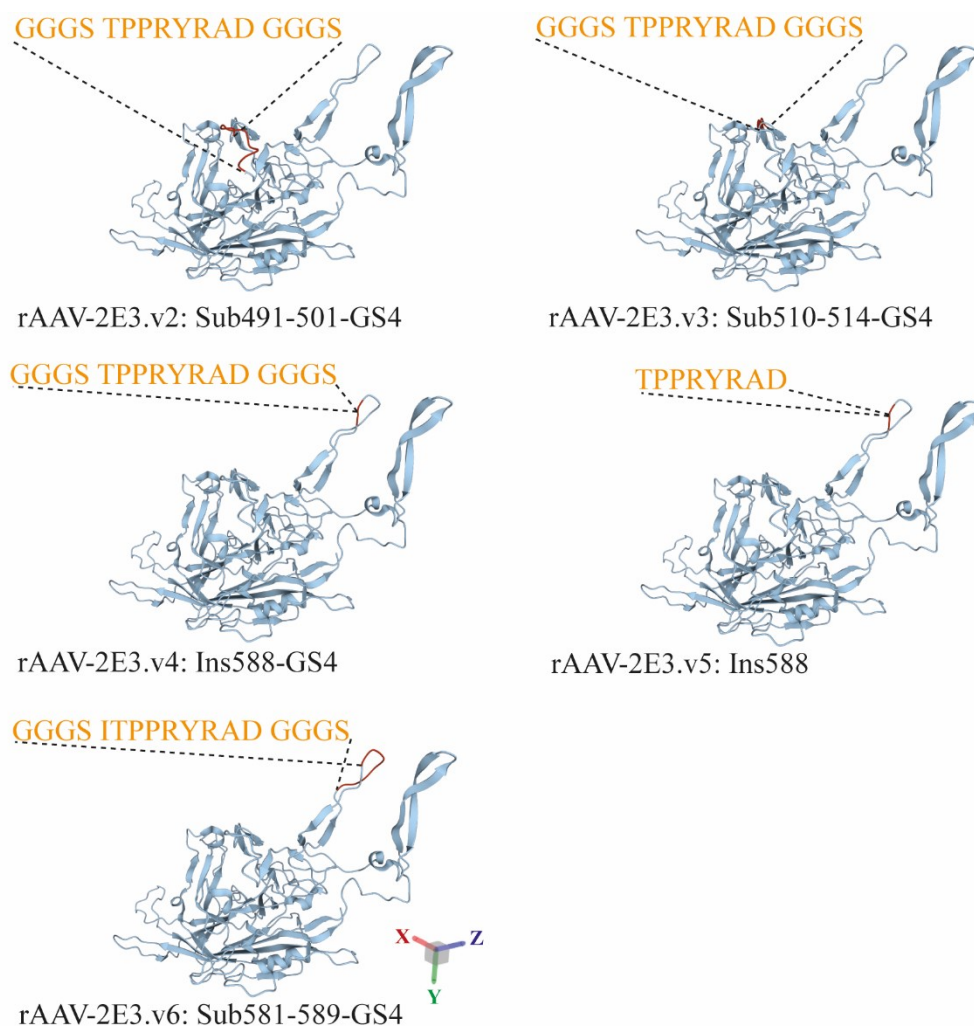


Figure 6: Ribbon drawing of the VP3 subunit with indicated capsid modifications (Kuklik et al. 2021). Five versions of VP3 capsid modifications (rAAV-2E3.v2; -v3; -v4; -v5 and -v6) were designed by insertions or substitutions with 2E3 epitope variants (orange) into the VP3 protein (blue). The site of capsid modification is indicated by dashed lines and modified sequence areas are shown in red. The name of the capsid modification and numbering of amino acid changes is written below. Sub = Substitution; Ins = Insertion; GS4 = 4×Gly-Ser linker. The VP3 ribbon structures (ID: 1LP3) are visualized and modified using the PDB tool (<https://rcsb.org>, access date 22.05.2021).

The packaging capacity (VG/mL) and vector yield (capsids/mL) after iodixanol purification of rAAV-2E3 viral variants and AAV2 were analyzed using ddPCR and ELISA (Figure 7A, B). All viral variants and AAV2 were produced in cell discs with an initial HEK-293H seeding density of 60×10^6 cells in 1.0 L volume. All AAVs were produced and purified in high titers (1.24×10^{12} to 4.98×10^{12} VG/mL) except for rAAV-2E3.v3 (2.25×10^{10} VG/mL) which was excluded from further analysis. The packaging capacity correlated with capsid yield although up to 8 × excess of capsids were observed. Electron microscopy of negatively

stained rAAV-2E3.v6 capsid variants were performed to visualize the capsid structure of a modified viral variant (Figure 7C). The typical icosahedral AAV capsid structure was unaltered in rAAV-2E3.v6 and mostly packaged viral particles were observed (Kuklik et al. 2021).

To prove 2E3 epitope insertion into AAV2 capsids, a western blot was conducted with anti-VP protein and anti-2E3 epitope binding antibodies. Anti-VP staining showed the typical pattern of VP1: VP2: VP3 proteins in the ratio of 1:1:10 of all analyzed AAV samples within a protein size of 90, 72, and 62 kDa. Anti-2E3 staining showed signals in all VP proteins except for the AAV2 batch, indicating that the epitope is presented 60× in the viral capsid (Figure 7D). rAAV-2E3 viral variants were immobilized on an MSD® standard plate and an ELISA assay was performed in comparison to AAV2 capsids to prove accessibility of 2E3 surface epitopes for anti-2E3 antibodies in a concentration dependent manner. A20 anti-VP protein staining was performed as a positive control, showing RLU signals of all rAAV viral variants (Figure 7E, F) (Kuklik et al. 2021).

Viral variant designs based on AAV2 could be produced but packaging capacity seemed to be influenced by capsid modification. Produced viral variants are detectable with widely known anti-VP protein antibodies (A20 and B1) (Wistuba et al. 1995, 1997; Grimm et al. 1999; Wobus et al. 2000) but can also be bound by anti-2E3 antibodies. Moreover, it was shown that modified viral variants show the expected ratio of viral capsid proteins VP1, VP2, and VP3 as well as the typical icosahedral capsid structure (Kuklik et al. 2021).

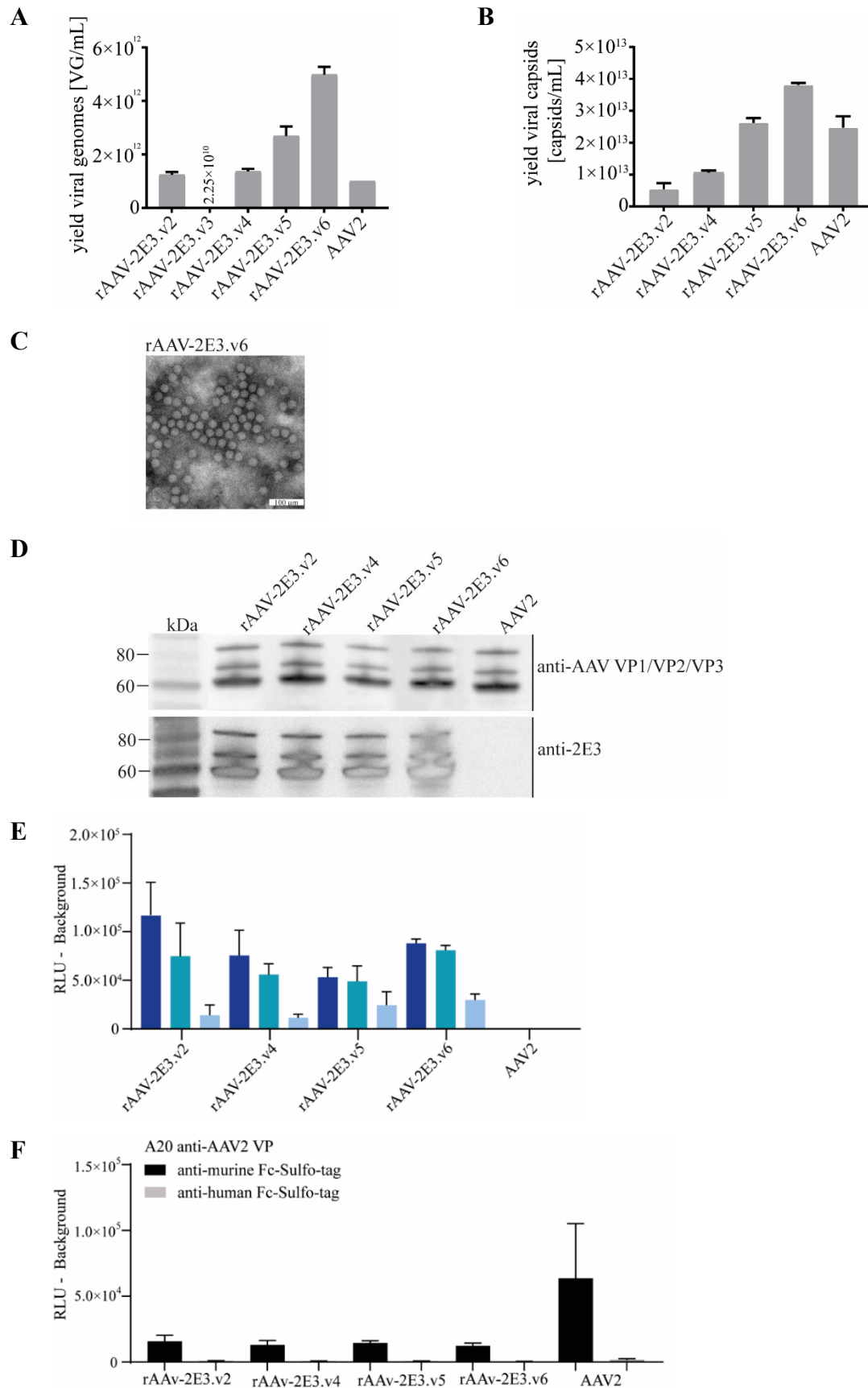


Figure 7: Characterization of novel rAAV-2E3 viral variants (Kuklik et al. 2021). **A)** ddPCR analysis of viral packaging based on the plasmid pFBsc-CMV-eGFP of rAAV-2E3.v2; -v3; -v4; v5; -v6 and AAV2. Experiments were performed in biological triplicates and presented as mean \pm SD. **B)** Titration ELISA assay of viral capsid yield of rAAV-2E3.v2; -v4; v5; -v6 and AAV2. Experiments were performed in biological triplicates of each batch and data are shown as mean \pm SD. **C)** Representative transmission electron microscopy of negative stained rAAV-2E3.v6 viral particles. Scalebar 100 μ m. **D)** Western blot of reduced rAAV-2E3 variants and AAV2. Detection of VP proteins (B1, Progen, Heidelberg, Germany) and 2E3 epitopes (anti-2E3 antibody). **E)** ELISA assay of immobilized rAAV-2E3 variants and AAV2 following incubation with anti-2E3 antibodies in serial dilutions 1: 1000 (dark blue); 1:10,000 (turquoise); 1:100,000 (light blue) and secondary antibody staining. **F)** Viral capsid immobilization control ELISA assay of rAAV-2E3 viral variants and AAV2 following detection of AAV2 VP proteins by an anti-human secondary antibody or anti-murine isotype control antibody. Data represent mean \pm SD of three independent experiments.

3.2 2E3 epitope viral capsid modifications influence transduction properties and HSPG binding compared to AAV2

The development of a specific retargeting mechanism requires the ablation of the natural AAV2 transduction properties. The transduction properties of novel rAAV-2E3 variants were tested on a wide panel of murine and human cell lines *in vitro*. Successful transduction was measured three days after incubation by flow cytometry and microscopy for GFP expression (Figure 8 A, B). AAV2 transduction at high VG/cell of 150,000 resulted in high proportions of GFP positive several cell lines (HEK 293, B16-F10, FL8-3B, and CT26-CL25). rAAV-2E3.v5 showed comparable proportions of GFP positive HEK 293, FL8-3B, and CT26-CL25 cells and low proportions of B16-F10, BEND.3, MC38, NIH3T3, and Renca GFP positive cells. The viral variant rAAV-2E3.v4 showed only high transduction of HEK 293 cells but overall low proportions of B16-F10, TrampC2, 4T1, BEND.3, MC38, NIH3T3, Renca, and CT26-CL25 GFP positive cells. Incubation of cells with the viral variants rAAV-2E3.v2 and rAAV-2E3.v6 resulted in very low proportions of GFP positive cells at background level. None of the capsid variants showed increased transduction properties (Kuklik et al. 2021).

Microscopy-derived data of HEK 293 cells incubated with the viral variants correspond with flow cytometry data. However, flow cytometry revealed fluorescence intensity differences of transduced cells. AAV2 transduction resulted in bright GFP signals while rAAV-2E3.v5

transduction resulted in 10× reduced GFP brightness. rAAV-2E3.v4 transduction decreased fluorescence brightness about 30×. Microscopy data confirms the absence of GFP signals after transduction with either rAAV-2E3.v2 or rAAV-2E3.v6 (Kuklik et al. 2021).

As AAV2 infection is initiated by capsid binding of HSPG on the cellular surface (Summerford and Samulski 1998), the interaction was mimicked with a heparin column *in vitro* (Opie et al. 2003; Zhang et al. 2013, 2019). About 2/3 of capsids of the positive control AAV2 bound heparin could be eluted with 2 M NaCl elution buffer. The variants rAAV-2E3.v2, -v4, and -v5 showed similar binding of heparin compared to AAV2. However, rAAV-2E3.v6 binding was significantly reduced (mean 83.5% ± 27.05, $p < 0.001$) as viral genomes could mainly be found in the flow-through and wash fractions of the column (Kuklik et al. 2021).

2E3 epitope insertions were able to ablate heparin-binding and negatively influence cell transduction *in vitro* depending on the modified capsid site (Figure 8C) (Kuklik et al. 2021).

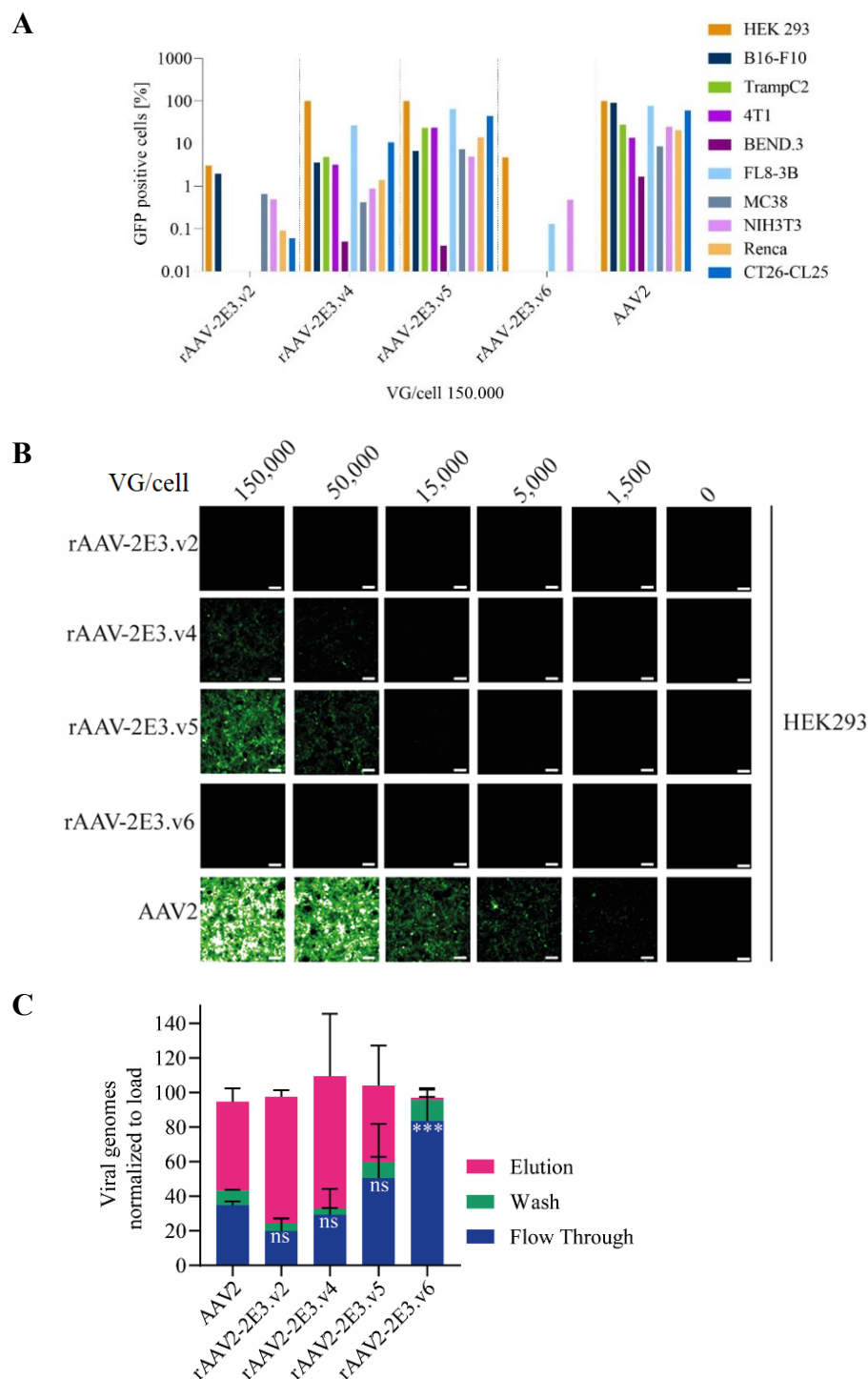


Figure 8: 2E3 epitope AAV2 capsid modification alters infectivity and heparin column binding compared to AAV2 (Kuklik et al. 2021) **A**) A panel of human and murine cell lines was screened for rAAV-2E.v2, -v4, -v5, -v6 and AAV2 transduction (VG/cell 150,000) following flow cytometry analysis of cellular proportions of GFP expression. **B**) HEK 293 cells were incubated with a dilution series of rAAV-2E3.v2, -v4, -v5, -v6 and AAV2 (VG/cell 150,000; 50,000; 15,000; 5,000 and 0.0) and GFP expression was documented after three days by fluorescence microscopy images. Scalebar 100 μ m. **C**) Heparin column binding of viral capsids was analyzed by ddPCR analysis of viral flow-through, wash and

elution fractions. Data were normalized to total amount of loaded viral genomes. Data represent the mean \pm SEM of two independent experiments. One-way ANOVA compared to AAV2 flow-through, Uncorrected Fisher's LSD, *** $p < 0,001$, ns = non-significant.

3.3 Design and production of bispecific antibodies engaging 2E3 epitopes and human FAP cell surface receptors

Bispecific antibodies were designed and produced to function as adapters between viral 2E3 epitopes and FAP cell surface receptors. Based on the previous publication by (Labrijn et al. 2013) knob-into-hole bispecific antibodies were produced with a C_{H3} K409R mutation (knob) or a complementary C_{H3} K409L mutation (hole). Furthermore, C_{H2} L243A and L235A were modified to reduce Fc-mediated effector functions as previously described (Xu et al. 2000). Bispecific antibodies (KiH-2E3-MO33, KiH-2E3-MO36, and isotype control KiH-2E3-Digoxigenin) were produced in HEK 293-6E cells and column purified by protein A, CEX, and SEC. Purified antibody fractions were analyzed by HPLC (Figure 9A-C) and SDS PAGE protein staining (Figure 9D) (Kuklik et al. 2021).

Bispecific antibodies KiH-2E3-MO33 and KiH-2E3-MO36 were purified in a single fraction with a mass of 143.9 kDa and 156.3 kDa respectively. KiH-2E3-Digoxigenin showed a peak with a slight shoulder that could not be removed by additional SEC purification and might be due to irregular glycosylation. Nevertheless, the peak showed a constant molar mass distribution (146.9 kDa) (Kuklik et al. 2021).

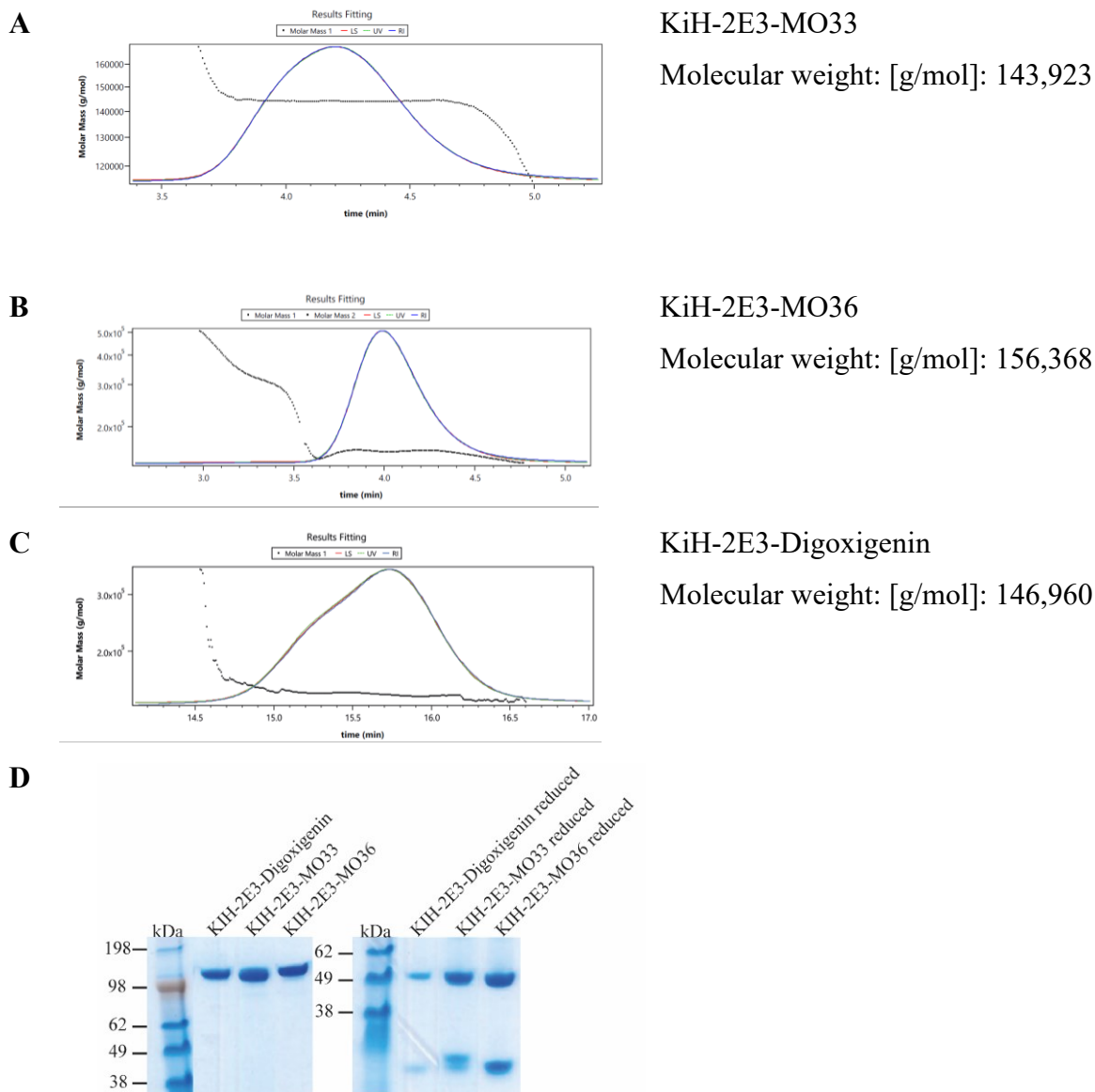


Figure 9: Quality control of knob-into-hole bispecific antibodies HPLC SEC of bispecific antibodies **A)** KiH-2E3-MO33, **B)** KiH-2E3-MO36 and **C)** KiH-2E3-Digoxigenin. Signals of light scatter (LS, red), ultraviolet (UV, green), and the refractive index (RI, black) are plotted, and the calculated molar mass of the peak is indicated at the right side of each graph. **D)** The size of purified bispecific antibodies KiH-2E3-MO33, KiH-2E3-MO36, and KiH-2E3-Digoxigenin was analyzed under reducing and non-reducing conditions by SDS PAGE and protein staining (Kuklik et al. 2021).

To exclude altered binding of cell surface receptors due to antibody Fc-modifications, a flow cytometry staining was performed of knob-into-hole bispecific antibodies (KiH-2E3-MO33, KiH-2E3-MO36) in comparison to their parental monospecific antibodies (MO33 IgG1, MO36 IgG1) and respective isotype controls (KiH-2E3-Digoxigenin and Digoxigenin IgG1). A shift of stained cell populations after incubation with MO33 IgG1 and KiH-2E3-

MO33 (MO33: 87.4%; KiH-2E3-MO33: 85.5% APC positive cells) as well as MO36 IgG1 and KiH-2E3-MO36 IgG1 (MO36: 79.2% and KiH-2E3-MO36: 81.8% APC positive cells) was measured (Figure 10A and B) (Kuklik et al.2021).

The binding of 2E3 epitopes by monospecific antibodies and bispecific antibodies was analyzed on immobilized rAAV-2E3.v6 and AAV2 viral capsids by ELISA. KiH-2E3-MO33, KiH-2E3-MO36, and KiH-2E3-Digoxigenin showed comparable binding signals to 2E3 epitopes but no interaction with AAV2 was measured (Figure 9C, D) (Kuklik et al. 2021).

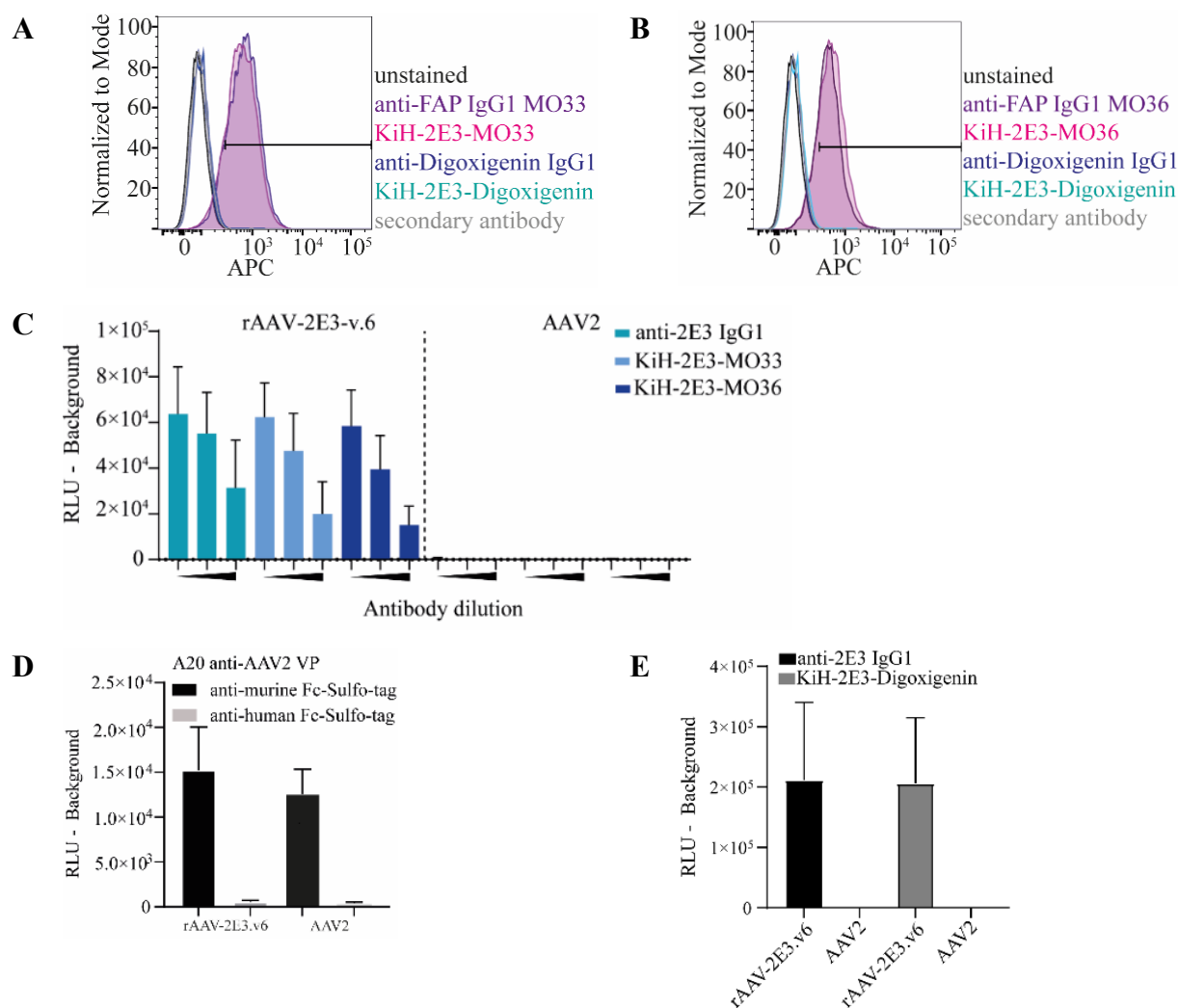


Figure 10: Bispecific antibodies show functional binding of FAP and 2E3 epitopes (Kuklik et al. 2021) **A)** MO33 and KiH-2E3-MO33 or **B)** MO36 and KiH-2E3-MO36 incubated with APC- labeled secondary antibody. **C)** ELISA of immobilized rAAV-2E3.v6 and AAV2 capsids incubated with anti-2E3 IgG1 and bispecific antibodies KiH-2E3-MO33 or KiH-2E3-MO36 in serial dilutions (black triangle, 1:1000; 1:10,000 and 1:100,000). Data show mean \pm SD of three independent experiments. **D)** ELISA assay of viral capsid immobilization and detection with antibody and secondary anti-human antibody or isotype anti-

murine secondary antibody. Data show mean \pm SD of three independent experiments **E**) ELISA of immobilized rAAV-2E3.v6 and AAV2 incubated with anti-2E3 IgG1 and KiH-2E3-Digoxigenin (1:500), following detection with anti-human secondary antibody. Data show mean \pm SD of three independent experiments.

A bridging assay was conducted using Octet HTX bio-layer interferometry (FortéBio, Fremont, CA, USA) to prove the production of bispecific antibodies. Streptavidin sensor tips were coupled with biotinylated 2E3-peptides (first spectral shift, #), followed by bispecific antibody binding (second spectral shift, ##) and finally binding of recombinant FAP or BSA labeled Digoxigenin (third spectral shift, ###) (Figure 11A-C). This proved the production of bispecific antibodies binding the distinct epitopes of 2E3 and FAP or Digoxigenin (Kuklik et al. 2021).

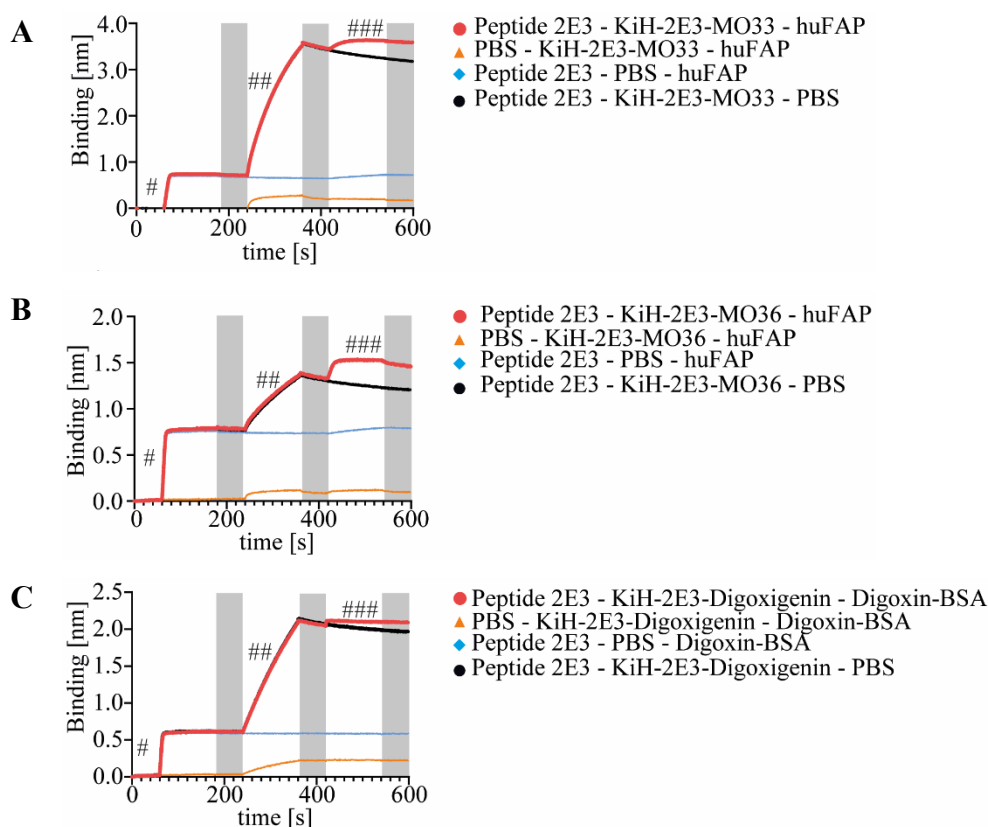


Figure 11: Octet HTX bio-layer interferometry proved simultaneously binding of 2E3 epitopes and recombinant proteins. (Kuklik et al. 2021) Bio-layer interferometry of **A**) KiH-2E3-MO33 **B**) KiH-2E3-MO36 and **C**) KiH-2E3-Digoxigenin antibodies. The first spectral shift was measured upon 2E3-biotin binding to streptavidin sensor tips (#). Bispecific antibody binding resulted in a second spectral shift (##) and a third spectral shift (###) was measured upon recombinant FAP binding or BSA-conjugated Digoxin binding. Wash steps between binding events are indicated by grey bars.

Internalization of FAP upon antibody binding was previously published (Baum et al. 2008; Fischer et al. 2012). The data were confirmed, and it was proven that also bispecific antibodies were internalized. All antibodies were Fc-conjugated to a pH-sensitive dye that emitted red fluorescence signals upon internalization in endosomes. HT1080 huFAP cells incubated with MO33 IgG1, MO36 IgG1, KiH-2E3-MO33, and KiH-2E3-MO36 labeled antibodies showed increasing red fluorescence signals throughout 5 h but cells incubated with respective isotype controls showed no distinct fluorescence signal (Figure 12) (Kuklik et al. 2021).

All in all, bispecific antibodies were generated that not only bind 2E3 epitopes and FAP cell surface receptors simultaneously but also induce FAP internalization upon antibody binding (Kuklik et al. 2021).

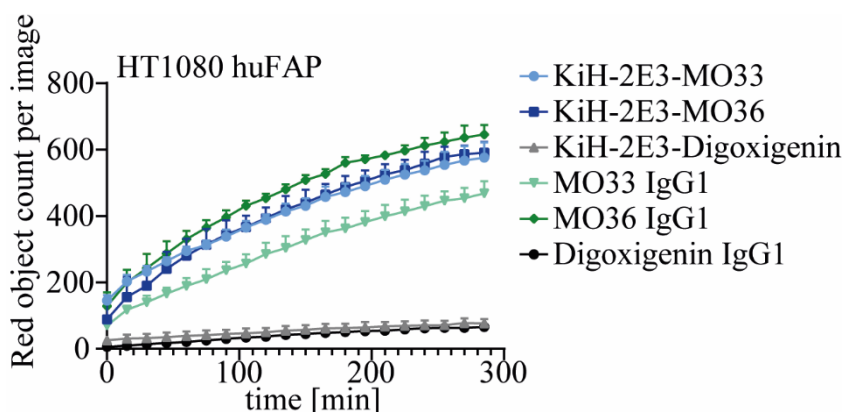


Figure 12: FAP receptors internalize independently of mono- or bispecific antibody binding (Kuklik et al. 2021). Monospecific parental antibodies, bispecific antibodies, and isotype control antibodies were labeled with Human Fabfluor-pH Red Antibody Labeling Dye (Sartorius, Göttingen, Germany) that emits a red fluorescence at low pH. HT1080 huFAP cells were incubated with labeled antibodies for 5 observation of red fluorescence signals. Data show mean \pm SD of two independent experiments.

3.4 *In vitro* targeting of FAP by AAV-antibody complexes

A retargeting approach to FAP was established *in vitro* by pre-incubation of purified rAAV-2E3 viral variants with KiH-2E3-FAP bispecific antibodies (MO33 or MO36). The virus was titrated in three dilutions steps (VG/cell 50,000; 15,000 and 5000) versus antibody dilutions starting at 7500 pg/ μ L in 1:10 dilution steps. The pre-incubated complex was incubated with HT1080 huFAP or HEK 293 huFAP cells for three days and viral-induced GFP expression was measured by flow cytometry. No GFP expression was measured by HT1080 huFAP cells incubated with rAAV-2E3.v2 at any antibody concentration (Figure 13A).

rAAV-2E3.v4 and rAAV-2E3.v5 incubated with Ht1080 huFAP cells resulted in high amounts of GFP expressing cells (up to 99% GFP positive cells) even without KiH-2E3-MO36. High amounts of bispecific antibodies seemed to correlate with decreasing proportions of GFP-positive cells. Due to the high background expression, a specific targeting effect could not be observed (Figure 13B, C). HT1080 huFAP cells incubated with a complex of rAAV-2E3.v6 (50,000 VG/cell) and KiH-2E3-MO36 (750 pg/ μ L) showed a significant increase $60.8\% \pm 17.32\%$ of GFP positive cells ($p < 0.01$). The proportion of GFP signals were depending on the ratio of antibodies per viral genome (Figure 13D).

A similar although weaker transduction could be observed with a complex of rAAV-2E3.v6:KiH-2E3-MO33 (50,000 VG/cell and 750 pg/ μ L) resulting in $7.59\% \pm 4.66\%$ GFP positive cells (Figure 13E). In a control experiment, it was proven that the transduction of HT1080 and HT1080 huFAP cells by rAAV2 (50,000 VG/cell) incubated with high amounts of bispecific antibodies was not altered in comparison to pure rAAV2 transduction (Figure 13F). (Kuklik et al. 2021).

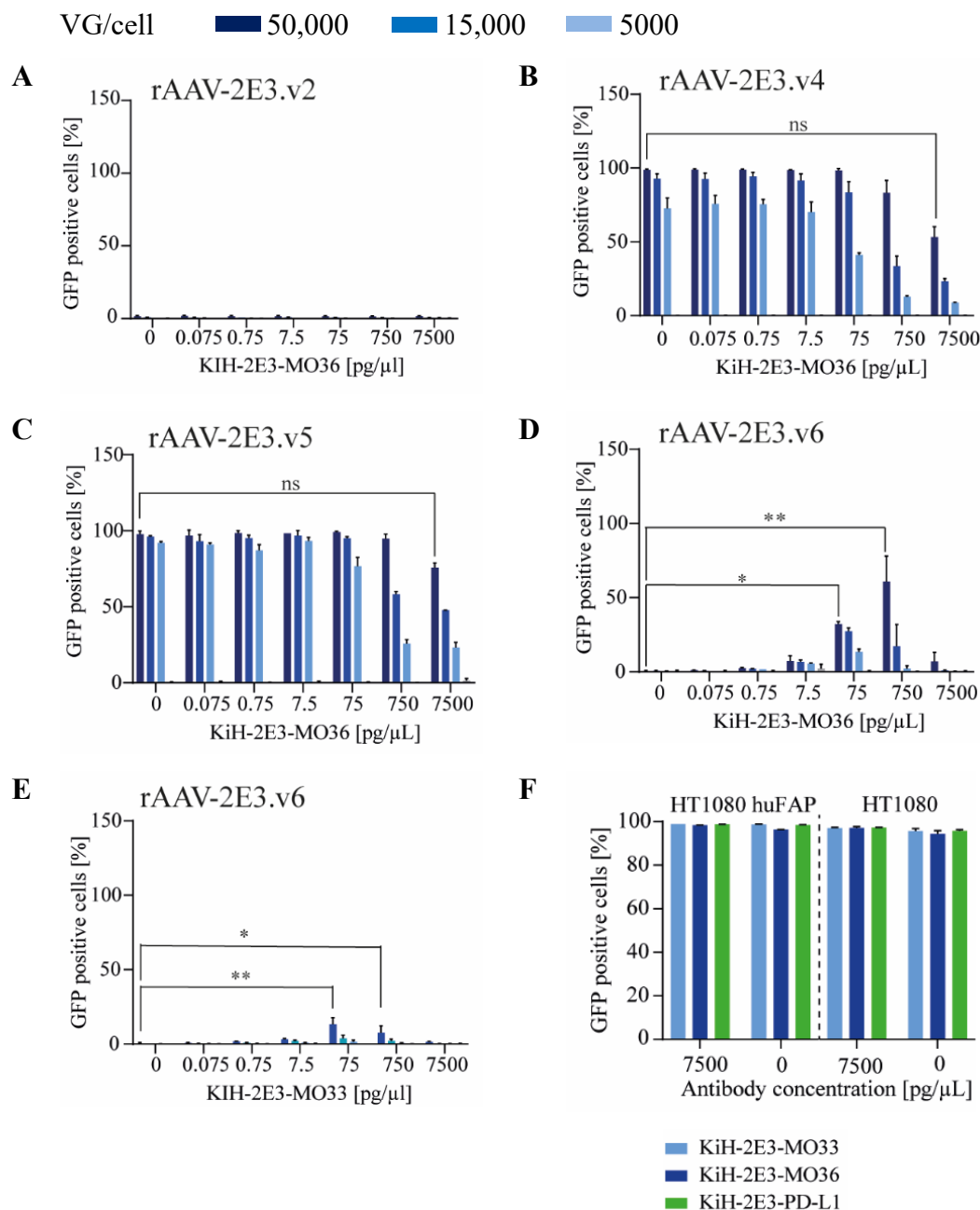


Figure 13: Establishment of a FAP targeting mechanism based on the complexation of rAAV-2E3 with bispecific antibodies Modified from (Kuklik et al. 2021), CC BY 4.0, <https://creativecommons.org/licenses/by/4.0/>. Flow cytometry analysis of GFP expressing HT1080 huFAP cells after incubation with titrations of antibody KiH-2E3-MO36 and **A**) rAAV-2E3.v2 **B**) rAAV-2E3.v4 **C**) rAAV-2E3.v5 **D**) rAAV-2E3.v6 used at 50,000 VG/cell (dark blue); 15,000 (VG/cell blue) and 5000 VG/cell (light blue). **E**) Repetition of the experiment using KiH-2E3-MO33 complexed with rAAV-2E3.v6 on HT1080 huFAP cells. one-way ANOVA, uncorrected Dunn's test *** $p < 0.001$, ns = non-significant. **F**) GFP expression of AAV2 transduced HT1080 huFAP or HT1080 cells is not affected by high doses of bispecific antibodies. Data show mean \pm SD.

The rAAV-2E3.v6: KiH-2E3-MO36 observed targeting effect was reproduced on HEK 293 huFAP expressing cells resulting in up to 71.32% \pm 13.78% GFP positive cells; $p < 0.01$ (50,000 VG/cell and 750 pg/ μ L antibody). The most efficient targeting of HEK 293 huFAP cells (63.39% \pm 5.77%; $p < 0.05$) by rAAV-2E3.v6: KiH-2E3-MO33 was observed at 50,000 VG/cell and 75 pg/ μ L antibody (Figure 14A and B) (Kuklik et al. 2021).

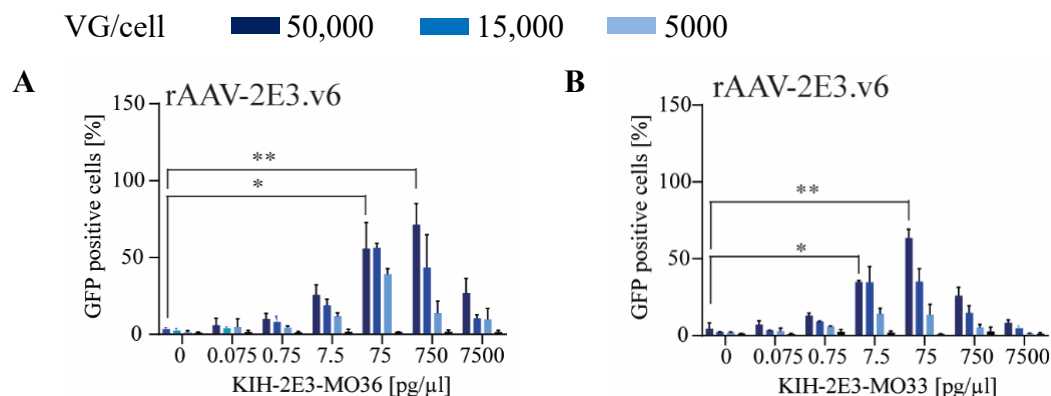


Figure 14: Reproduction of bispecific antibody-mediated rAAV-2E3.v6 retargeting to HEK 293 hu-FAP cells. A) Targeting experiment reproduction on HEK 293 huFAP expressing cells transduced by rAAV-2E3.v6 complexed with KiH-2E3-MO36 (Kuklik et al. 2021) or B) KiH-2E3-MO33. Data show mean \pm SD of two independent experiments, one-way ANOVA, Uncorrected Dunn's test, * $p < 0.05$; ** $p < 0.01$.

Direct comparison of GFP expression levels of HT1080 huFAP cells incubated with rAAV2, rAAV-2E3.v6, or rAAV-2E3.v6 coupled with bispecific antibodies (KiH-2E3-MO33 or KiH-2E3-MO36 at 2.5 ng/ μ L) revealed significant lack of transduction of rAAV-2E3.v6 (mean percent GFP positive cells 0.83 ± 0.11) compared to rAAV2 (mean percent of rAAV2 GFP positive cells 97.81 ± 0.92 $p < 0.001$). GFP expression was increased 13 fold upon rAAV-2E3.v6 interaction with KiH-2E3-MO33 and 57 fold upon interaction with KiH-2E3-MO36 (mean AAV-2E3.v6:KiH-2E3-MO36 GFP positive cells $57.7\% \pm 11.9\%$ $p < 0.001$) (Figure 15) (Kuklik et al. 2021).

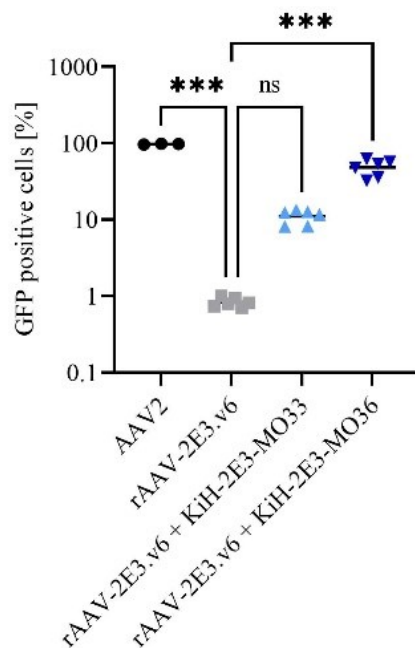


Figure 15: Reproduction of bispecific antibody-mediated rAAV-2E3.v6 retargeting to HEK 293 hu-FAP cells (Kuklik et al. 2021). GFP expression levels of HT1080 huFAP cells transduced with AAV2, rAAV-2E3.v6, rAAV-2E3.v6:KiH-2E3-MO33, and rAAV-2E3.v6:KiH-2E3-MO36 at 50,000 VG/cell and 2.5 ng/ μ L bispecific antibody normalized to AAV2 transduction levels. One-way ANOVA, uncorrected Dunn's test *** $p < 0.001$, ns = non-significant.

As antibody complexed rAAV-2E3.v6 showed FAP targeting, the optimal ratio of antibody per viral genome was examined and the specific antibody binding was evaluated. A dose-response curve of absolute amounts of antibody per rAAV-2E3.v6 genome was recorded using KiH-2E3-MO33 and KiH-2E3-MO36 and HT1080 huFAP cells (Figure 16A, B). Not only the percentage of GFP positive cells was analyzed but also the medium fluorescence intensity (MFI) (Figure 16C). Significant high proportions of GFP expressing cells and high MFI levels were measured at 180 KiH-2E3-MO33 antibodies per rAAV-2E3.v6 genome in comparison to rAAV-2E3.v6 without antibody incubation (Mean percent of GFP positive cells 13.99 ± 4.23 ; $p < 0.0001$). Incubation of KiH-2E3-MO36 with rAAV-2E3.v6 resulted in highest GFP expression levels at 600 antibodies per viral genome (Mean percent of GFP positive cells 48.28 ± 10.93 ; $p < 0.0001$). The curve shape corresponded with the MFI curve of GFP expressing cells. The transduction of cells showed strong dependence on the optimal

ratio of antibody per viral genome, as low antibody amounts and high antibody amounts negatively influenced the numbers of GFP expressing cells (Kuklik et al. 2021).

The targeting of HT1080 huFAP cells was dependent on the expression of FAP, as FAP negative cells showed no GFP expression after incubation with rAAV-2E3.v6 complexed with either KiH-2E3-MO33 or KiH-2E3-MO36 (Figure 16D). Additionally, it was shown that the antibody-mediated binding of FAP was a necessity for cell targeting since bispecific isotype antibodies (KiH-2E3-Digoxigenin) complexed with rAAV-2E3.v6 did not lead to GFP expression (Figure 16A, B). In contrast, the positive control rAAV2 transduced up to 99% GFP positive cells with MFIs in the range of 2×10^6 - 3×10^6 at comparative levels of VG/cell (Figure 16E, F).

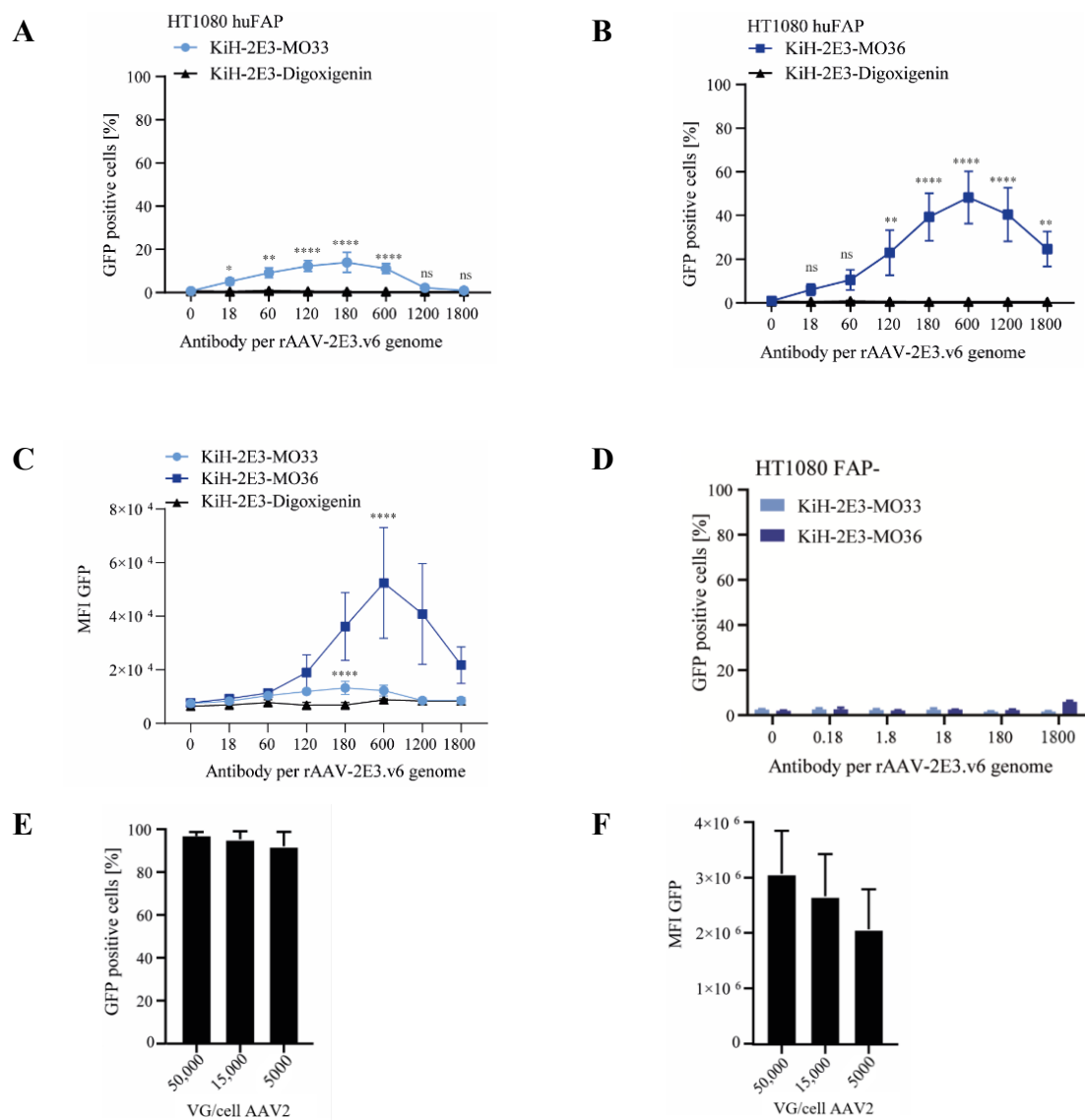


Figure 16: Retargeting of rAAV-2E3.v6 is dependent on the epitope binding and ratio of KiH-antibody per viral genome (Kuklik et al. 2021). Flow cytometry analysis of proportions of GFP positive cells incubated with rAAV-2E3.v6 and bispecific antibody dilutions of isotype control and **A)** KiH-2E3-MO33:rAAV-2E3.v6 or **B)** KiH-2E3-MO36. **C)** MFI of cells targeted with KiH-2E3-MO33:rAAV-2E3.v6, KiH-2E3-MO36:rAAV-2E3.v6 or KiH-2E3-Digoxigenin:rAAV-2E3.v6. Data show mean \pm SD of two independent experiments, one-way ANOVA, Uncorrected Dunn's test, * $p < 0.05$; ** $p < 0.01$, ns= non-significant. **D)** HT1080 wt cells show no GFP signal after incubation with KiH-2E3-MO33 or KiH-2E3-MO36 complexed with rAAV-2E3.v6. Data show mean \pm SD of three independent experiments, one-way ANOVA, Uncorrected Dunn's test groups compared to rAAV-2E3.v6 without bispecific antibody, * $p < 0.05$; ** $p < 0.01$; **** $p < 0.0001$. **E)** HT1080 huFAP cells were incubated with AAV2 (50,000; 15,000 and 5000 VG/cell) following flow cytometry measurement of proportional GFP expression and **(F)** MFI. Data show mean \pm SD.

3.5 Bispecific antibody-mediated targeting is highly epitope- and independent of heparin interaction

MO33 and MO36 interact with human FAP as previously described (Brocks et al. 2001). Furthermore, MO36 interacts with murine FAP and human FAP with similar affinity while the affinity of MO33 to murine FAP is reduced. Successful transduction of HT1080 huFAP and HT1080 muFAP by complexes of rAAV-2E3.v6:KiH-2E3-MO33 or rAAV-2E3.v6:KiH-2E3-MO36 was successfully shown. However, the retargeting efficiency was significantly decreased for both bispecific antibodies on muFAP expressing cells compared to huFAP expressing cells (fold change rAAV-2E3.v6:KiH-2E3-MO36: 0.35 ± 0.02 ; $p < 0.05$ and fold change rAAV-2E3.v6:KiH-2E3-MO33: 0.28 ± 0.04 ; $p < 0.05$) (Figure 17A) (Kuklik et al. 2021).

The human FAP binding antibody BIBH1 is known to interact only with human FAP but not murine FAP (Hofheinz et al. 2003; Tahtis et al. 2003) and was used in this study as a competitor for FAP binding and receptor availability. HT1080 huFAP and HT1080 muFAP cells were pre-incubated with increasing concentrations of BIBH1 following incubation with rAAV-2E3.v6:KiH-2E3-MO33 or rAAV-2E3.v6:KiH-2E3-MO36. GFP expression was measured by flow cytometry. Proportions of GFP expressing cells were normalized to data obtained from cells treated with 0 $\mu\text{g/mL}$ BIBH1. Increasing amounts of BIBH1 reduce the proportions of GFP positive cells after incubation with rAAV-2E3.v6:KiH-2E3-MO33. A significant drop of expression was measured at a BIBH1 concentration of 1000 $\mu\text{g/mL}$ ($15.2\% \pm 7.0\%$ GFP positive cells; $p < 0.01$). A weaker effect of BIBH1 on rAAV-2E3.v6:KiH-2E3-MO36 transduction was observed at the highest BIBH1 concentration ($61.94\% \pm 13.24\%$ GFP positive cells; $p < 0.01$). No significant effect was observed after co-incubation of BIBH1 and KiH-2E3-MO33 or KiH-2E3-MO36 with rAAV-2E3.v6 on HT1080 muFAP cells as expected (Figure 17B, C) (Kuklik et al. 2021).

Specific 2E3 epitope binding by bispecific antibodies was measured in a competition assay with increasing concentrations of soluble 2E3 peptide or 2E3 mutation plus rAAV-2E3.v6:KiH-2E3-MO33 or rAAV-2E3.v6:KiH-2E3-MO36. Flow cytometry measured proportions of GFP positive cells were normalized to data obtained from samples incubated with 0.0 mg/mL 2E3 peptide. The GFP expression levels of HT1080 huFAP incubated with these complexes were decreasing with increasing 2E3 peptide concentrations. 2E3 mutated

peptides showed no influence on cellular GFP expression (Figure 17D, E) (Kuklik et al. 2021)

As shown in chapter 3.2, rAAV-2E3.v6 showed reduced heparin column binding compared to other rAAV-2E3 capsid variants and AAV2. This effect was confirmed in cell culture by culturing HT1080 huFAP cells with increasing amounts of heparin sodium following incubation with AAV2, rAAV-2E3.v4, rAAV-2E3.v5 and rAAV-2E3.v6:KiH-2E3-MO36. Increasing amounts of heparin interfered with the GFP expression of cells incubated with AAV2, rAAV-2E3.v4, and rAAV-2E3.v5. GFP expression levels of cells treated with rAAV-2E3.v6:KiH-2E3-MO36 remained unaffected by any heparin concentrations (Figure 17F) (Kuklik et al. 2021).

Finally, the transduction efficiency was analyzed under the influence of purified human intravenous immunoglobulins (IVIGs) that naturally contain AAV neutralizing antibodies (Moskalenko et al. 2000; Huttner et al. 2003; Mingozi et al. 2013; Mingozi and High 2017; Kuranda et al. 2018). Transduction of AAV2 as well as KiH-2E3-MO36:rAAV-2E3.v6 was negatively influenced with increasing IVIG concentrations (AAV2 $IC_{50} = 0.114$ mg/mL and rAAV-2E3.v5:KiH-2E3-MO36 $IC_{50} = 0.182$ mg/mL). Therefore, capsid modifications and pre-bound antibodies may not rescue rAAV-2E3.v6 of neutralizing antibody binding *in vivo*.

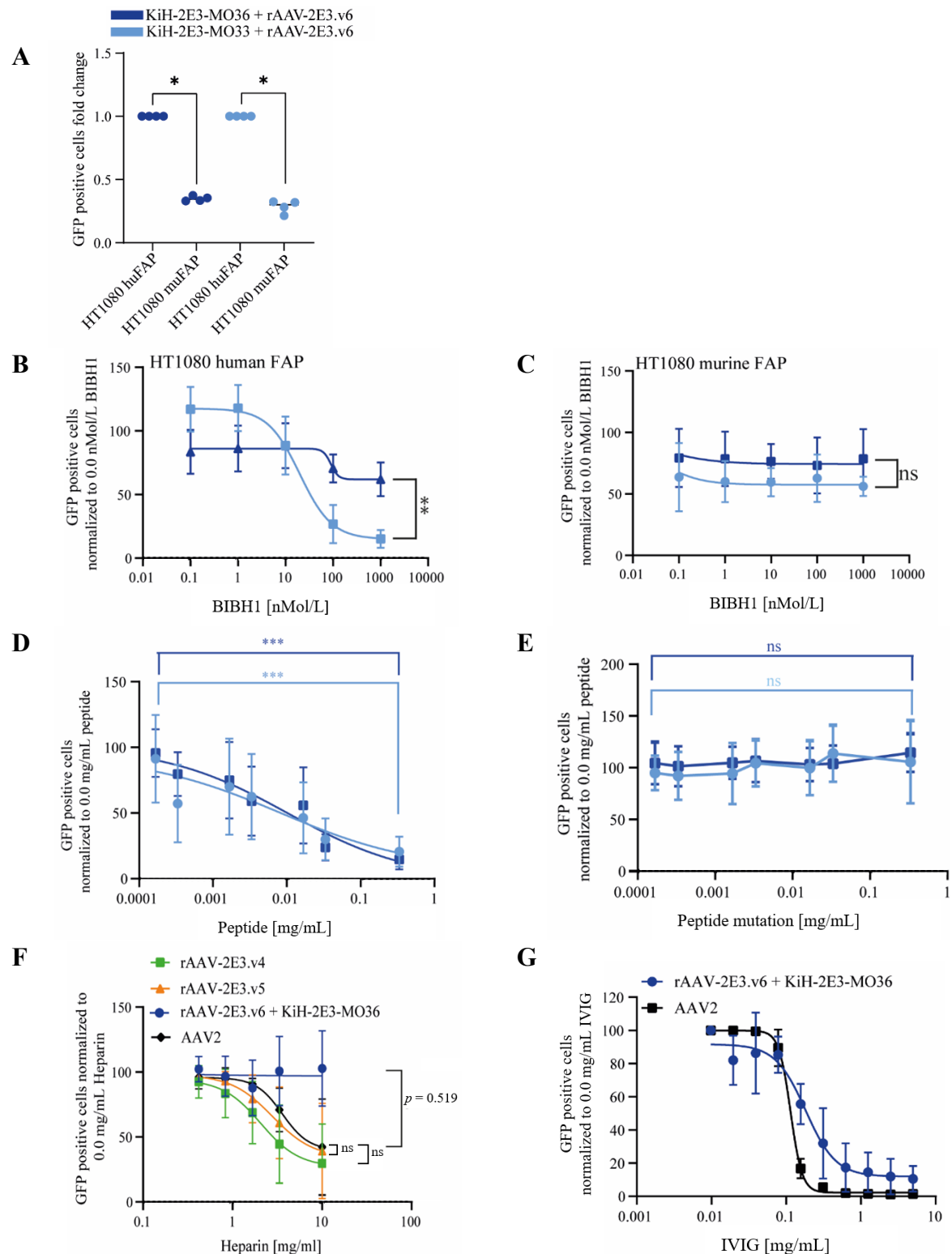


Figure 17: Bispecific antibody rAAV-2E3.v6 retargeting is influenced by competitors and neutralizing antibodies but not heparin (Kuklik et al. 2021) Flow cytometry analysis of proportions of GFP positive cells normalized to expression levels without competitor agents. rAAV-2E3.v6:KiH-2E3-MO33 is shown in light blue, rAAV-2E3.v6:KiH-2E3-MO36 is shown in dark blue. **A)** Efficiency of KiH-2E3-MO33 or KiH-2E3-MO36 complexed with rAAV-2E3.v6 transduction of HT1080 huFAP or muFAP-mediated cells. Data

show mean \pm SD of two independent experiments, Mann Whitney test, * $p < 0.05$. **B)** Increasing concentrations of BIBH1 compete with KiH-2E3-MO33 and KiH-2E3-MO36-rAAV-2E3.v6 for targeting HT1080 huFAP cells or **C)** HT1080 muFAP cells. Data show mean \pm SD of three independent experiments, Mann Whitney test, ** $p < 0.01$; ns = non-significant. **D)** Competition of soluble 2E3 peptide or **E)** soluble 2E3 mutation with KiH-2E3-MO33 or KiH-2E3-MO36 for binding of rAAV-2E3.v6 following transduction of HT1080 huFAP cells. Data show mean \pm SD of three independent experiments, Mann Whitney test, *** $p < 0.001$; ns = non-significant. **F)** Transduction of HT1080 huFAP cells with AAV2, rAAV-2E3.v4, rAAV-2E3.v5 or KiH-2E3-MO36:rAAV-2E3.v6 in presence of increasing heparin concentrations. Data show mean \pm SD of four independent experiments, Mann Whitney test. GFP expression of cells in all experiments was measured by flow cytometry. **G)** Transduction of AAV2 and AAV-2E3.v6:KiH-2E3-MO36 with increasing concentrations of human intravenous immunoglobulins (IVIGs). Data show mean \pm SD of two independent experiments, Mann Whitney test, ns = non-significant.

3.6 Viral uptake is dependent on bispecific antibody binding

It was observed that rAAV-2E3.v6 alone does not induce GFP expression and that the GFP expression levels of cells incubated with KiH-2E3-MO36:rAAV-2E3.v6 were lower compared to those exposed to AAV2. Therefore, the internalization protein biosynthesis kinetic of rAAV-2E3.v6 was analyzed by qPCR and flow cytometry in comparison to KiH-2E3-MO36:rAAV-2E3.v6 and AAV2 (Figure 18).

Low amounts of rAAV-2E3.v6 viral genomes per cell and transcripts at the detection limit were measured resulting consequently in the lowest amounts of GFP positive cells within 72 h observation after transduction. Viral genomes of KiH-2E3-MO36:rAAV-2E3.v6 were observed after 6h with a peak at 24h after transduction. Relative transcript levels of rAAV-2E3.v6 complexed with KiH-2E3-MO36 reached a peak at 24h and maximal GFP expression levels were measured at 48h after transduction. Viral genomes and transcript levels of rAAV-2E3.v6:KiH-2E3-MO36 were significantly enhanced compared to those derived from rAAV-2E3.v6 at 24h after transduction (mean $1,807 \pm 756.9$ viral gDNA per cell, $p < 0.05$ and mean 0.008 ± 0.004 delta delta ct GFP, $p < 0.01$) (Figure 18A, B).

A trend of enhanced GFP expression levels and MFI of cells transduced with rAAV-2E3.v6:KiH-2E3-MO36 compared to cells transduced with rAAV-2E3.v6 was observed within 6 h and 24h after transduction (Figure 18C, D).

Significantly high levels of AAV2 viral genomes per cell compared to KiH-2E3-MO36:rAAV-2E3.v6 were measured at 24 h after transduction (mean $4,855 \pm 1,717$ AAV2 viral genomes per cell, * $p < 0.05$) and rAAV-2E3.v6 (** $p < 0.001$). 100 fold higher transcript levels of AAV2 cargo were measured compared to KiH-2E3-MO36:rAAV-2E3.v6 at 24 h after transduction. Furthermore, it was observed that the relative transcript levels of AAV2 genomes were significantly enhanced compared to those measured of rAAV-2E3.v6 (mean 1.24 ± 0.52 delta delta ct GFP, *** $p < 0.001$). Cells transduced with AAV2 showed maximal GFP protein expression at 24 h showing 4× increased proportions of GFP positive cells and 40× enhanced MFI levels compared to cells transduced with rAAV-2E3.v6. GFP protein expression of AAV2 was significantly enhanced compared to rAAV-2E3.v6 (mean $99.94\% \pm 0.01\%$ GFP positive cells, ** $p < 0.01$, and mean $8,192,870 \pm 1,689,008$ MFI, ** $p < 0.01$).

All in all, these experiments show an expected kinetic of genome detection, transcripts, and finally protein expression. rAAV-2E3.v6 does not enter HT1080 huFAP cells without the support of bispecific antibodies. The internalization kinetics of rAAV-2E3.v6:KiH-2E3-MO36 is similar to AAV2 based on genomes per cell and transcripts. However, higher amounts of AAV2 genomes are found at early timepoints leading to higher transcript levels, faster protein expression, and accelerated GFP protein levels.

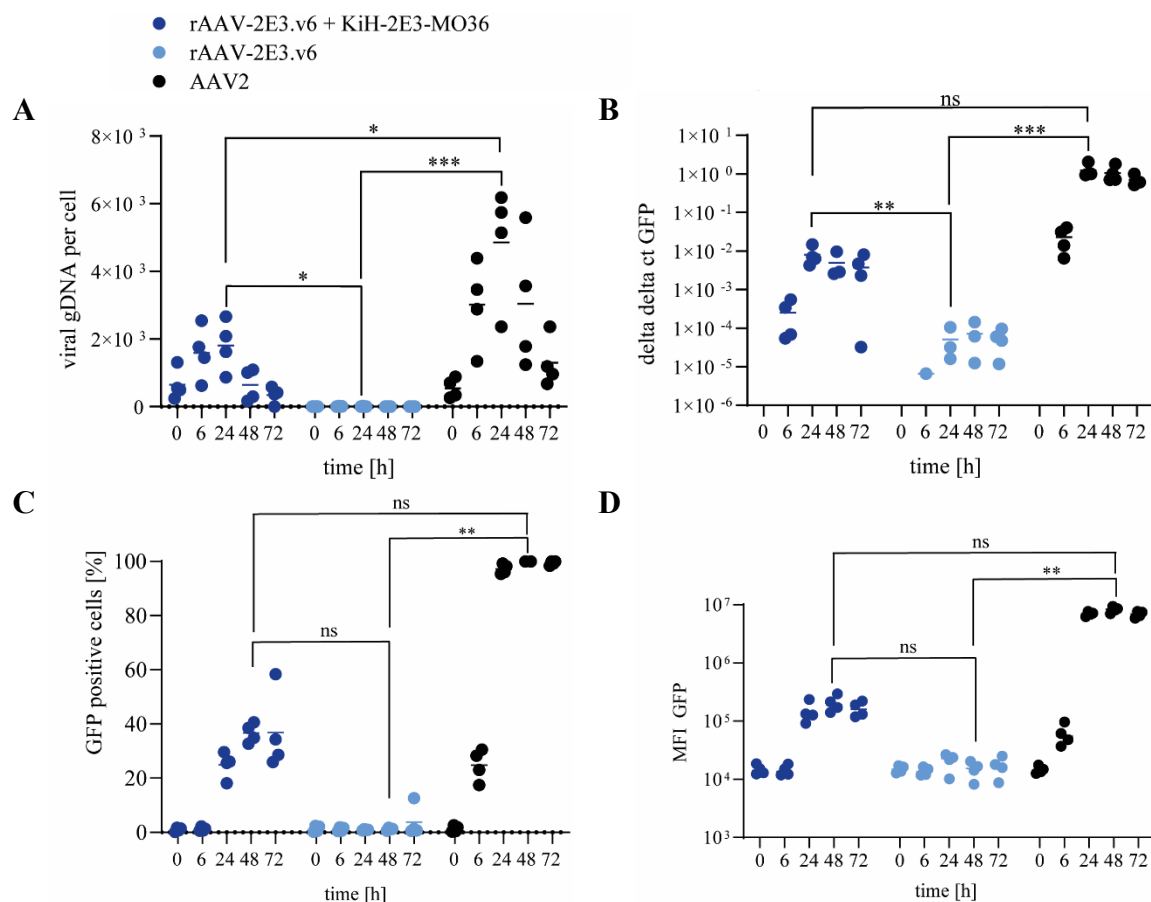


Figure 18: Comparison of viral internalization and transgene expression kinetics of rAAV-2E3.v6 and AAV2 The internalization kinetics of rAAV-2E3.v6, rAAV-2E3.:KiH-2E3-MO36 in comparison to AAV2 was analyzed using Ht1080 huFAP cells within 0, 6, 24, 48 and 72 hours. **A)** Internalized viral genomes and **B)** AAV genomic transcripts were analyzed by qPCR. **C)** The percentage of GFP positive cells and **D)** GFP MFI were analyzed by flow cytometry. Data sets show scatter plot of individual samples and mean of four independent experiments, one-way ANOVA, Uncorrected Dunn's test, * $p < 0.05$; ** $p < 0.01$; *** $p < 0.001$, ns = non-significant.

3.7 Targeting of PD-L1 by modular bispecific antibody exchange

Having established a reliable FAP retargeting mechanism based on rAAV-2E3.v6, the system was adapted to target PD-L1 by simple “Fab-arm exchange” with the hole-antibody anti-PD-L1 binding antibody avelumab. This resulted in the bispecific antibody KiH-2E3-PD-L1. Visible were the longer kappa light chains (107 amino acids) and shorter lambda light chains (105 amino acids) of the purified bispecific antibody after reducing SDS PAGE and protein staining (Figure 19A) (Kuklik et al. 2021).

Flow cytometry staining of HT1080 huFAP incubated with avelumab, KiH-2E3-PD-L1, respective isotype controls, and APC-labelled anti-human Fc secondary antibody indicated a clear shift of PD-L1 positive cells. This proved native PD-L1 receptor expression of HT1080-huFAP cells as described earlier (Park et al. 2018; Teruya et al. 2019). HT1080-huFAP cells stained with bispecific or monospecific antibodies resulted in two separate peaks. The slight differences of PD-L1 positive may be due to small differences in antibody concentrations, altered affinities, or purities (avelumab: 92.8%; KiH-2E3-PD-L1: 99.0% APC positive cells). However, this experiment proved PD-L1 expression of HT1080 cells and binding of mono- and bispecific antibodies (Figure 19B) (Kuklik et al. 2021).

KiH-2E3-PD-L1 proved to bind immobilized rAAV-2E3.v6 but not AAV2 indicating the specific interaction of KiH-2E3-PD-L1 with 2E3 epitopes (Figure 19C). Immobilization of AAV viral capsids was proven by anti-VP staining via A20 antibodies and respective secondary antibody isotype controls (Figure 19D) (Kuklik et al. 2021).

Re-targeting of rAAV-2E3.v6 was conducted by pre-incubation with either KiH-2E3-PD-L1 or KiH-2E3-MO36 antibodies following incubation of the complex on HT1080 huFAP cells. Flow cytometry analysis of GFP positive cells proved successful retargeting via PD-L1 and FAP binding. Both antibodies showed a significant increase of GFP positive cells compared to control groups with a ratio of 180 bispecific antibodies per rAAV-2E3.v6 (KiH-2E3-PD-L1: percentage of GFP positive cells $22.73\% \pm 11.28\%$; $p < 0.0001$ and KiH-2E3-MO36: percentage of GFP positive cells $50.19\% \pm 13.78\%$; $p < 0.001$) (Figure 19E). The curve of proportions of GFP positive cells correlated with the MFI dataset (Figure 19F). FAP targeting by KiH-2E3-MO36 seemed to be more efficient than targeting PD-L1. However, the data sets integrated well into the overall range of transduced cells of KiH-2E3-MO33 and KiH-2E3-MO36. This indicated that the transduction efficiency was dependent on antibody-epitope interactions and may not be influenced by differences in native expression or receptor overexpression (Kuklik et al. 2021).

In summary, a modular targeting approach based on new AAV2 capsid variants was developed enabling the targeting of distinct cell-surface receptors by 'Fab-arm exchange' of bispecific antibodies (Kuklik et al. 2021).

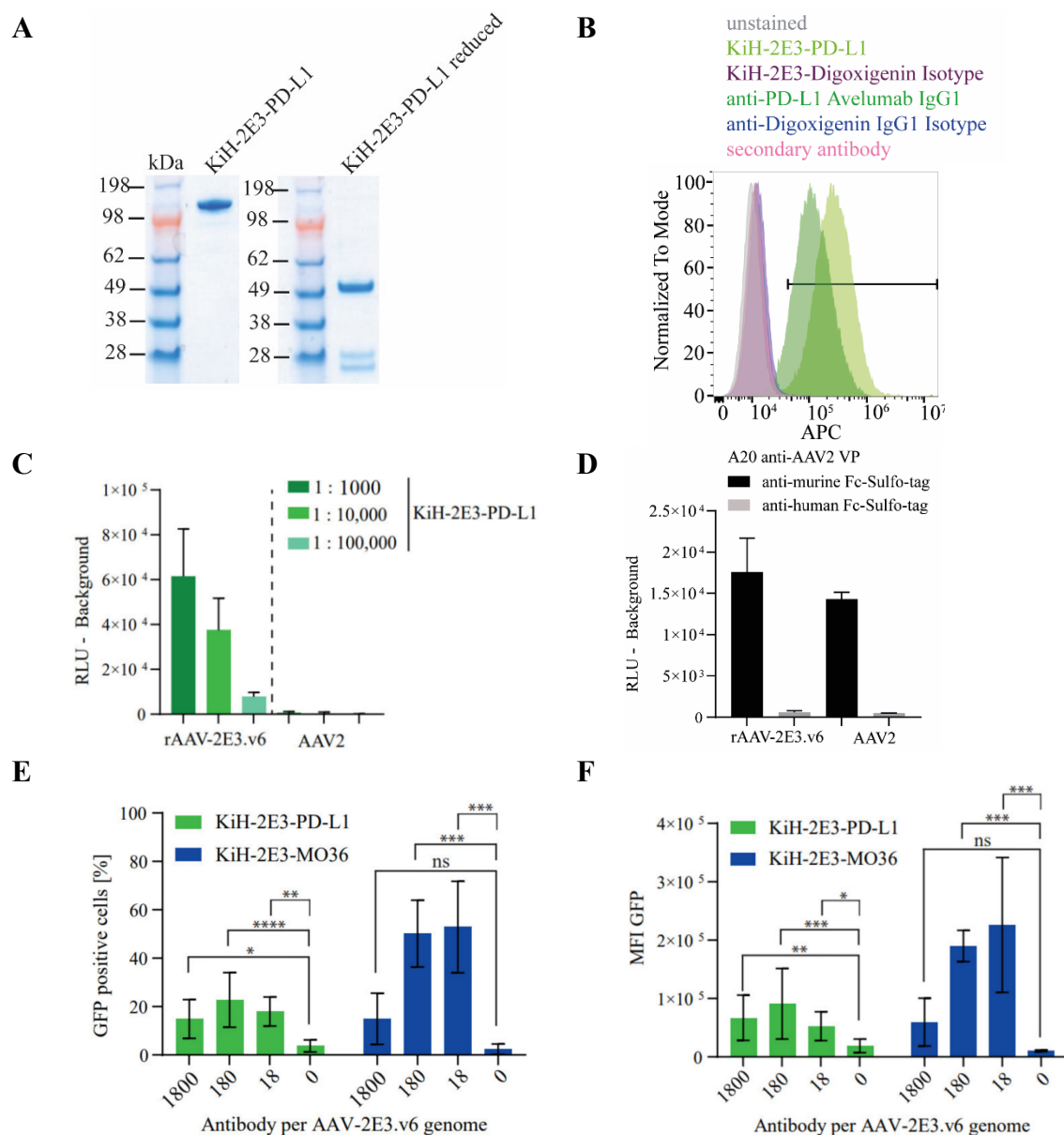


Figure 19: ‘Fab-arm exchange’ enabled the production of KiH-2E3-PD-L1 and modular targeting of PD-L1 with rAAV-2E3.v6 (Kuklik et al. 2021) **A**) SDS PAGE of purified KiH-2E3-PD-L1 composed of knob-2E3 (kappa light chains) and hole-avelumab (lambda light chains). **B**) Flow cytometry staining of HT1080 huFAP cells with monospecific avelumab (anti-PD-L1), KiH-2E3-PD-L1 and isotype controls. **C**) ELISA assay of immobilized rAAV-2E3.v6 binding by KiH-2E3-PD-L1 **D**) Control staining of immobilized rAAV-2E3.v6 and AAV2 using anti-VP A20 (Progen, Heidelberg, Germany). Specific anti-murine Fc staining was proven with the isotype control antibody anti-human Fc (MSD® Rockville, MD, USA). **E**) Flow cytometry analysis of GFP positive HT1080 huFAP cells after transduction with rAAV-2E3.v6:KiH-2E3-PD-L1 or KiH-2E3-MO36 and **F**) MFI. Data show mean \pm SD of three independent experiments; one-way ANOVA, uncorrected Dunn’s test, * $p < 0.05$; ** $p < 0.01$; *** $p < 0.001$, **** $p < 0.0001$, ns = non-significant.

3.8 Development of a murine xenograft HT1080 huFAP tumor model and processing of reagents for *in vivo* experiments

A murine xenograft tumor model was established at Charles River, Wilmington, MA, USA to analyze detargeting of rAAV-2E3.v6 as well as the targeting of HT1080 huFAP tumor tissue with the complex of rAAV-2E3.v6:KiH-2E3-MO36. HT1080 huFAP cells and HT1080 cells were injected subcutaneously into two groups of mice to compare FAP expression levels. HT1080 derived tumors grew unbiased of injected number of cells or over-expression of FAP (Figure 20A, B). 27 days after injection tumors started to reach a size of 2000 mm³, and animals were sacrificed. Immunohistochemistry analysis of Formalin-Fixed Paraffin-Embedded tissues proved FAP expression independent of the injected amount of HT1080 huFAP cells, while HT1080 tumors did not express FAP (Figure 20C, D). As the lowest number of injected cells resulted in reliable and fast tumor growth, it was decided to use this model for further *in vivo* studies.

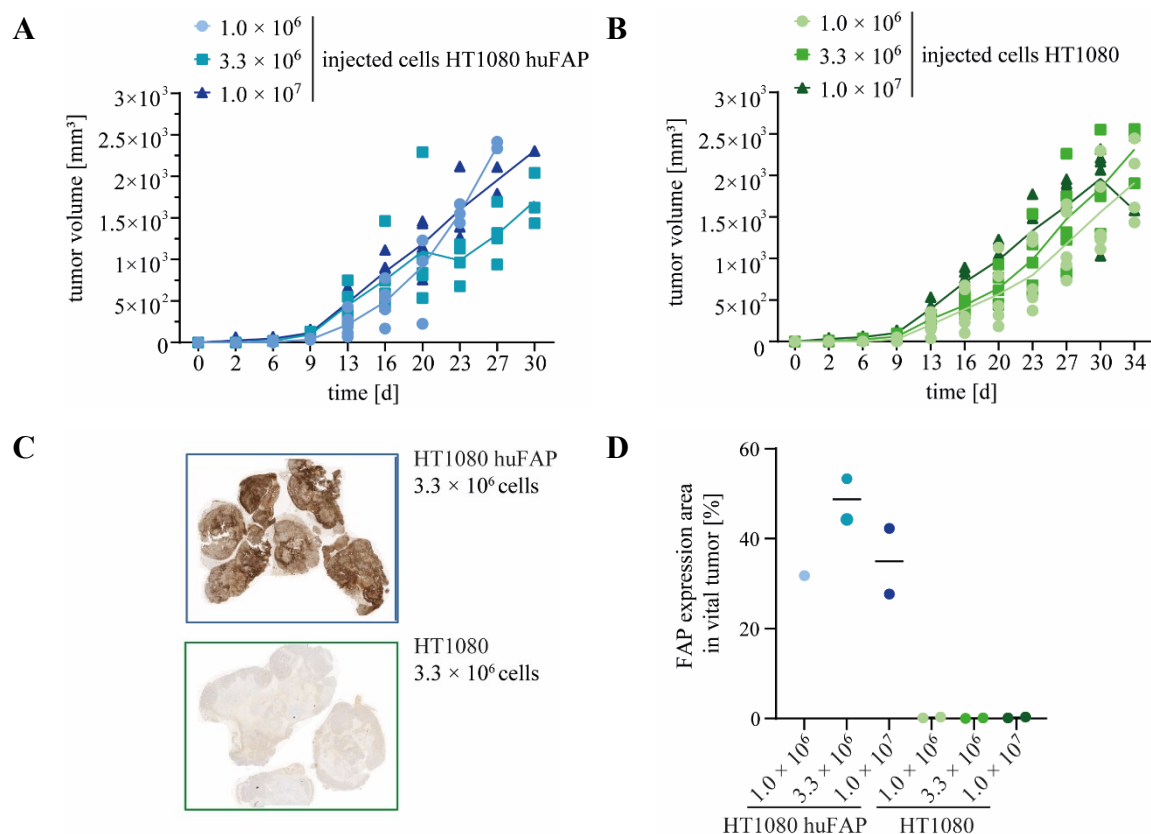


Figure 20: Establishment of an HT1080 huFAP xenograft model A) HT1080 huFAP cells and B) HT1080 cells were injected subcutaneously into the flank of NSG mice at different concentrations per group (1.0×10^6 , 3.3×10^6 , or 1.0×10^7 cells per animal). Tumor

growth was observed until the maximal tumor volume of 2000 mm³ was reached. **C)** Transmitted light microscopy images of anti-FAP stained tumor samples. One exemplary image of each tumor is shown derived from an initial injection of 3.3×10^6 cells per animal. **D)** Dot plot of the proportional FAP expressed area in vital tumor tissue.

Pharmacokinetics of KiH-2E3-MO33 and KiH-2E3-MO36 were measured to evaluate the best suited FAP binding antibody for *in vivo* experiments. After a single dose injection of 10 mg/kg antibody per animal, the antibody plasma concentrations were analyzed for 6 days. The highest human antibody plasma concentration was measured directly after antibody injection. Both antibodies showed a similar half-life of about 13 days and a calculated mean residence time of 17 to 19 days (Table 31). As both antibodies show similar pharmacokinetic parameters, it was decided that KiH-2E3-MO36 should be used for *in vivo* experiments, as higher amounts of targeted cells were obtained by complexing with rAAV-2E3.v6 *in vitro*

Table 31: Pharmacokinetic parameters of bispecific antibodies

	KiH-2E3-MO33	KiH-2E3-MO36
Parameter	Mean \pm stdev	Mean \pm stdev
C _{max} [nmol/L]	1706.7 \pm 532.0	1950.0 \pm 254.6
T _{max} [h]	0.0	0.0
T _{1/2} [h]	326.0 \pm 58.3	291.5 \pm 37.5
MRT _{disp} [h]	464.3 \pm 85.7	414.5 \pm 54.4

As the transduction kinetics of viral variants should be detectable during *in vivo* studies, AAV2 and rAAV-2E3.v6 were produced with the cargo plasmid pAAV-CMV-Fluc. This plasmid resulted in a single AAV genome expressing firefly luciferase. Both viral variants showed high packaging capacity and equivalent vector yield after equivalent transduction and purification steps. (Table 32). An ELISA assay with immobilized rAAV-2E3.v6 capsids were performed to prove unaltered 2E3 antibody binding. All anti-2E3 antibody variants bound to rAAV-2E3.v6 likewise to monospecific anti-2E3 (Figure 21A) without any cross reaction to AAV2 capsids (Figure 21B). Control experiments proved that rAAV2-E3.v6 and AAV2 were detected by anti-VP antibodies and respective secondary antibody staining (Figure 21C).

Table 32: Yield of AAV variants with Fluc expression plasmid

Viral variant	Packaging capacity [VG/mL]	Vector yield [Capsids/mL]
AAV2-Fluc	$2.28 \times 10^{13} \pm 18.0$	$1.17 \times 10^{14} \pm 3.05 \times 10^{12}$
rAAV-2E3.v6-Fluc	$5.54 \times 10^{13} \pm 4.41$	$4.51 \times 10^{14} \pm 4.96 \times 10^{13}$

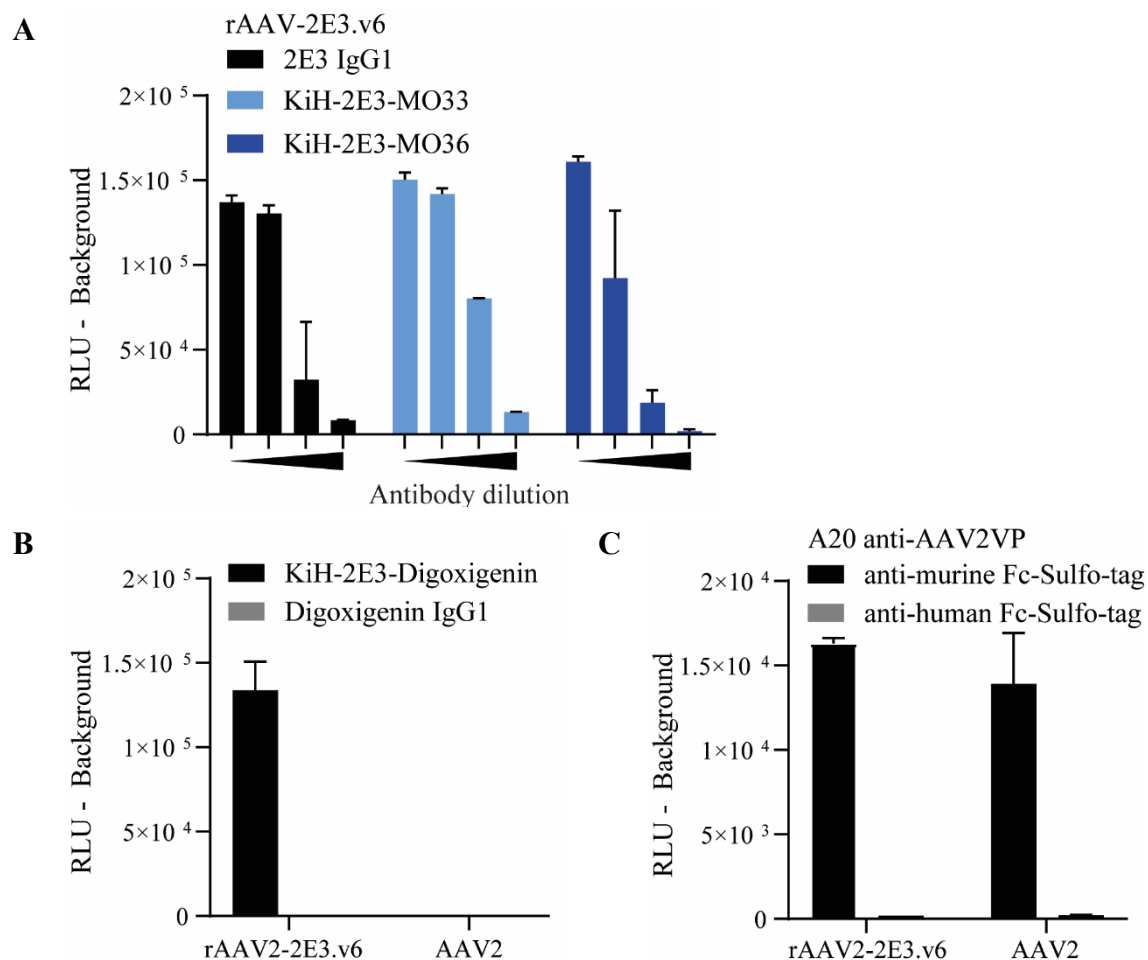


Figure 21: Cargo alterations did not influence antibody binding of viral capsids **A)** ELISA assay of immobilized rAAV-2E3.v6 incubated with monospecific anti-2E3 IgG1 or bispecific antibodies KiH-2E3-MO33 or KiH-2E3-MO36 in serial dilutions (black triangle, 1:500; 1:1000; 1:10,000 and 1:100,000). Data show mean \pm SD. **B)** ELISA assay of immobilized rAAV-2E3.v6 and AAV2 incubated with anti-2E3 IgG1 and KiH-2E3-Digoxigenin (dilution 1:500). Data show mean \pm SD. **C)** Control staining of viral capsids following incubation with A20 anti-VP proteins (Progen, Heidelberg, Germany). Specific binding of secondary antibody (anti-murine FC-Sulfo-tag) was compared to anti-human Fc-Sulfo-tag secondary antibody (MSD® Rockville, MD, USA). Data show mean \pm SD.

HT1080 huFAP cells were transduced with either AAV2 or rAAV-2E3.v6 that were previously incubated with a serial dilution of KiH-2E3-MO36 following the detection of firefly luciferase light signals after 72 h. Significantly high firefly luciferase signals were obtained after AAV2 transduction of 50,000 VG/cell (1.69×10^6 RLU $\pm 3.48 \times 10^4$, $p < 0.05$) compared to 2500 VG/cell (Figure 22A). Firefly luciferase expression levels of HT1080 huFAP cells incubated with rAAV-2E3.v6 were dependent on the dose of KiH-2E3-MO36. The expression peak was measured at 600 bispecific antibodies per viral genome (4.37×10^3 RLU $\pm 1.81 \times 10^3$, $p < 0.001$) (Figure 22B). However, AAV2 mediated transduction resulted in 400 \times higher RLU expression levels at equal amounts of viral genomes per cell. As rAAV-2E3.v6 showed low firefly luciferase signals *in vitro*, it was decided to use high doses of viral genomes (2.0×10^{12} VG per animal) to enable luciferase detection via *In Vivo* Imaging Systems (IVIS).

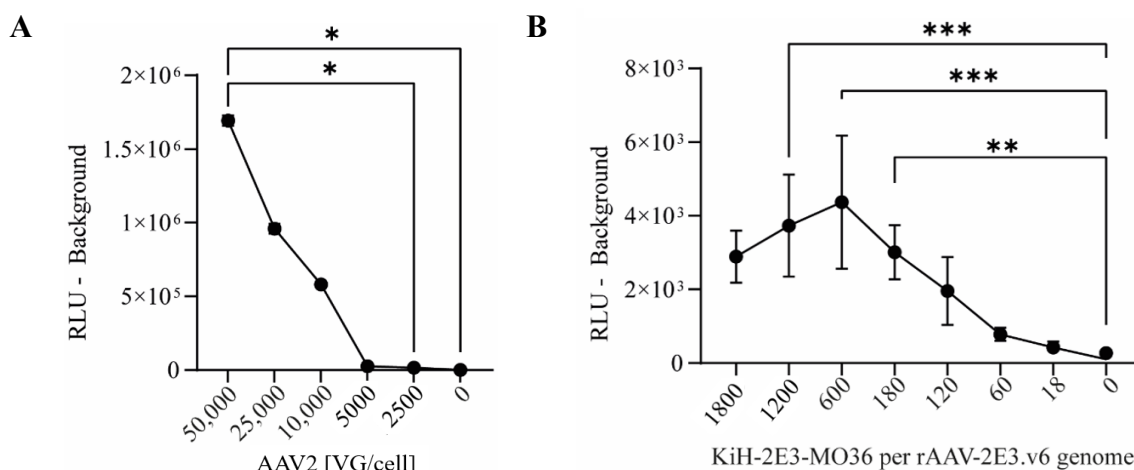


Figure 22: HT1080 huFAP firefly luciferase expression after AAV2 and rAAV-2E3.v6 transduction *in vitro* **A)** HT1080 huFAP expression of firefly luciferase after incubation with dilutions of AAV2 (50,000 to 0 VG/cell), data show mean \pm SD, one-way ANOVA, Uncorrected Dunn's test, * $p < 0.05$. **B)** HT1080 huFAP expression of firefly luciferase after incubation with 50,000 VG/cell rAAV-2E3.v6 complexed with a dilution series of KiH-2E3.v6, data show mean \pm SD of two independent experiments, one-way ANOVA, Uncorrected Dunn's test, * $p < 0.05$; ** $p < 0.01$; *** $p < 0.001$.

3.9 Targeting of rAAV-2E3.v6 reveals tissue detargeting but no tumor targeting

In vivo experiments were conducted at Charles River Discovery Research Services, North Carolina, USA. The study was designed based on *in vitro* data with NSG mice injected with HT1080 huFAP tumors. The animals were divided into the following groups with different

treatments: Group 1 rAAV-2E3.v6:KiH-2E3-MO36; Group 2 rAAV-2E3.v6:KiH-2E3-Digoxigenin, Group 3 AAV2 plus KiH-2E3-Digoxigenin and Group 4 untreated animals (Table 29). Animals of all groups showed minimal loss of body weight and a comparable increase of tumor volume during the study (Figure 23 A, B). Firefly luciferase expression was regularly measured and representative images of each group within days 1 to 18 are shown in (Figure 24). Mice injected with AAV2 showed luciferase expression in the right hypochondriac region after 4 days ($\sim 1 \times 10^5$ photons/s/cm²/sr) and the signal increased until day 18 ($\sim 1 \times 10^6$ photons/s/cm²/sr) (Figure 24). The mean firefly luciferase signals indicated that only animals treated with AAV2 showed significantly increased light signals at day 18 compared to day 1 ($3.33 \times 10^7 \pm 6.50 \times 10^6$ photons/s, $p < 0.05$) (Figure 23C). Mice injected with rAAV-2E3.v6:KiH-2E3-MO36 or rAAV-2E3.v6:KiH-2E3-Digoxigenin showed low-level light signals on the right flank region but no tissue or group-specific light signals (Figure 23C and Figure 24). At the end of the study, animals of groups 1 and 2 were shaved in the upper abdominal region. Dorsolateral and ventral images were taken with a focus on liver and tumor regions to increase photon emission sensitivity. However, no elevated luminescence signals could be detected within any group or region of interest (Figure 23D).

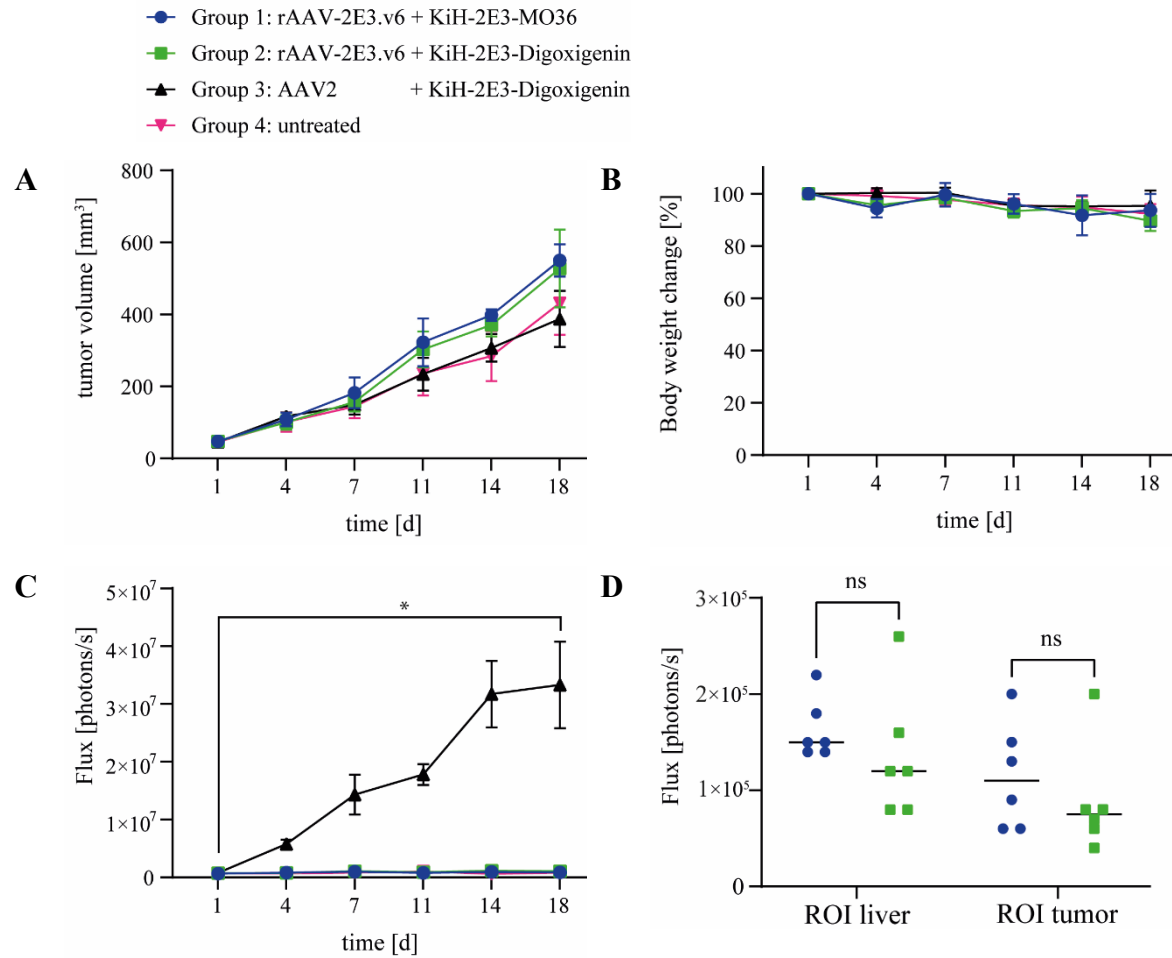


Figure 23: Comprehensive overview of *in vivo* study data A) The tumor volume, B) body weight change, and C) whole body bioluminescence of all animals was measured over 18 days. D) Bioluminescence imaging of liver and tumor of group 1 and group 2 at day 19. Data show mean \pm SD, Mann Whitney test, * $p < 0.05$, ns = non-significant.

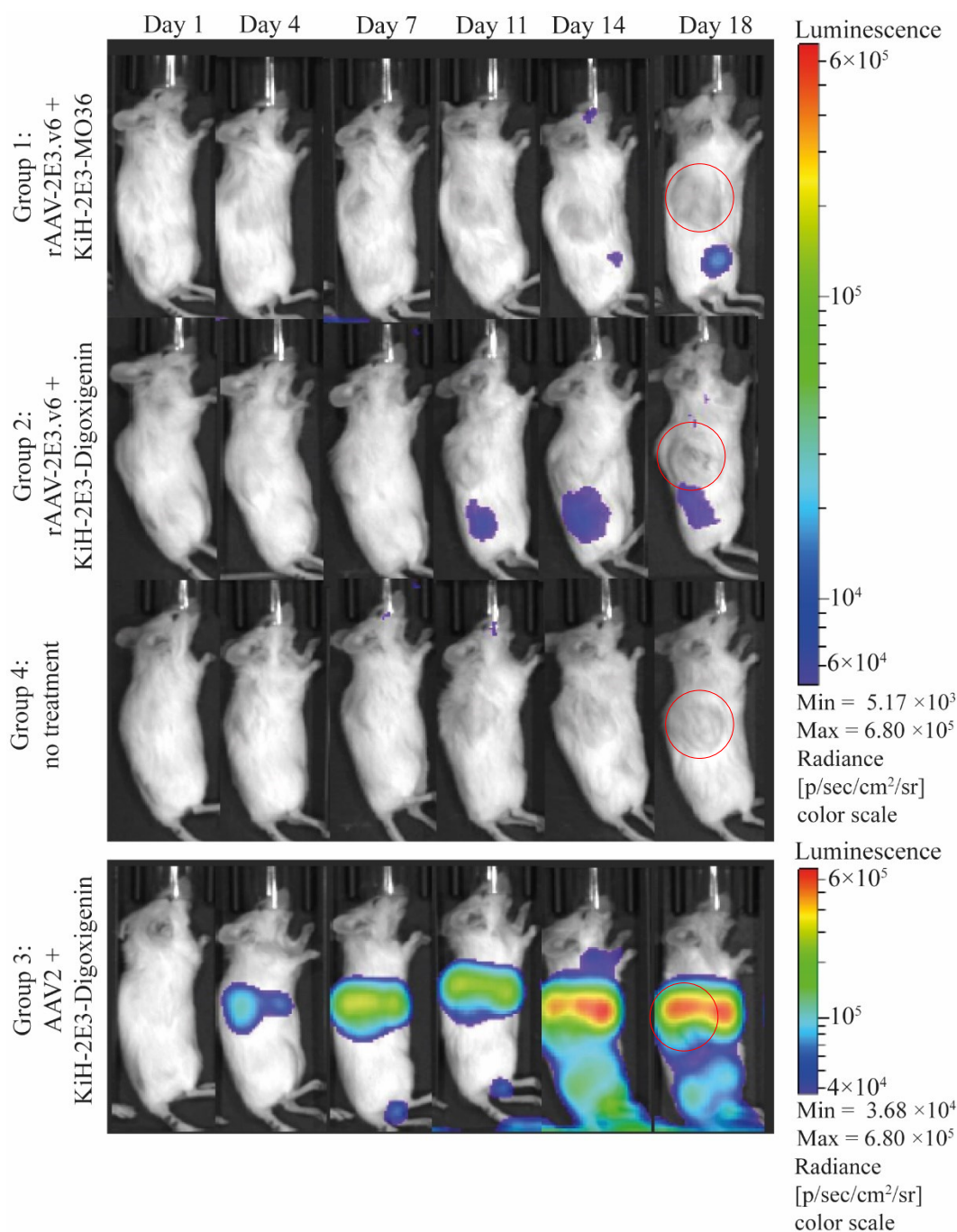


Figure 24: Whole-body bioluminescence imaging of firefly luciferase expression. Animals of all groups received a subcutaneous injection of HT1080 huFAP cells. Group 1 was treated with rAAV-2E3.v6:KiH-2E3-MO36, Group 2 was treated with rAAV-2E3.v6:KiH-2E3-Digoxigenin, Group 3 was treated with AAV2:KiH-2E3-Digoxigenin, and Group 4 received no treatment. Firefly luciferase expression was measured by whole-body bioluminescence imaging and representative images of single animals of each group were shown. Luminescence signals of group 3 were scaled independent from groups 1, 2, and 4 since luminescence signals were incomparatively higher. Tumor formations were exemplarily indicated by red circles on day 18.

At the study endpoint (day 19) the tissues of the liver, lung, heart, and tumor were harvested and divided into three parts 1) qPCR of AAV genomes, 2) luciferase assay of homogenized tissues lysates and 3) immunohistochemistry of FFPE fixed tumors to analyze FAP expression and tumor tissue vascularization.

Significant amounts of viral genomes could only be detected heart ($5.71 \times 10^6 \pm 2.72 \times 10^6$, $p < 0.05$), liver ($7.99 \times 10^6 \pm 4.57 \times 10^6$, $p < 0.01$) and lung lysates ($3.17 \times 10^6 \pm 1.49 \times 10^6$, $p < 0.01$) of group 1 compared to viral genomes detected in respective tissues of group 2. No viral genomes were detected in tumor lysates ($5.21 \times 10^5 \pm 8.99 \times 10^5$, ns) within group 1. The highest amounts of AAV2 genomes could be measured in liver and heart tissues. rAAV-2E3.v6 treated animals showed no detectable viral genomes in any analyzed tissue within group 1 or group 2 (Figure 25A).

Comparable results were obtained after analysis of firefly luciferase activity. Significantly increased luciferase activity per mg protein was observed in animal tissue lysates that were previously treated with AAV2. Heart (median 16.53 ± 11.27 RLU/mg protein, $p < 0.05$) and liver (median 13.73 ± 5.22 RLU/mg protein, $p < 0.01$) but not lung and tumor samples showed increased luciferase signals compared to tissue lysates of animals treated with rAAV-2E3.v6. No luciferase signals were measured in any tissue of the control group 4 (Figure 25B).

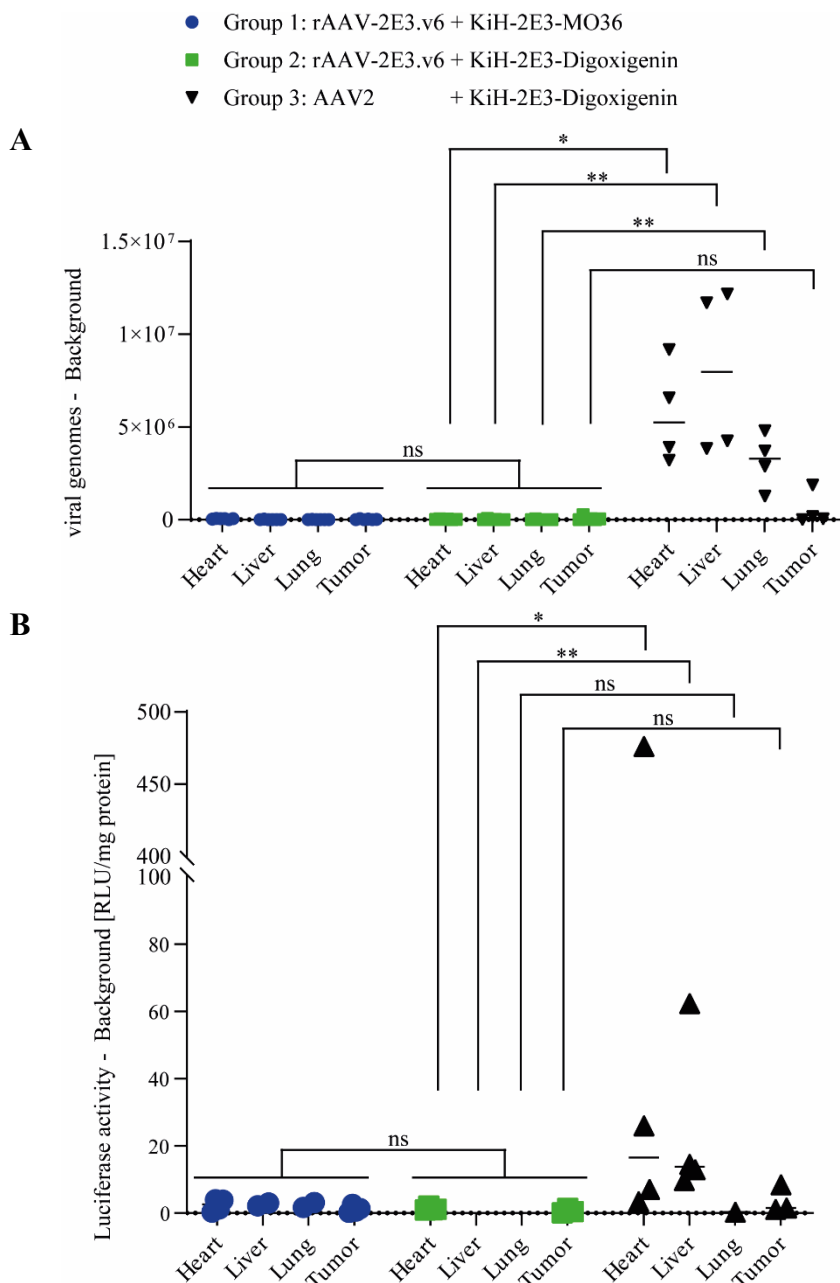


Figure 25: Detection of AAV genomes and luciferase activity in homogenized tissues **A)** Viral genomes could be detected by qPCR in tissue lysates of group 3 (AAV2 + KiH-2E3-Digoxigenin). Signals were normalized to baseline signals of group 4 (untreated animals). Graphs show scattered plot data of individual samples and group median, one-way ANOVA, Uncorrected Dunn's test, * $p < 0.05$; ** $p < 0.01$, ns = non-significant. **B)** Luciferase signals per mg protein were detected only in tissue lysates of group 3. Signals were normalized to baseline signals of group 4 (untreated animals). Graphs show scattered plot data of individual samples and group median, one-way ANOVA, Uncorrected Dunn's test, * $p < 0.05$; ** $p < 0.01$, ns = non-significant.

Immunohistochemistry staining of FFPE fixed tumors proved strong FAP in vital tumor areas independently of the treatment of the four groups (Figure 26A). Tumor vascularization was analyzed by anti-CD31 staining, a marker of vascularization and micro vessels (Wehrhan F. et al. 2011). Tumors showed low-1 vascularization independently of the treatment (Figure 26B). Images of anti-CD31 and anti-FAP stainings of representative tumors of each group showed uneven patches of CD31 expression levels that did not overlap with regions of high FAP expression (Figure 26C). Low vascularization levels might have resulted in low penetration of AAVs and antibodies into tumor tissues and therefore have prevented efficient tumor targeting *in vivo*.

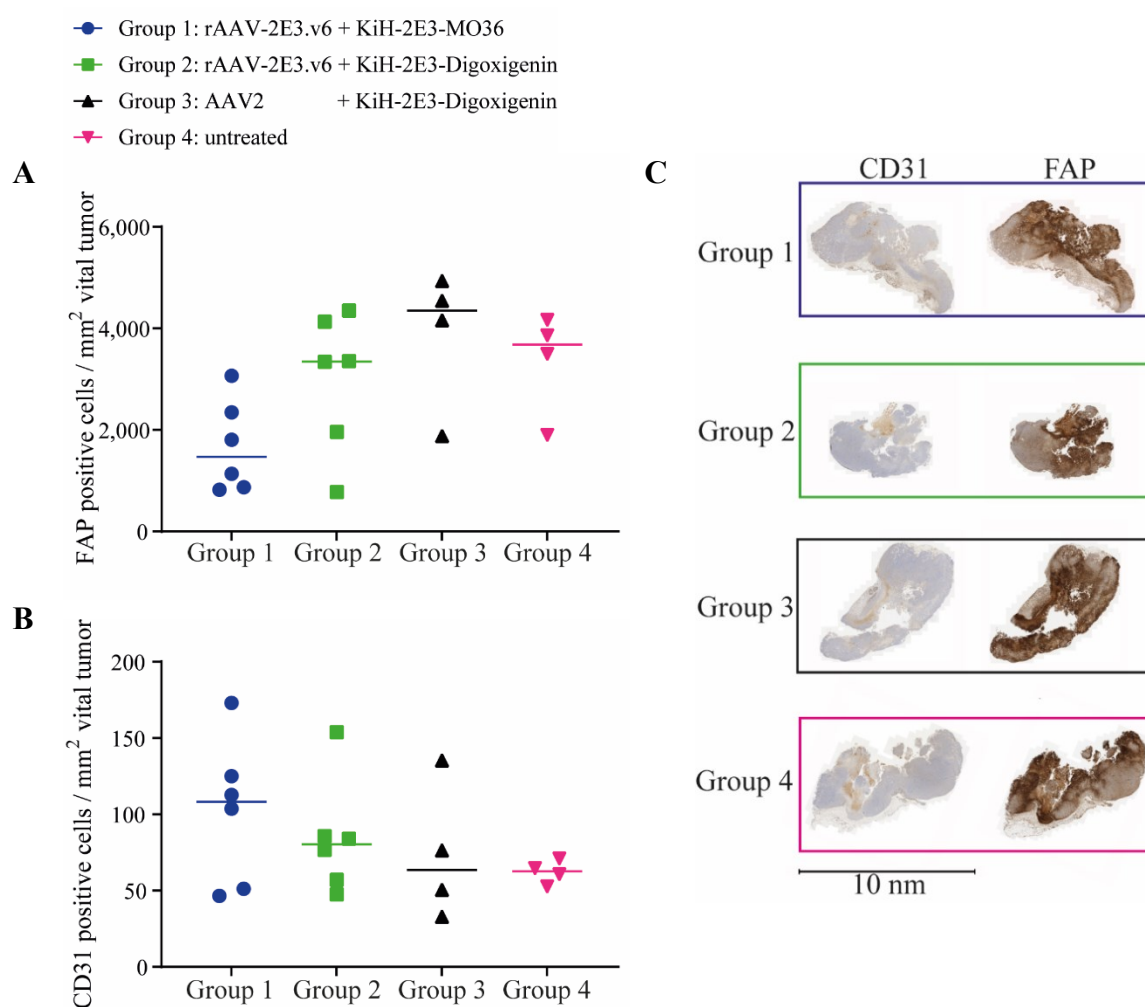


Figure 26: HT1080 huFAP tumor tissues showed strong FAP expression but low vascularization Immunohistochemistry analysis of HT1080 huFAP tumor tissues. **A)** FAP expression within vital tumor areas of individual groups. Individual samples and the group median are shown. **B)** CD31 positive tumor areas of individual groups. Individual samples and the group median are shown. **C)** Overview of anti-CD31 and anti-FAP immunohistochemistry stainings of one representative FFPE-fixed tumor per group. Scalebar 10 nm.

4 Discussion

4.1 Impact of capsid design of rAAV-2E3 viral variants on production and transduction properties

To develop a modular AAV retargeting platform, novel AAV2 based viral variants were designed and produced. The aim was to insert a short PCSK9 derived epitope named 2E3 into five capsid regions to abrogate HSPG or integrin $\alpha 5\beta 1$ binding. By this detargeted viral variants with a tag for antibody binding were developed. Four rAAV-2E3 viral variants (rAAV-2E3.v2, -.v4, -.v5 and -.v6) were producible with epitopes within distinct capsid surface structures. ELISA assays proved that the epitopes were exposed to the capsid surface and therefore allowed anti-2E3 antibody binding. The epitope was detectable in every VP protein, indicating exposure of 60 epitopes per viral capsid. rAAV-2E3.v6 was proven by EM to contain viral capsids of the typical icosahedral structure (Atchison et al. 1966; Xie et al. 2002). Along with the electron microscopy and ddPCR data and in agreement with our previously evaluated production protocol, novel rAAV variants were produced with high packaging capacity and low impurities. A strikingly high excess of viral capsids in comparison to vector yield was analyzed based on ELISA measurements. According to the established purification protocol, mostly full vectors should be purified after iodixanol-based ultracentrifugation (Strobel et al. 2015). It might be possible that those capsid-modified AAVs were not suited to be compared with an AAV2 standard provided by the AAV2 Titration ELISA kit. Other serotype-independent methods such as capillary electrophoresis SDS in combination with ddPCR or liquid chromatography–mass spectrometry might be better-suited methods to measure viral capsids and genomes precisely.

Integrin $\alpha 5\beta 1$ binding and internalization is mediated by the AAV2 capsid motif NGR (511-513) (Asokan et al. 2006). Therefore, the region 491 to 514 was chosen for substitutions with GS-linker framed TPPRYRAD epitope (rAAV-2E3.v2 and rAAV-2E3.v3). Substitution of four capsid amino acids (510 to 514) with 16 epitope amino acids resulted in rAAV-2E3.v3 that was not producible. It is assumed that a short sequence exchanged with a large epitope within this region may interfere with efficient capsid assembly. As this capsid variant was not producible, it was excluded from further experiments. The substitution of nine capsid amino acids (491-501) next to the NGR motif with the same 2E3 epitope was well tolerated (rAAV-2E3.v2) and resulted in viral variants with desired detargeting on every tested

cell line *in vitro*. However, heparin binding was not impaired for this variant compared to AAV2. Therefore, it is assumed that this viral modification impaired further co-receptor binding, such as integrin $\alpha 5\beta 1$ or AAVr. This might influence viral uptake or viral trafficking. To prove this hypothesis further experiments are needed to examine if receptor binding is impaired, and which specific receptor may be involved in the uptake and transport of this viral variant. (Kuklik et al 2021).

The variable loop eight and especially the position 587 of the AAV2 capsid is known to tolerate capsid modifications that interfere with HSPG binding (Ried et al. 2002; Vihinen-Ranta et al. 2002; Xie et al. 2002; Gurda et al. 2013; Büning and Srivastava 2019; Kim et al. 2019). This study confirmed that epitope insertions between eight to sixteen amino acids (rAAV-2E3.v4 and rAAV-2E3.v5) as well as large substitutions of seven capsid amino acids with seventeen new amino acids (rAAV-2E3.v6) were well tolerated resulting in viral vectors that were producible in high titers. Increasing alterations of loop eight resulted in severely reduced transduction efficiency of the capsids. AAV2 did infect HEK 293, B16-F10, FL8-3B, and CT26-CL25 cells most efficiently. Decreased transduction was observed with AAV2-2E3.v5 (eight amino acids insertions) and AAV2-2E3.v4 (sixteen amino acids insertions). Although loop eight is altered in both variants, impaired heparin binding could not be observed. Differences in expression levels may be due to lower heparin affinity, impaired co-receptor binding, or impaired intracellular trafficking of modified viral variants. The most severely impaired transduction was observed with the seventeen amino acid substitution of rAAV-2E3.v6, as no cargo expression after incubation with this viral variant could be measured even at high titers. rAAV-2E3.v6 showed significantly impaired heparin binding compared to AAV2. It is assumed that the exchange of the two amino acids R585 and R588 of the five amino acid-HSPG motif (R484, R487, R585, R588, and K532) with a sequence of neutral charge abolishes heparin binding and by this infection (Opie et al. 2003; Grieger et al. 2006).

In conclusion, four out of five rAAV-2E3 viral capsid designs were producible with an exposed 2E3 tag on the capsid surface. Modified capsids show altered and even abolished transduction in extents that correlated with the modification level of the capsids. Transduction characteristics of individual variants were not predictable (Kuklik et al. 2021).

4.2 Design and production of bispecific antibodies

The modular targeting mechanism established in this study required convertible bispecific adapters to bind 2E3 modified viral capsids as well as the individual target receptors. For this purpose, knob-into-hole bispecific antibodies were designed which shared the same 2E3 binding arm ('knob') and differed in their receptor binding arm ('hole') as described earlier (Labrijn et al. 2013). An IgG-based bispecific format was chosen, as the Fc-part supported not only stability, serum half-life (Johnson et al. 2010; Brinkmann and Kontermann 2017) but also allowed for efficient purification via established protocols (Bauer et al. 1980; Grodzki and Berenstein 2009; Fishman and Berg 2019). As Fc-effector functions were not needed in this study, C_H2 point mutations L234A/L235A (Xu et al. 2000) were inserted into all antibody Fc-domains (Kuklik et al. 2021).

Four bispecific knob-into-hole bispecific antibodies were developed and purified, all containing the 2E3 binding arm but different receptor or molecule binding: FAP (MO33 and MO36), PD-L1 (avelumab), or Digoxigenin (isotype control). The bispecific antibody production protocol was established with KiH-2E3-MO33, KiH-2E3-MO36, and KiH-2E3-Digoxigenin. According to quality control experiments and established production protocols (Labrijn et al. 2013; Goulet et al. 2018), clean bispecific antibody fractions of desired size and equal distribution of light chains were purified. HPLC analytical SEC revealed clean productions with a single peak around 143 to 156 g/mol and constant mass distribution, indicating that clean antibody fractions were purified. KiH-2E3-Digoxigenin productions showed a slight shoulder in every production, which could not be removed by CEX or SEC and may indicate a tendency of this antibody to form aggregates or fractions with diverse glycosylation patterns. However, the antibody showed a mass of 146 g/mol was proven to bind 2E3 as well as BSA-conjugated digoxin. Aggregations may be overcome by the adjustment of the storage buffer. Mass spectrometry could be performed to prove the production of 1:1 paired knob-into-hole antibodies and a consistent glycosylation pattern.

Bispecificity of antibodies was proven by an HTX bio-layer interferometry bridging assay as well as in cell culture experiments. It was shown by flow cytometry staining of target cells and ELISA experiments, that all bispecific antibodies retain specific target binding at comparable levels as their respective parental monospecific antibodies. Finally, it was visualized that bispecific antibodies (KiH-2E3-MO33 and KiH-2E3-MO36) induced receptor internalization in cell culture within 30 min after incubation. Red fluorescence signals indicated that

internalization occurred in cell compartments with low pH. These were very likely endosomes, due to their cellular localization, acidity, and uptake of extracellular proteins. This confirmed previous findings reporting FAP uptake by dynamin-dependent endocytosis that rapidly occurred after 20 min (Baum et al. 2008; Fischer et al. 2012; Ruger et al. 2014). With those experiments, it was shown that functional antibodies were produced with desired bispecific binding characteristics and the induction of receptor-mediated endocytosis (Kuklik et al. 2021).

Having established a bispecific-antibody production protocol, results were transferred to a KiH-2E3-PD-L1 production. Bispecific antibodies proved to bind PD-L1 receptors and 2E3 epitopes. Flow cytometry staining of HT1080 huFAP expressing cells revealed native PD-L1 expression next to stably transfected FAP expression. Therefore, this cell line was suited for PD-L1 retargeting experiments. The purified bispecific antibody was successfully used in retargeting experiments of rAAV-2E3.v6 to PD-L1 HT1080 huFAP expressing cells. It was concluded that bispecific antibodies were produced. Furthermore, antibody-PD-L1 binding proved to induce receptor internalization in HT1080 cells as described earlier (Park et al. 2018; Teruya et al. 2019; Jin et al. 2020; Kuklik et al. 2021).

In summary, the design, production, purification, and quality control of bispecific antibodies was established, which allowed flexible production of different bispecific antibodies based on a knob-into-hole scaffold. The produced antibodies showed specific epitope and target receptor engagement comparable to parental monospecific antibodies.

4.3 Establishment of a highly specific retargeting mechanism based on bispecific antibodies binding rAAV-2E3 viral variants and FAP receptors

The retargeting mechanism was established *in vitro* using HEK 293 and HT1080 cells stably expressing huFAP (Park et al. 1999). KiH-2E3-MO36 was titrated against dilutions of rAAV-2E3.v2, -.v4, -.v5 and -.v6. rAAV-2E3.v4 and rAAV-2E3.v5 complexed with bispecific antibodies did show high background expression and a retargeting effect could not be observed. However, high bispecific antibody concentrations correlated with a trend of reduced transduction, while AAV2 preincubated with bispecific antibodies did not show altered transduction. High amounts of bispecific antibodies bound to rAAV-2E3 capsids may

have formed high molecular weight complexes, which were too big for internalization and therefore blocked transduction (Kuklik et al. 2021).

It was not possible to reverse the abolished rAAV-2E3.v2 transduction to FAP expressing cells by bispecific antibody binding. It can be excluded, that rAAV-2E3.v2 showed blocked transduction because of impaired HSPG binding, as rAAV-2E3.v2 showed no altered binding to heparin columns compared to AAV2. Potentially, the 2E3 substitution influenced the NGR motif negatively so the binding of integrin $\alpha 5\beta 1$ or other co-receptors needed for internalization was blocked. This modification might have also impacted the trafficking and unpackaging of the viral variants and hindered, therefore, gene expression. The trafficking of AAV variants could be analyzed in further experiments by immunofluorescence staining and microscopy analysis. The presence of viral genomes within the cell could be measured by qPCR.

It was shown that the AAV2 capsid region 491 to 514 was sensitive to large substitutions which had a drastic effect on produced rAAV-2E3 variants. Furthermore, simple insertions of epitopes within loop eight R587 did not overcome HSPG binding, and retargeting was not possible. Therefore, the variants rAAV-2E3.v2, -.v4, and -.v5 did not meet the criteria of both de- and retargeting and were not further analyzed in this study.

Uncoupled rAAV-2E3.v6 did not transduce either HEK or HT1080 huFAP expressing cells but increasing proportions of GFP expressing cells and respectively MFIs were directly connected to dilutions of KiH-2E3-MO36. This effect was reproduced with KiH-2E3-MO33:rAAV-2E3.v6 on both cell lines. Further control experiments revealed that transduction required expression of FAP and specific antibody-receptor binding, as isotype antibodies did not alter transduction levels. It was concluded that a FAP specific antibody-media retargeting mechanism was established. Higher amounts of transduced cells were generally observed with increased levels of AAVs per cell. The used number of viral genomes per cell (5000 to 50.000 VG/cell) used in this study was in line with previously published doses of engineered AAVs (Ried et al. 2002; Zhang et al. 2019; Feiner et al. 2020).

The described retargeting mechanism was dependent on an optimal ratio of bispecific antibodies between 180 and 600 per viral genome and the used bispecific antibody. This retargeting effect was visualized in a dose-response curve. Insufficient amounts of bispecific antibody per viral genome (<120:1) decreased transduction possibly due to inadequate binding

events. High amounts of antibody:viral genome ratios (>1200:1) decreased transduction may be due to extreme excess of unbound bispecific antibodies blocking FAP receptors, as unbound antibodies have not been depleted after complexing with rAAV-2E3 capsids. Additionally, it was possible that excessive amounts of bispecific antibodies could form large molecular complexes that did block cellular uptake. However, an excess of bispecific antibodies for efficient retargeting was necessary. Based on these data and the antibody binding curves, it was concluded that the 2E3 epitope on viral surfaces might not be bound with high affinity and that cell targeting demanded available additional adaptors to promote efficient cellular binding (Kuklik et al. 2021). Additionally, it is very likely that the required dose of antibodies must be increased if the AAV batch contains higher amounts of empty capsids.

The bispecific antibody KiH-2E3-MO36 leads to higher amounts and MFIs of GFP positive cells compared to KiH-2E3-MO33. Both bispecific antibodies enabled retargeting to huFAP as well as muFAP expressing cells. But the targeting of muFAP was significantly reduced compared to huFAP. Such differences may be related to distinct FAP epitopes and consequently, affinities as already described for MO33 (Brocks et al. 2001). Differences in transduction may furthermore be influenced by lower expression levels of muFAP compared to huFAP. Affinities of bispecific antibodies could be measured by Biacore affinity measurements of immobilized AAV-2E3.v6 capsids. ddPCR in combination with flow cytometry staining could be used to measure muFAP and huFAP transcripts and cell surface receptor densities of different cell lines (Kuklik et al. 2021).

Specific KiH-antibody interaction with either 2E3 epitopes as well as huFAP was proven by competition experiments. Soluble 2E3 epitopes successfully competed for bispecific antibody binding and by this inhibited retargeting of rAAV-2E3.v6 in a dose-dependent manner, while mutated epitopes showed no effect on cellular targeting. This proved, that bispecific antibody retargeting was exclusively dependent on 2E3 epitope binding. BIBH1 was described as an efficient huFAP but not a muFAP binding antibody (Hofheinz et al. 2003; Tahtis et al. 2003). Competition with BIBH1 strongly inhibited KiH-2E3-MO33 huFAP targeting, inhibited KiH-2E3-MO36 huFAP targeting moderately, and showed no effect on muFAP targeting. BIBH1 binding may reduce available FAP receptors by inducing internalization or overlapping epitopes with MO33. In conclusion, it was shown that retargeting was highly specific for 2E3 epitopes and binding of both human and muFAP and were likely influenced by targeted epitope and affinity. This targeting mechanism was independent of

HSPG binding, but it could not be excluded that binding of co-receptor, such as integrin $\alpha 5\beta 1$, were still important for internalization (Kuklik et al. 2021).

Systemically administered AAV gene therapies suffer from a high prevalence of AAV binding antibodies in humans that inhibit optimal therapies (Moskalenko et al. 2000; Huttner et al. 2003; Mingozzi et al. 2013; Mingozzi and High 2017; Kuranda et al. 2018). Therefore, the development of AAV variants that escape antibody neutralization, is very important for gene therapy approaches. Even though shielding from neutralizing antibodies was not declared objective of the viral capsid modifications that were designed in this study, it was analyzed, if rAAV-2E3.v6 complexed with KiH-2E3-MO36 tolerated higher amounts of human IVIGs compared to AAV2. Dose-response curves of IVIGs showed slight shifts of GFP expressing cells transduced with rAAV-2E3.v6:KiH-2E3-MO36 and AAV2. But a prominent effect was not observed, even though the position 587 was described as an immunogenic position and ligand insertions have successfully abolished antibody neutralizing effects (Huttner et al. 2003).

As relevant differences of MFIs and transduced cells were observed after incubation with AAV2 or rAAV-2E3.v6 with and without KiH-2E3-MO36 proportions, the kinetics of viral uptake, transcripts, and protein expression was analyzed over 72 h.

High AAV2 and KiH-2E3-MO36:rAAV-2E3.v6 genome uptake were measured within 6 to 24 h after incubation leading to a peak of transcript synthesis at 24 h and the consequent peak of protein expression at 48 h after incubation. As rAAV-2E3.v6 genomes were measured in cell lysates close to the detection limit at any time point, it was concluded that the cellular entry of sole rAAV-2E3.v6 was blocked and was only restored with KiH-2E3-MO36 induced FAP binding. 2.5 times more AAV2 genomes than KiH-2E3-MO36:rAAV-2E3.v6 genomes were found after 24 h, resulting in consequently higher transcript and protein expression levels. If differences in transcript levels are influenced by altered trafficking or unpackaging of capsids is unknown yet. The viral trafficking could be analyzed by fluorescence microscopy staining of viral capsids and various cellular compartments at different time points. Further co-incubation with various inhibitors influencing viral uptake and cellular transport and analysis by fluorescence microscopy as described in (Fischer et al. 2012) would reveal the cellular trafficking in detail. Even though statistical analysis did not show significant differences in GFP expression levels induced by AAV2 or KiH-2E3-

MO36:rAAV-2E3.v6, a clear and reproducible trend of higher AAV2 transduction was observed. Increased levels of AAV2 uptake in comparison to retargeted rAAV-2E3.v6 could be explained by differences in cellular attachment. HSPG might show expression levels and high amounts of direct viral attachment sites compared to FAP that is indirectly bound of the viral through a bispecific antibody.

The experiments showed, that a novel rAAV-2E3.v6 viral variant was developed that does not infect cells. This blocked transduction was likely due to inhibited HSPG binding. The use of bispecific antibodies, such as KiH-2E3-MO36, reversed cellular binding. Internalization kinetics of natural transduction and retargeted viral transduction wash were observed to be equal. Higher AAV2 expression levels were derived from higher uptake of AAV2 genomes in comparison to rAAV-2E3.v6:KIH-2E3-MO36. If further co-receptors are needed for internalization of rAAV-2E3.v6 is unknown as well as the internalization pathway of retargeted viral variants. The internalization pathway and uncoating of the modified viral variants may further influence viral genome expression.

4.4 Modular Fab-arm exchange enabled rAAV-2E3.v6 retargeting of PD-L1 receptors

After a successful FAP targeting system was established based on rAAV-2E3.v6 and bispecific antibodies, the system was transferred by simple ‘Fab-arm exchange’ towards the membrane-anchored protein PD-L1. HT1080 huFAP cells were used in these experiments that were known to express PD-L1 natively (Park et al. 2018; Teruya et al. 2019) in contrast to previously used stably transfected FAP. Successful rAAV-2E3.v6 PD-L1 retargeting was observed at bispecific antibody per viral genome ratios similar to doses observed for rAAV-2E3.v6 retargeting by KiH-2E3-MO36 and KiH-2E3-MO33. Within direct comparison to KiH-2E3-MO36 mediated FAP targeting, lower proportions of transduced cells and MFIs were observed for PD-L1 retargeting of rAAV-2E3.v6. But the amounts of transduced cells by KiH-2E3-PD-L1:rAAV-2E3.v6 are in line with GFP positive cells after incubation with KiH-2E3-MO33:rAAV-2E3.v6. Therefore, GFP expression levels may not exclusively result from differences in cell surface receptor expression levels but also receptor affinity and receptor internalization rates.

By using simple 'Fab-arm exchange' it was possible to reuse the viral variant rAAV-2E3.v6 for retargeting towards a different cell surface receptor PD-L. The retargeting protocol could be directly transferred to the new bispecific antibody without modifications.

4.5 The developed retargeting mechanism is not directly conferrable to *in vivo* models

Murine xenograft models injected with HT1080-huFAP cells were developed, to analyze rAAV-2E3.v6 detargeting along with KiH-2E3-MO36:rAAV-2E3.v6 retargeting *in vivo*. It was proven that NSG mice tolerated subcutaneously injected HT1080 huFAP cells independently of the injected number of cells. Cells at any injected concentration formed fast-growing tumors within nine days, which was in line with previous findings (Weng et al. 2012). Tumors showed strong expression of huFAP in the end of the study. It was decided to use the lowest number of injected HT1080 huFAP cells for further *in vivo* experiments, as this amount was proven to reliably induce tumor formation with a size not exceeding 2000 mm³ until the end of the study. This provided a sufficient time window to observe AAV-induced reporter plasmid expression.

The PK parameters of bispecific antibodies KiH-2E3-MO33 and KiH-2E3-MO36 were analyzed to choose the best-suited antibody for *in vivo* experiments. Both antibodies showed similar PK- parameters with a half-time in line with previously reported parameters of IgGs (Kontermann 2011; Ryman and Meibohm 2017; Liu 2018; Basu et al. 2020). As PK parameters did not significantly differ among both antibodies, it was decided to use KiH-2E3-MO36 in further *in vivo* experiments. This antibody in combination with rAAV-2E3.v6 has robustly shown higher transduction signals according to flow cytometry data.

As rAAV-2E3.v6 mediated cargo expression should be detectable *in vivo* over time, firefly luciferase was chosen as reporter gene. Due to the size of ITRs, CMV promoter, and firefly luciferase (2.8 kb), single-stranded viral vectors were produced. Binding properties of KiH-2E3 bispecific antibodies to this new batch of rAAV-2E3.v6 was successfully confirmed by ELISA. Detection of firefly luciferase of HT1080 huFAP cells incubated with AAV2 or KiH-2E3-MO36:rAAV-2E3.v6 confirmed cargo functionality. AAV2 transduction resulted in 400 × upregulated transgene expression levels compared to KiH-2E3-MO36:rAAV-2E3.v6. Due to the big gap in expression levels, it was decided to use a high dose of rAAV-

2E3.v6 viral genomes per mouse (2.0×10^{12} VG) to ensure detection of possibly faint expression signals.

The retargeting mechanism was challenged *in vivo* by an intravenous injection of an upscaled ratio of rAAV-2E3.v6:KiH-2E3-MO36 into HT1080 huFAP tumor- mice. To discriminate retargeting from unspecific tissue infection, KiH-2E3-Digoxigenin:rAAV-2E3.v6 was chosen as negative control. AAV2 mixed with KiH-2E3-Digoxigenin was used as positive control and to exclude any side effects induced by bispecific antibodies. AAV2 induced strong firefly luciferase expression in the right hypochondriac region 4 days after injection but rAAV-2E3.v6 bearing expression was not observed in any group at any time point. Light-sensitive close-up images of liver and tumor regions did not detect luciferase signals.

Neither increased rAAV-2E3.v6 viral genomes nor firefly luciferase activity could be measured in any tissue lysate. These data indicate that rAAV-2E3.v6 is a viral variant with completely abolished tropism. FAP-specific retargeting could not be shown by coupling to KiH-2E3.v6 *in vivo*. The lack of firefly luciferase expression of rAAV-2E3.v6 cannot be related to inactive cargo expression, as AAV2 induced firefly luciferase expression was detectable in liver and heart tissue and viral genomes were detectable in liver, heart, and lung tissue. These data confirmed the AAV2 tropism described earlier (Xiao et al. 1996, 1997, 1998a; Fisher et al. 1997; Snyder et al. 1997; Bartlett et al. 1998; Arruda et al. 2005; Hacker et al. 2005; Palomeque et al. 2007). A single heart lysate showed upregulated luciferase expression levels within group three. As every tissue was divided into three parts for qPCR, luciferase assay, and histology, it could occur that different tissue areas were compared with unequal viral genome distribution. As all animals received dosing based on one master mix per group, it can be excluded, that single animals received different viral dosing.

Based on this data, it can be concluded, that rAAV-2E3.v6 is a novel viral variant that was not able to transduce heart, liver, lung, tumor, or likely any other murine tissue. However, it is yet unclear which tissue absorbs and consequently degraded rAAV-2E3.v6 and antibody samples. This could be analyzed by further *in vivo* experiments and the analysis of multiple tissues such as spleen, kidney, or tissue of the digestive system.

Tumor FAP expression was confirmed at the end of the study, but only low-level expression of the vascularization marker CD31 was measured by histology. This raises the possibility,

that the small tumors at the time of viral injection were not sufficiently vascularized and by this not accessible for binding of antibody:viral complexes.

The *in vitro* established retargeting mechanism based on KiH-2E3-MO36 could not be transferred to the *in vivo* model. Several factors of this experiment should be examined and improved, such as the chosen *in vivo* model and the stability of the antibody:viral complex. First, it should be analyzed, if the HT1080 huFAP derived tumor is well vascularized at the time of dosing and by this accessible for intravenously injected antibody:viral complexes. This could be analyzed by immunohistochemistry of the vascularization marker CD31 of tumors at different time points after cellular injection. HT1080 cells are described to show vascularization and neo-vessels through the entire tumor tissue and even express angiogenic markers, but all these data were measured 20 to 24 days after cellular injection (Misra et al. 2012; Weng et al. 2012). If Ht1080 tumors already show vascularization after one week of growth is yet unknown but a necessity for tumor targeting.

Secondly, the stability of KiH-2E3-MO36:rAAV-2E3.v6 complexes should be measured, which could be done by Biacore affinity measurements of immobilized AAV-2E3.v6 capsids. Given the fact that efficient retargeting *in vitro* was only achieved in excess of bispecific antibodies and low and defined volume, it is likely that not enough bispecific antibodies are in proximity to rAAV-2E3.v6 *in vivo*. KiH-2E3-MO36:rAAV-2E3.v6 complexes may dissolve quickly in the vascular system with no change to form new complexes. The KiH-2E3-MO36 antibody could be modified by affinity maturation for FAP and 2E3 binding. Matured bispecific antibodies in combinations of high and low antigen affinity should be tested within *in vivo* experiments in combination with rAAV-2E3.v6 to analyze antibody:viral complex stability and receptor interaction.

KiH-2E3-MO36:rAAV-2E3.v6 complexes must be in contact with FAP receptors long enough for receptor-mediated endocytosis and this condition might not be fulfilled, if the dosing is performed intravenously. In comparison, intratumoral injection could be performed to analyze, if uptake of KiH-2E3-MO36:rAAV-2E3.v6 into tumor cells is possible in general. Uptake of bispecific antibody:rAAV complexes could also be analyzed in older and therefore better vascularized tumors *in vivo*. Animals bearing a tumor for 24 days could be injected with AAVs and sacrificed after three to five days. This short incubation time would

not allow detection of a firefly luciferase kinetic. However, viral genomes within different tissue lysates could be detected by qPCR.

Successful *in vivo* retargeting of capsid modified AAV by multispecific antibody binding was successfully shown in 2019. The study shows targeting of liver, intestine and pancreas tissue using a similar mechanism as described in this study (Kyratsous et al. 2019). These data support the functionality of established mechanism, that has the potential to show successful *in vivo* retargeting after antibody affinity maturation in combination with targeting accessible antigens.

4.6 Conclusion

In this study, novel capsids of AAV2 were rationally designed, produced, and characterized. The AAV2 capsid modification based on PCSK9 derived epitopes (2E3) and resulted in defeated tropism. By using bispecific antibodies that were binding both capsid inserted epitope and a set of target receptors (FAP or PD-L1), a modular targeting mechanism was developed *in vitro* (Kuklik et al. 2021).

AAV capsids areas were modified that were known to be crucial for viral host cell interaction and internalization. However, the impact of epitope insertions and viral transduction characteristics were not predictable. In this study, one of five rational capsid designs (rAAV-2E3.v6) met the criteria of detargeting and retargeting to novel receptors by bispecific antibody binding. The abolished tropism was directly linked with the absence of two amino acids R585 and R588 of the HSPG binding motif (Summerford and Samulski 1998; Kern et al. 2003; Zhang et al. 2013) that resulted in lost heparin binding and even abolished tissue targeting *in vivo*. However, it is unknown if further co-receptor binding was altered by the capsid modification (Kuklik et al. 2021).

Several bispecific antibodies were successfully developed and produced that were proven to simultaneously bind 2E3 epitopes and the cell surface receptors FAP, PD-L1 or the control molecule Digoxigenin. However, the affinity to neither 2E3 epitope nor receptor was measured and binding strength might be improved in future to optimize efficient target binding. The bispecific antibody production was a straightforward approach. It enabled the translation of available antibody sequences into a KiH format, that allowed fast production via well described purification protocols (Bauer et al. 1980; Grodzki and Berenstein 2009; Labrijn et al. 2013; Fishman and Berg 2019; Kuklik et al. 2021).

The cell surface receptors FAP and PD-L1 were chosen as targets, as both are disease relevant markers and have not been used as AAV gene therapy targets before. Antibodies binding FAP or PD-L1 were well characterized, and target receptors were known to internalize upon antibody binding (Rettig et al. 1988; Brocks et al. 2001; Mersmann et al. 2001; Hofheinz et al. 2003; Scott et al. 2003; Tahtis et al. 2003; Fischer et al. 2012; Contreras-Sandoval et al. 2014; Collins and Gulley 2018; Li et al. 2018; Gurung et al. 2020; Jin et al. 2020). Receptor internalization upon antibody binding was considered as an important target characteristic to allow for retargeted AAV infections. However, the precise internalization pathway was not investigated in this study.

PD-L1 is a marker that is highly expressed in cancer tissue and tumor microenvironment (Ghebeh et al. 2006; Patel and Kurzrock 2015; Cheng et al. 2018; Li et al. 2019) and FAP is solely expressed in diseased adult tissue, e.g., the tumor microenvironment (Garin-Chesa et al. 1990; Busek et al. 2018). Therefore, the described approach has the potential to target the main proportion of solid human cancers (Kuklik et al. 2021).

A specific retargeting mechanism was established based on FAP binding and was converted to PD-L1 targeting *in vitro*. The transduction of rAAV-2E3 complexed with bispecific antibody was dependent on the 2E3 capsid epitope and cell surface receptor antibody binding. The viral transduction was independent of HSPG interaction. However, it is unknown, if further co-receptors were needed for internalization. The destruction of naturally evolved HSPG binding and retargeting via novel receptors resulted in significantly lower transduction rates compared to natural AAV2 infection. This might be due to abundantly expressed HSPG on the cell surface with various interaction sites on AAV2 capsids. In contrast with the retargeting mechanism that is dependent on assumingly fewer expressed cell surface receptors as well as the correct interaction of 2E3 epitope, antibody, and receptor at the same time. The retargeting approach was transferrable to PD-L1 cell surface receptors and seemed to be independent of stably transfected or native receptor expression. Therefore, it is supposed that various internalizing cell surface receptors might be suitable for a bispecific antibody- retargeting approach. By this, a modular and flexible targeting system was developed for *in vitro* applications. The retargeting success will depend on receptor internalization rates, receptor density, epitope, and antibody affinity (Kuklik et al. 2021).

In vivo experiments confirmed rAAV-2E3.v6 detargeting from animal tissues especially liver that is the main targeted organ of wt AAV2 (Xiao et al. 1998a). However, bispecific antibody:viral complexes did not result in transduced tumor tissues. Further improvements of the system could enable *in vivo* tumor targeting by modifying antibody 2E3 affinity, the timing of dosing at optimal tumor vascularization levels or examination of different *in vivo* administration routes.

The development of an advanced gene therapy approach for clinical settings would require the analysis of anti-2E3 antibodies binding human PCSK9. It must be excluded that PCSK9 and related protein signaling pathways that are influencing the lipoprotein homeostasis and low-density lipoprotein concentrations are not influenced by this gene therapy approach (Schiele 2013; Weinreich and Frishman 2014). This might require alterations of the capsid inserted 2E3 epitope and antibody affinity maturation to exclude human PCSK9 binding.

It is conceivable that this retargeting system is transferrable to other AAV serotypes, as AAVs show a common capsid structure with identical, homologous overlapping variable regions (Padron et al. 2005; Büning and Srivastava 2019). Therefore, the 2E3 epitope substitution within loop VIII might be equally tolerated in other serotypes, which would enable a serotype transferable retargeting approach.

Within this study, a valuable AAV2 capsid modification together with novel bispecific antibodies as target adaptors were developed. This approach allows to rapidly screen gene therapy targets *in vitro* based on a single AAV capsid modification and modular bispecific antibody. Additionally, this system has the potential to be expanded across species boundaries as well as AAV serotypes.

5 Summary

Human gene therapy is a growing and promising field to treat and potentially cure acquired diseases. Recombinant Adeno-associated vectors type 2 (rAAV2) became advantageous for gene therapy approaches due to its low immunogenicity, low frequency of genomic integration, and lack of toxicity while providing a long-term genome expression after transduction. However, a limiting factor of systemic delivery of AAV-based gene therapies is the lack of tissue-specific AAV capsid variants.

This study demonstrated that the insertion of the human Proprotein-Convertase Subtilisin/Kexin Type 9 (PCSK9) derived short, linear epitope 2E3 can be inserted into various surface loops of AAV2 capsid proteins. 2E3 epitope sequence substitution in loop eight of the viral capsid protein resulted in abolished heparin sulfate-proteoglycan binding. Consequently, a detargeted capsid variant was developed proven by *in vitro* and *in vivo* experiments.

The 2E3 epitope served as tag for bispecific antibodies that were combined from an anti-2E3 antibody with target receptor binding antibodies. The targeted receptors FAP (Fibroblast activation protein) or PD-L1 (programmed death-ligand 1) are both disease-relevant markers within the tumor microenvironment and cancer cells. Both receptors have been successfully targeted in this study and were used as AAV gene therapy targets for the first time.

The developed platform allowed selective targeting of desired cell surface receptors *in vitro* based on a single AAV modification and modular adaptor antibodies. Although this approach could not be easily transferred to target solid tumor tissue *in vivo*, binding improvements and optimized disease models may allow *in vivo* targeting in future. Yet this platform can serve as a valuable tool to target cells in mixed cultures, to investigate the role of disease-relevant cell types or to serve as a base for the rapid identification of novel receptors for gene-therapy approaches.

6 References

- Acharya, P. S., Zukas, A., Chandan, V., Katzenstein, A. L., & Puré, E. (2006). Fibroblast activation protein: a serine protease expressed at the remodeling interface in idiopathic pulmonary fibrosis. *Human pathology*, 37(3), 352–360.
<https://doi.org/10.1016/j.humpath.2005.11.020>
- Ahmadzadeh, M., Johnson, L. A., Heemskerk, B., Wunderlich, J. R., Dudley, M. E., White, D. E., & Rosenberg, S. A. (2009). Tumor antigen-specific CD8 T cells infiltrating the tumor express high levels of PD-1 and are functionally impaired. *Blood*, 114(8), 1537–1544. <https://doi.org/10.1182/blood-2008-12-195792>
- Akache, B., Grimm, D., Pandey, K., Yant, S. R., Xu, H., & Kay, M. A. (2006). The 37/67-kilodalton laminin receptor is a receptor for adeno-associated virus serotypes 8, 2, 3, and 9. *Journal of virology*, 80(19), 9831–9836. <https://doi.org/10.1128/JVI.00878-06>
- Arruda, V. R., Stedman, H. H., Nichols, T. C., Haskins, M. E., Nicholson, M., Herzog, R. W., Couto, L. B., & High, K. A. (2005). Regional intravascular delivery of AAV-2-F.IX to skeletal muscle achieves long-term correction of hemophilia B in a large animal model. *Blood*, 105(9), 3458–3464
- Asokan, A., Hamra, J. B., Govindasamy, L., Agbandje-McKenna, M., & Samulski, R. J. (2006). Adeno-associated virus type 2 contains an integrin alpha5beta1 binding domain essential for viral cell entry. *Journal of virology*, 80(18), 8961–8969.
<https://doi.org/10.1128/JVI.00843-06>
- Atchison, R. W., Casto, B. C., & Hammon, W. M. (1965). Adenovirus-Associated Defective Virus Particles. *Science (New York, N.Y.)*, 149(3685), 754–756.
<https://doi.org/10.1126/science.149.3685.754>
- Atchison, R. W., Casto, B. C., & Hammon, W. M. (1966). Electron microscopy of adeno-associated virus (AAV) in cell cultures. *Virology*, 29(2), 353–357.
[https://doi.org/10.1016/0042-6822\(66\)90045-6](https://doi.org/10.1016/0042-6822(66)90045-6)
- Atwell, S., Ridgway, J. B., Wells, J. A., & Carter, P. (1997). Stable heterodimers from remodeling the domain interface of a homodimer using a phage display library. *Journal of molecular biology*, 270(1), 26–35. <https://doi.org/10.1006/jmbi.1997.1116>
- Bartel, M. A., Weinstein, J. R., & Schaffer, D. V. (2012). Directed evolution of novel adeno-associated viruses for therapeutic gene delivery. *Gene therapy*, 19(6), 694–700.
<https://doi.org/10.1038/gt.2012.20>
- Bartlett, J. S., Kleinschmidt, J., Boucher, R. C., & Samulski, R. J. (1999). Targeted adeno-associated virus vector transduction of nonpermissive cells mediated by a bispecific F(ab'gamma)2 antibody. *Nature biotechnology*, 17(2), 181–186.
<https://doi.org/10.1038/6185>

- Bartlett, J. S., Samulski, R. J., & McCown, T. J. (1998). Selective and rapid uptake of adeno-associated virus type 2 in brain. *Human gene therapy*, 9(8), 1181–1186. <https://doi.org/10.1089/hum.1998.9.8-1181>
- Bartlett, J. S., Wilcher, R., & Samulski, R. J. (2000). Infectious entry pathway of adeno-associated virus and adeno-associated virus vectors. *Journal of virology*, 74(6), 2777–2785. <https://doi.org/10.1128/jvi.74.6.2777-2785.2000>
- Basu, S., Lien, Y., Vozmediano, V., Schlender, J. F., Eissing, T., Schmidt, S., & Niederalt, C. (2020). Physiologically Based Pharmacokinetic Modeling of Monoclonal Antibodies in Pediatric Populations Using PK-Sim. *Frontiers in pharmacology*, 11, 868. <https://doi.org/10.3389/fphar.2020.00868>
- Baudino T. A. (2015). Targeted Cancer Therapy: The Next Generation of Cancer Treatment. *Current drug discovery technologies*, 12(1), 3–20. <https://doi.org/10.2174/1570163812666150602144310>
- Bauer, K., Bayer, P. M., Deutsch, E., & Gabl, F. (1980). Binding of enzyme-IgG complexes in human serum to Protein-A Sepharose CL-4B. *Clinical chemistry*, 26(2), 297–300
- Bauer, S., Jendro, M. C., Wadle, A., Kleber, S., Stenner, F., Dinser, R., Reich, A., Faccin, E., Gödde, S., Dinges, H., Müller-Ladner, U., & Renner, C. (2006). Fibroblast activation protein is expressed by rheumatoid myofibroblast-like synoviocytes. *Arthritis research & therapy*, 8(6), R171. <https://doi.org/10.1186/ar2080>
- Baum, P., Müller, D., Rüger, R., & Kontermann, R. E. (2007). Single-chain Fv immunoliposomes for the targeting of fibroblast activation protein-expressing tumor stromal cells. *Journal of drug targeting*, 15(6), 399–406. <https://doi.org/10.1080/10611860701453034>
- Becerra, S. P., Rose, J. A., Hardy, M., Baroudy, B. M., & Anderson, C. W. (1985). Direct mapping of adeno-associated virus capsid proteins B and C: a possible ACG initiation codon. *Proceedings of the National Academy of Sciences of the United States of America*, 82(23), 7919–7923. <https://doi.org/10.1073/pnas.82.23.7919>
- Berns, K. I., & Giraud, C. (1996). Biology of adeno-associated virus. *Current topics in microbiology and immunology*, 218, 1–23. https://doi.org/10.1007/978-3-642-80207-2_1
- Berns, K. I., & Linden, R. M. (1995). The cryptic life style of adeno-associated virus. *BioEssays : news and reviews in molecular, cellular and developmental biology*, 17(3), 237–245. <https://doi.org/10.1002/bies.950170310>
- Bleker, S., Sonntag, F., & Kleinschmidt, J. A. (2005). Mutational analysis of narrow pores at the fivefold symmetry axes of adeno-associated virus type 2 capsids reveals a dual role in genome packaging and activation of phospholipase A2 activity. *Journal of virology*, 79(4), 2528–2540. <https://doi.org/10.1128/JVI.79.4.2528-2540.2005>

- Bramlage, B., Brinkmann, U., Croasdale, R., Dill, S., Dormeyer, W., Georges, G., Grote, M., Haas, A., Hoffmann, E., Ickenstein, L.M., Jahn-Hofmann, K., John, M., Metz, S., Mundigl, O., Scheuer, W., Stracke, J.O., (2009) Bi-Specific Digoxigenin Binding Antibodies. Patent WO-2011003780-A1.
- Brinkmann, U., & Kontermann, R. E. (2017). The making of bispecific antibodies. *mAbs*, 9(2), 182–212. <https://doi.org/10.1080/19420862.2016.1268307>
- Brocks, B., Garin-Chesa, P., Behrle, E., Park, J. E., Rettig, W. J., Pfizenmaier, K., & Moosmayer, D. (2001). Species-crossreactive scFv against the tumor stroma marker "fibroblast activation protein" selected by phage display from an immunized FAP-/- knock-out mouse. *Molecular medicine (Cambridge, Mass.)*, 7(7), 461–469.
- Büning, H., Huber, A., Zhang, L., Meumann, N., & Hacker, U. (2015). Engineering the AAV capsid to optimize vector-host-interactions. *Current opinion in pharmacology*, 24, 94–104. <https://doi.org/10.1016/j.coph.2015.08.002>
- Büning, H., & Srivastava, A. (2019). Capsid Modifications for Targeting and Improving the Efficacy of AAV Vectors. *Molecular therapy. Methods & clinical development*, 12, 248–265. <https://doi.org/10.1016/j.omtm.2019.01.008>
- Buller, R. M., & Rose, J. A. (1978). Characterization of adenovirus-associated virus-induced polypeptides in KB cells. *Journal of virology*, 25(1), 331–338. <https://doi.org/10.1128/JVI.25.1.331-338.1978>
- Burr, M. L., Sparbier, C. E., Chan, Y. C., Williamson, J. C., Woods, K., Beavis, P. A., Lam, E., Henderson, M. A., Bell, C. C., Stolzenburg, S., Gilan, O., Bloor, S., Noori, T., Morgens, D. W., Bassik, M. C., Neeson, P. J., Behren, A., Darcy, P. K., Dawson, S. J., Voskoboinik, I., ... Dawson, M. A. (2017). CMTM6 maintains the expression of PD-L1 and regulates anti-tumour immunity. *Nature*, 549(7670), 101–105. <https://doi.org/10.1038/nature23643>
- Busek, P., Mateu, R., Zubal, M., Kotackova, L., & Sedo, A. (2018). Targeting fibroblast activation protein in cancer - Prospects and caveats. *Frontiers in bioscience (Landmark edition)*, 23, 1933–1968. <https://doi.org/10.2741/4682>
- Cao, M., You, H., & Hermonat, P. L. (2014). The X gene of adeno-associated virus 2 (AAV2) is involved in viral DNA replication. *PloS one*, 9(8), e104596. <https://doi.org/10.1371/journal.pone.0104596>
- Carlisle, R. C., Benjamin, R., Briggs, S. S., Sumner-Jones, S., McIntosh, J., Gill, D., Hyde, S., Nathwani, A., Subr, V., Ulbrich, K., Seymour, L. W., & Fisher, K. D. (2008). Coating of adeno-associated virus with reactive polymers can ablate virus tropism, enable retargeting and provide resistance to neutralising antisera. *The journal of gene medicine*, 10(4), 400–411. <https://doi.org/10.1002/jgm.1161>
- Carter B. J. (2004). Adeno-associated virus and the development of adeno-associated virus vectors: a historical perspective. *Molecular therapy : the journal of the American Society of Gene Therapy*, 10(6), 981–989. <https://doi.org/10.1016/j.ymthe.2004.09.011>

- Chang, L. S., Shi, Y., & Shenk, T. (1989). Adeno-associated virus P5 promoter contains an adenovirus E1A-inducible element and a binding site for the major late transcription factor. *Journal of virology*, 63(8), 3479–3488. <https://doi.org/10.1128/JVI.63.8.3479-3488.1989>
- Cheng, Y., Li, H., Deng, Y., Tai, Y., Zeng, K., Zhang, Y., Liu, W., Zhang, Q., & Yang, Y. (2018). Cancer-associated fibroblasts induce PDL1+ neutrophils through the IL6-STAT3 pathway that foster immune suppression in hepatocellular carcinoma. *Cell death & disease*, 9(4), 422. <https://doi.org/10.1038/s41419-018-0458-4>
- Choi, H. J., Kim, Y. J., Lee, S., & Kim, Y. S. (2013). A heterodimeric Fc-based bispecific antibody simultaneously targeting VEGFR-2 and Met exhibits potent antitumor activity. *Molecular cancer therapeutics*, 12(12), 2748–2759. <https://doi.org/10.1158/1535-7163.MCT-13-0628>
- Chung, K. M., Hsu, S. C., Chu, Y. R., Lin, M. Y., Jiaang, W. T., Chen, R. H., & Chen, X. (2014). Fibroblast activation protein (FAP) is essential for the migration of bone marrow mesenchymal stem cells through RhoA activation. *PloS one*, 9(2), e88772. <https://doi.org/10.1371/journal.pone.0088772>
- Colella, P., Ronzitti, G., & Mingozzi, F. (2017). Emerging Issues in AAV-Mediated In Vivo Gene Therapy. *Molecular therapy. Methods & clinical development*, 8, 87–104. <https://doi.org/10.1016/j.omtm.2017.11.007>
- Collins, J. M., & Gulley, J. L. (2019). Product review: avelumab, an anti-PD-L1 antibody. *Human vaccines & immunotherapeutics*, 15(4), 891–908. <https://doi.org/10.1080/21645515.2018.1551671>
- Contreras-Sandoval, A. M., Merino, M., Vasquez, M., Trocóniz, I. F., Berraondo, P., & Garrido, M. J. (2016). Correlation between anti-PD-L1 tumor concentrations and tumor-specific and nonspecific biomarkers in a melanoma mouse model. *Oncotarget*, 7(47), 76891–76901. <https://doi.org/10.18632/oncotarget.12727>
- Davies, D. R., Chacko, S. (1993) Antibody structure. *Accounts Chem Res* 26:421–427. <https://doi.org/10.1021/ar00032a005>
- Davis, J. H., Aperlo, C., Li, Y., Kurosawa, E., Lan, Y., Lo, K. M., & Huston, J. S. (2010). SEEDbodies: fusion proteins based on strand-exchange engineered domain (SEED) CH3 heterodimers in an Fc analogue platform for asymmetric binders or immunofusions and bispecific antibodies. *Protein engineering, design & selection : PEDS*, 23(4), 195–202. <https://doi.org/10.1093/protein/gzp094>
- Daya, S., & Berns, K. I. (2008). Gene therapy using adeno-associated virus vectors. *Clinical microbiology reviews*, 21(4), 583–593. <https://doi.org/10.1128/CMR.00008-08>
- Deisenhofer J. (1981). Crystallographic refinement and atomic models of a human Fc fragment and its complex with fragment B of protein A from *Staphylococcus aureus* at 2.9- and 2.8-Å resolution. *Biochemistry*, 20(9), 2361–2370.

- Dong, H., Zhu, G., Tamada, K., & Chen, L. (1999). B7-H1, a third member of the B7 family, co-stimulates T-cell proliferation and interleukin-10 secretion. *Nature medicine*, 5(12), 1365–1369. <https://doi.org/10.1038/70932>
- Duan, D., Li, Q., Kao, A. W., Yue, Y., Pessin, J. E., & Engelhardt, J. F. (1999). Dynamin is required for recombinant adeno-associated virus type 2 infection. *Journal of virology*, 73(12), 10371–10376. <https://doi.org/10.1128/JVI.73.12.10371-10376.1999>
- Dudek, A. M., Zabaleta, N., Zinn, E., Pillay, S., Zengel, J., Porter, C., Franceschini, J. S., Estelien, R., Carette, J. E., Zhou, G. L., & Vandenberghe, L. H. (2020). GPR108 Is a Highly Conserved AAV Entry Factor. *Molecular therapy : the journal of the American Society of Gene Therapy*, 28(2), 367–381. <https://doi.org/10.1016/j.ymthe.2019.11.005>
- Duque, S., Joussemet, B., Riviere, C., Marais, T., Dubreil, L., Douar, A. M., Fyfe, J., Moullier, P., Colle, M. A., & Barkats, M. (2009). Intravenous administration of self-complementary AAV9 enables transgene delivery to adult motor neurons. *Molecular therapy : the journal of the American Society of Gene Therapy*, 17(7), 1187–1196. <https://doi.org/10.1038/mt.2009.71>
- Durocher, Y., Perret, S., & Kamen, A. (2002). High-level and high-throughput recombinant protein production by transient transfection of suspension-growing human 293-EBNA1 cells. *Nucleic acids research*, 30(2), E9. <https://doi.org/10.1093/nar/30.2.e9>
- Eichhoff, A. M., Börner, K., Albrecht, B., Schäfer, W., Baum, N., Haag, F., Körbelin, J., Trepel, M., Braren, I., Grimm, D., Adriouch, S., & Koch-Nolte, F. (2019). Nanobody-Enhanced Targeting of AAV Gene Therapy Vectors. *Molecular therapy. Methods & clinical development*, 15, 211–220. <https://doi.org/10.1016/j.omtm.2019.09.003>
- Elmore, Z. C., Patrick Havlik, L., Oh, D. K., Anderson, L., Daaboul, G., Devlin, G. W., Vincent, H. A., & Asokan, A. (2021). The membrane associated accessory protein is an adeno-associated viral egress factor. *Nature communications*, 12(1), 6239. <https://doi.org/10.1038/s41467-021-26485-4>
- Erles, K., Seböková, P., & Schlehofer, J. R. (1999). Update on the prevalence of serum antibodies (IgG and IgM) to adeno-associated virus (AAV). *Journal of medical virology*, 59(3), 406–411. [https://doi.org/10.1002/\(sici\)1096-9071\(199911\)59:3<406::aid-jmv22>3.0.co;2-n](https://doi.org/10.1002/(sici)1096-9071(199911)59:3<406::aid-jmv22>3.0.co;2-n)
- Fein, D. E., Limberis, M. P., Maloney, S. F., Heath, J. M., Wilson, J. M., & Diamond, S. L. (2009). Cationic lipid formulations alter the in vivo tropism of AAV2/9 vector in lung. *Molecular therapy : the journal of the American Society of Gene Therapy*, 17(12), 2078–2087. <https://doi.org/10.1038/mt.2009.173>
- Feiner, R. C., Kemker, I., Krutzke, L., Allmendinger, E., Mandell, D. J., Sewald, N., Kochanek, S., & Müller, K. M. (2020). EGFR-Binding Peptides: From Computational Design towards Tumor-Targeting of Adeno-Associated Virus Capsids. *International journal of molecular sciences*, 21(24), 9535. <https://doi.org/10.3390/ijms21249535>

- Feiner, R. C., Teschner, J., Teschner, K. E., Radukic, M. T., Baumann, T., Hagen, S., Hannappel, Y., Biere, N., Anselmetti, D., Arndt, K. M., & Müller, K. M. (2019). rAAV Engineering for Capsid-Protein Enzyme Insertions and Mosaicism Reveals Resilience to Mutational, Structural and Thermal Perturbations. *International journal of molecular sciences*, 20(22), 5702. <https://doi.org/10.3390/ijms20225702>
- Ferrari, F. K., Xiao, X., McCarty, D., & Samulski, R. J. (1997). New developments in the generation of Ad-free, high-titer rAAV gene therapy vectors. *Nature medicine*, 3(11), 1295–1297. <https://doi.org/10.1038/nm1197-1295>
- Fischer, E., Chaitanya, K., Wüest, T., Wadle, A., Scott, A. M., van den Broek, M., Schibli, R., Bauer, S., & Renner, C. (2012). Radioimmunotherapy of fibroblast activation protein positive tumors by rapidly internalizing antibodies. *Clinical cancer research : an official journal of the American Association for Cancer Research*, 18(22), 6208–6218. <https://doi.org/10.1158/1078-0432.CCR-12-0644>
- Fisher, K. J., Jooss, K., Alston, J., Yang, Y., Haecker, S. E., High, K., Pathak, R., Raper, S. E., & Wilson, J. M. (1997). Recombinant adeno-associated virus for muscle directed gene therapy. *Nature medicine*, 3(3), 306–312. <https://doi.org/10.1038/nm0397-306>
- Fishman, J. B., & Berg, E. A. (2019). Protein A and Protein G Purification of Antibodies. *Cold Spring Harbor protocols*, 2019(1), 10.1101/pdb.prot099143. <https://doi.org/10.1101/pdb.prot099143>
- Freeman, G. J., Long, A. J., Iwai, Y., Bourque, K., Chernova, T., Nishimura, H., Fitz, L. J., Malenkovich, N., Okazaki, T., Byrne, M. C., Horton, H. F., Fouser, L., Carter, L., Ling, V., Bowman, M. R., Carreno, B. M., Collins, M., Wood, C. R., & Honjo, T. (2000). Engagement of the PD-1 immunoinhibitory receptor by a novel B7 family member leads to negative regulation of lymphocyte activation. *The Journal of experimental medicine*, 192(7), 1027–1034. <https://doi.org/10.1084/jem.192.7.1027>
- Fu, H., Muenzer, J., Samulski, R. J., Breese, G., Sifford, J., Zeng, X., & McCarty, D. M. (2003). Self-complementary adeno-associated virus serotype 2 vector: global distribution and broad dispersion of AAV-mediated transgene expression in mouse brain. *Molecular therapy : the journal of the American Society of Gene Therapy*, 8(6), 911–917. <https://doi.org/10.1016/j.ymthe.2003.08.021>
- Galibert, L., Hyvönen, A., Eriksson, R., Mattola, S., Aho, V., Salminen, S., Albers, J. D., Peltola, S. K., Weman, S., Nieminen, T., Ylä-Herttuala, S., Lesch, H. P., Vihinen-Ranta, M., & Airene, K. J. (2021). Functional roles of the membrane-associated AAV protein MAAP. *Scientific reports*, 11(1), 21698. <https://doi.org/10.1038/s41598-021-01220-7>
- Garin-Chesa, P., Old, L. J., & Rettig, W. J. (1990). Cell surface glycoprotein of reactive stromal fibroblasts as a potential antibody target in human epithelial cancers. *Proceedings of the National Academy of Sciences of the United States of America*, 87(18), 7235–7239. <https://doi.org/10.1073/pnas.87.18.7235>

- Georg-Fries, B., Biederlack, S., Wolf, J., & zur Hausen, H. (1984). Analysis of proteins, helper dependence, and seroepidemiology of a new human parvovirus. *Virology*, 134(1), 64–71. [https://doi.org/10.1016/0042-6822\(84\)90272-1](https://doi.org/10.1016/0042-6822(84)90272-1)
- Ghebeh, H., Mohammed, S., Al-Omair, A., Qattan, A., Lehe, C., Al-Qudaihi, G., Elkum, N., Alshabanah, M., Bin Amer, S., Tulbah, A., Ajarim, D., Al-Tweigeri, T., & Dermime, S. (2006). The B7-H1 (PD-L1) T lymphocyte-inhibitory molecule is expressed in breast cancer patients with infiltrating ductal carcinoma: correlation with important high-risk prognostic factors. *Neoplasia (New York, N.Y.)*, 8(3), 190–198. <https://doi.org/10.1593/neo.05733>
- Gigout, L., Rebollo, P., Clement, N., Warrington, K. H., Jr, Muzyczka, N., Linden, R. M., & Weber, T. (2005). Altering AAV tropism with mosaic viral capsids. *Molecular therapy : the journal of the American Society of Gene Therapy*, 11(6), 856–865. <https://doi.org/10.1016/j.ymthe.2005.03.005>
- Girod, A., Wobus, C. E., Zádori, Z., Ried, M., Leike, K., Tijssen, P., Kleinschmidt, J. A., & Hallek, M. (2002). The VP1 capsid protein of adeno-associated virus type 2 is carrying a phospholipase A2 domain required for virus infectivity. *The Journal of general virology*, 83(Pt 5), 973–978. <https://doi.org/10.1099/0022-1317-83-5-973>
- Gonçalves M. A. (2005). Adeno-associated virus: from defective virus to effective vector. *Virology journal*, 2, 43. <https://doi.org/10.1186/1743-422X-2-43>
- Goulet, D. R., Orcutt, S. J., Zwolak, A., Rispens, T., Labrijn, A. F., de Jong, R. N., Atkins, W. M., & Chiu, M. L. (2018). Kinetic mechanism of controlled Fab-arm exchange for the formation of bispecific immunoglobulin G1 antibodies. *The Journal of biological chemistry*, 293(2), 651–661. <https://doi.org/10.1074/jbc.RA117.000303>
- Govindasamy, L., Padron, E., McKenna, R., Muzyczka, N., Kaludov, N., Chiorini, J. A., & Agbandje-McKenna, M. (2006). Structurally mapping the diverse phenotype of adeno-associated virus serotype 4. *Journal of virology*, 80(23), 11556–11570. <https://doi.org/10.1128/JVI.01536-06>
- Graille, M., Stura, E. A., Corper, A. L., Sutton, B. J., Taussig, M. J., Charbonnier, J. B., & Silverman, G. J. (2000). Crystal structure of a *Staphylococcus aureus* protein A domain complexed with the Fab fragment of a human IgM antibody: structural basis for recognition of B-cell receptors and superantigen activity. *Proceedings of the National Academy of Sciences of the United States of America*, 97(10), 5399–5404. <https://doi.org/10.1073/pnas.97.10.5399>
- Graham, F. L., Smiley, J., Russell, W. C., & Nairn, R. (1977). Characteristics of a human cell line transformed by DNA from human adenovirus type 5. *The Journal of general virology*, 36(1), 59–74. <https://doi.org/10.1099/0022-1317-36-1-59>

- Gray, S. J., Blake, B. L., Criswell, H. E., Nicolson, S. C., Samulski, R. J., McCown, T. J., & Li, W. (2010). Directed evolution of a novel adeno-associated virus (AAV) vector that crosses the seizure-compromised blood-brain barrier (BBB). *Molecular therapy : the journal of the American Society of Gene Therapy*, 18(3), 570–578. <https://doi.org/10.1038/mt.2009.292>
- Grieger, J. C., & Samulski, R. J. (2005). Packaging capacity of adeno-associated virus serotypes: impact of larger genomes on infectivity and postentry steps. *Journal of virology*, 79(15), 9933–9944. <https://doi.org/10.1128/JVI.79.15.9933-9944.2005>
- Grieger, J. C., Snowdy, S., & Samulski, R. J. (2006). Separate basic region motifs within the adeno-associated virus capsid proteins are essential for infectivity and assembly. *Journal of virology*, 80(11), 5199–5210. <https://doi.org/10.1128/JVI.02723-05>
- Grimm, D., Kern, A., Pawlita, M., Ferrari, F., Samulski, R., & Kleinschmidt, J. (1999). Titration of AAV-2 particles via a novel capsid ELISA: packaging of genomes can limit production of recombinant AAV-2. *Gene therapy*, 6(7), 1322–1330. <https://doi.org/10.1038/sj.gt.3300946>
- Grodzki, A. C., & Berenstein, E. (2010). Antibody purification: affinity chromatography - protein A and protein G Sepharose. *Methods in molecular biology (Clifton, N.J.)*, 588, 33–41. https://doi.org/10.1007/978-1-59745-324-0_5
- Gunasekaran, K., Pentony, M., Shen, M., Garrett, L., Forte, C., Woodward, A., Ng, S. B., Born, T., Retter, M., Manchulenko, K., Sweet, H., Foltz, I. N., Wittekind, M., & Yan, W. (2010). Enhancing antibody Fc heterodimer formation through electrostatic steering effects: applications to bispecific molecules and monovalent IgG. *The Journal of biological chemistry*, 285(25), 19637–19646. <https://doi.org/10.1074/jbc.M110.117382>
- Gurda, B. L., DiMattia, M. A., Miller, E. B., Bennett, A., McKenna, R., Weichert, W. S., Nelson, C. D., Chen, W. J., Muzyczka, N., Olson, N. H., Sinkovits, R. S., Chiorini, J. A., Zolotutkhin, S., Kozyreva, O. G., Samulski, R. J., Baker, T. S., Parrish, C. R., & Agbandje-McKenna, M. (2013). Capsid antibodies to different adeno-associated virus serotypes bind common regions. *Journal of virology*, 87(16), 9111–9124. <https://doi.org/10.1128/JVI.00622-13>
- Gurung, S., Khan, F., Gunassekaran, G. R., Yoo, J. D., Poongkavithai Vadevoo, S. M., Permpoon, U., Kim, S. H., Kim, H. J., Kim, I. S., Han, H., Park, J. H., Kim, S., & Lee, B. (2020). Phage display-identified PD-L1-binding peptides reinvigorate T-cell activity and inhibit tumor progression. *Biomaterials*, 247, 119984. <https://doi.org/10.1016/j.biomaterials.2020.119984>
- Hacker, U. T., Wingenfeld, L., Kofler, D. M., Schuhmann, N. K., Lutz, S., Herold, T., King, S. B., Gerner, F. M., Perabo, L., Rabinowitz, J., McCarty, D. M., Samulski, R. J., Hallek, M., & Büning, H. (2005). Adeno-associated virus serotypes 1 to 5 mediated tumor cell directed gene transfer and improvement of transduction efficiency. *The journal of gene medicine*, 7(11), 1429–1438. <https://doi.org/10.1002/jgm.782>

- Hauck, B., Chen, L., & Xiao, W. (2003). Generation and characterization of chimeric recombinant AAV vectors. *Molecular therapy : the journal of the American Society of Gene Therapy*, 7(3), 419–425. [https://doi.org/10.1016/s1525-0016\(03\)00012-1](https://doi.org/10.1016/s1525-0016(03)00012-1)
- Hermonat, P. L., Labow, M. A., Wright, R., Berns, K. I., & Muzyczka, N. (1984). Genetics of adeno-associated virus: isolation and preliminary characterization of adeno-associated virus type 2 mutants. *Journal of virology*, 51(2), 329–339. <https://doi.org/10.1128/JVI.51.2.329-339.1984>
- Hindson, B. J., Ness, K. D., Masquelier, D. A., Belgrader, P., Heredia, N. J., Makarewicz, A. J., Bright, I. J., Lucero, M. Y., Hiddessen, A. L., Legler, T. C., Kitano, T. K., Hodel, M. R., Petersen, J. F., Wyatt, P. W., Steenblock, E. R., Shah, P. H., Bousse, L. J., Troup, C. B., Mellen, J. C., Wittmann, D. K., ... Colston, B. W. (2011). High-throughput droplet digital PCR system for absolute quantitation of DNA copy number. *Analytical chemistry*, 83(22), 8604–8610. <https://doi.org/10.1021/ac202028g>
- Hofheinz, R. D., al-Batran, S. E., Hartmann, F., Hartung, G., Jäger, D., Renner, C., Tanswell, P., Kunz, U., Amelsberg, A., Kuthan, H., & Stehle, G. (2003). Stromal antigen targeting by a humanised monoclonal antibody: an early phase II trial of si-brotuzumab in patients with metastatic colorectal cancer. *Onkologie*, 26(1), 44–48. <https://doi.org/10.1159/000069863>
- Hoggan, M. D., Blacklow, N. R., & Rowe, W. P. (1966). Studies of small DNA viruses found in various adenovirus preparations: physical, biological, and immunological characteristics. *Proceedings of the National Academy of Sciences of the United States of America*, 55(6), 1467–1474. <https://doi.org/10.1073/pnas.55.6.1467>
- Hoque, M., Ishizu, K., Matsumoto, A., Han, S. I., Arisaka, F., Takayama, M., Suzuki, K., Kato, K., Kanda, T., Watanabe, H., & Handa, H. (1999). Nuclear transport of the major capsid protein is essential for adeno-associated virus capsid formation. *Journal of virology*, 73(9), 7912–7915. <https://doi.org/10.1128/JVI.73.9.7912-7915.1999>
- Huston, J. S., Mudgett-Hunter, M., Tai, M. S., McCartney, J., Warren, F., Haber, E., & Oppermann, H. (1991). Protein engineering of single-chain Fv analogs and fusion proteins. *Methods in enzymology*, 203, 46–88. [https://doi.org/10.1016/0076-6879\(91\)03005-2](https://doi.org/10.1016/0076-6879(91)03005-2)
- Huttner, N. A., Girod, A., Perabo, L., Edbauer, D., Kleinschmidt, J. A., Büning, H., & Hallek, M. (2003). Genetic modifications of the adeno-associated virus type 2 capsid reduce the affinity and the neutralizing effects of human serum antibodies. *Gene therapy*, 10(26), 2139–2147. <https://doi.org/10.1038/sj.gt.3302123>
- Im, D. S., & Muzyczka, N. (1990). The AAV origin binding protein Rep68 is an ATP-dependent site-specific endonuclease with DNA helicase activity. *Cell*, 61(3), 447–457. [https://doi.org/10.1016/0092-8674\(90\)90526-k](https://doi.org/10.1016/0092-8674(90)90526-k)
- Inbar, D., Hochman, J., & Givol, D. (1972). Localization of antibody-combining sites within the variable portions of heavy and light chains. *Proceedings of the National Academy of Sciences of the United States of America*, 69(9), 2659–2662. <https://doi.org/10.1073/pnas.69.9.2659>

- Janik, J. E., Huston, M. M., & Rose, J. A. (1984). Adeno-associated virus proteins: origin of the capsid components. *Journal of virology*, 52(2), 591–597. <https://doi.org/10.1128/JVI.52.2.591-597.1984>
- Janik, J. E., Huston, M. M., Cho, K., & Rose, J. A. (1989). Efficient synthesis of adeno-associated virus structural proteins requires both adenovirus DNA binding protein and VA I RNA. *Virology*, 168(2), 320–329. [https://doi.org/10.1016/0042-6822\(89\)90272-9](https://doi.org/10.1016/0042-6822(89)90272-9)
- Jin, H., D'Urso, V., Neuteboom, B., McKenna, S. D., Schweickhardt, R., Gross, A. W., Fomekong Nanfack, Y., Paoletti, A., Carter, C., Toleikis, L., Fluck, M., Scheuenpflug, J., & Cai, T. (2021). Avelumab internalization by human circulating immune cells is mediated by both Fc gamma receptor and PD-L1 binding. *Oncoimmunology*, 10(1), 1958590. <https://doi.org/10.1080/2162402X.2021.1958590>
- Johnson, S., Burke, S., Huang, L., Gorlatov, S., Li, H., Wang, W., Zhang, W., Tuailon, N., Rainey, J., Barat, B., Yang, Y., Jin, L., Ciccarone, V., Moore, P. A., Koenig, S., & Bonvini, E. (2010). Effector cell recruitment with novel Fv-based dual-affinity re-targeting protein leads to potent tumor cytolysis and in vivo B-cell depletion. *Journal of molecular biology*, 399(3), 436–449. <https://doi.org/10.1016/j.jmb.2010.04.001>
- Kaepffel, C., Beattie, S. G., Fronza, R., van Logtenstein, R., Salmon, F., Schmidt, S., Wolf, S., Nowrouzi, A., Glimm, H., von Kalle, C., Petry, H., Gaudet, D., & Schmidt, M. (2013). A largely random AAV integration profile after LPLD gene therapy. *Nature medicine*, 19(7), 889–891. <https://doi.org/10.1038/nm.3230>
- Kashiwakura, Y., Tamayose, K., Iwabuchi, K., Hirai, Y., Shimada, T., Matsumoto, K., Nakamura, T., Watanabe, M., Oshimi, K., & Daida, H. (2005). Hepatocyte growth factor receptor is a coreceptor for adeno-associated virus type 2 infection. *Journal of virology*, 79(1), 609–614. <https://doi.org/10.1128/JVI.79.1.609-614.2005>
- Kern, A., Schmidt, K., Leder, C., Müller, O. J., Wobus, C. E., Bettinger, K., Von der Lieth, C. W., King, J. A., & Kleinschmidt, J. A. (2003). Identification of a heparin-binding motif on adeno-associated virus type 2 capsids. *Journal of virology*, 77(20), 11072–11081. <https://doi.org/10.1128/jvi.77.20.11072-11081.2003>
- Kim, S. H., Lee, S., Lee, H., Cho, M., Schaffer, D. V., & Jang, J. H. (2019). AAVR-Displaying Interfaces: Serotype-Independent Adeno-Associated Virus Capture and Local Delivery Systems. *Molecular therapy. Nucleic acids*, 18, 432–443. <https://doi.org/10.1016/j.omtn.2019.09.015>
- King, J. A., Dubielzig, R., Grimm, D., & Kleinschmidt, J. A. (2001). DNA helicase-mediated packaging of adeno-associated virus type 2 genomes into preformed capsids. *The EMBO journal*, 20(12), 3282–3291. <https://doi.org/10.1093/emboj/20.12.3282>
- Köhler, G., & Milstein, C. (1975). Continuous cultures of fused cells secreting antibody of predefined specificity. *Nature*, 256(5517), 495–497. <https://doi.org/10.1038/256495a0>
- Kontermann R. E. (2005). Recombinant bispecific antibodies for cancer therapy. *Acta pharmacologica Sinica*, 26(1), 1–9. <https://doi.org/10.1111/j.1745-7254.2005.00008.x>

- Kontermann R. E. (2011). Strategies for extended serum half-life of protein therapeutics. *Current opinion in biotechnology*, 22(6), 868–876. <https://doi.org/10.1016/j.cop-bio.2011.06.012>
- Kotin, R. M., Siniscalco, M., Samulski, R. J., Zhu, X. D., Hunter, L., Laughlin, C. A., McLaughlin, S., Muzyczka, N., Rocchi, M., & Berns, K. I. (1990). Site-specific integration by adeno-associated virus. *Proceedings of the National Academy of Sciences of the United States of America*, 87(6), 2211–2215. <https://doi.org/10.1073/pnas.87.6.2211>
- Kotterman, M. A., Chalberg, T. W., & Schaffer, D. V. (2015). Viral Vectors for Gene Therapy: Translational and Clinical Outlook. *Annual review of biomedical engineering*, 17, 63–89. <https://doi.org/10.1146/annurev-bioeng-071813-104938>
- Kuklik, J., Michelfelder, S., Schiele, F., Kreuz, S., Lamla, T., Müller, P., & Park, J. E. (2021). Development of a Bispecific Antibody-Based Platform for Retargeting of Capsid Modified AAV Vectors. *International journal of molecular sciences*, 22(15), 8355. <https://doi.org/10.3390/ijms22158355>
- Kuranda, K., Jean-Alphonse, P., Leborgne, C., Hardet, R., Collaud, F., Marmier, S., Costa Verdera, H., Ronzitti, G., Veron, P., & Mingozi, F. (2018). Exposure to wild-type AAV drives distinct capsid immunity profiles in humans. *The Journal of clinical investigation*, 128(12), 5267–5279. <https://doi.org/10.1172/JCI122372>
- Kurzeder, C., Koppold, B., Sauer, G., Pabst, S., Kreienberg, R., & Deissler, H. (2007). CD9 promotes adeno-associated virus type 2 infection of mammary carcinoma cells with low cell surface expression of heparan sulphate proteoglycans. *International journal of molecular medicine*, 19(2), 325–333.
- Kyratsous, C., Murphy, A.J., Wang, C., Sabin, L. (2019) Tropism-modified recombinant viral vectors and uses thereof for the targeted introduction of genetic material into human cells. Patent WO/2019/006043.
- Labrijn, A. F., Buijsse, A. O., van den Bremer, E. T., Verwilligen, A. Y., Bleeker, W. K., Thorpe, S. J., Killestein, J., Polman, C. H., Aalberse, R. C., Schuurman, J., van de Winkel, J. G., & Parren, P. W. (2009). Therapeutic IgG4 antibodies engage in Fab-arm exchange with endogenous human IgG4 in vivo. *Nature biotechnology*, 27(8), 767–771. <https://doi.org/10.1038/nbt.1553>
- Labrijn, A. F., Meesters, J. I., de Goeij, B. E., van den Bremer, E. T., Neijssen, J., van Kampen, M. D., Strumane, K., Verploegen, S., Kundu, A., Gramer, M. J., van Berkel, P. H., van de Winkel, J. G., Schuurman, J., & Parren, P. W. (2013). Efficient generation of stable bispecific IgG1 by controlled Fab-arm exchange. *Proceedings of the National Academy of Sciences of the United States of America*, 110(13), 5145–5150. <https://doi.org/10.1073/pnas.1220145110>

- Leaver-Fay, A., Froning, K. J., Atwell, S., Aldaz, H., Pustilnik, A., Lu, F., Huang, F., Yuan, R., Hassanali, S., Chamberlain, A. K., Fitchett, J. R., Demarest, S. J., & Kuhlman, B. (2016). Computationally Designed Bispecific Antibodies using Negative State Repertoires. *Structure (London, England : 1993)*, 24(4), 641–651. <https://doi.org/10.1016/j.str.2016.02.013>
- Lee, G. K., Maheshri, N., Kaspar, B., & Schaffer, D. V. (2005). PEG conjugation moderately protects adeno-associated viral vectors against antibody neutralization. *Biotechnology and bioengineering*, 92(1), 24–34. <https://doi.org/10.1002/bit.20562>
- Levy, M. T., McCaughan, G. W., Abbott, C. A., Park, J. E., Cunningham, A. M., Müller, E., Rettig, W. J., & Gorrell, M. D. (1999). Fibroblast activation protein: a cell surface dipeptidyl peptidase and gelatinase expressed by stellate cells at the tissue remodelling interface in human cirrhosis. *Hepatology (Baltimore, Md.)*, 29(6), 1768–1778. <https://doi.org/10.1002/hep.510290631>
- Li, C. W., Lim, S. O., Chung, E. M., Kim, Y. S., Park, A. H., Yao, J., Cha, J. H., Xia, W., Chan, L. C., Kim, T., Chang, S. S., Lee, H. H., Chou, C. K., Liu, Y. L., Yeh, H. C., Perillo, E. P., Dunn, A. K., Kuo, C. W., Khoo, K. H., Hsu, J. L., Wu, Y., Hsu, J.-M., Yamaguchi, H., Huang, T.-H., Sahin, A. A., Hortobagyi, G. N., Yoo, S. S., Hung, M. C. (2018). Eradication of Triple-Negative Breast Cancer Cells by Targeting Glycosylated PD-L1. *Cancer cell*, 33(2), 187–201. <https://doi.org/10.1016/j.ccell.2018.01.009>
- Li, Z., Zhou, J., Zhang, J., Li, S., Wang, H., & Du, J. (2019). Cancer-associated fibroblasts promote PD-L1 expression in mice cancer cells via secreting CXCL5. *International journal of cancer*, 145(7), 1946–1957. <https://doi.org/10.1002/ijc.32278>
- Liu L. (2018). Pharmacokinetics of monoclonal antibodies and Fc-fusion proteins. *Protein & cell*, 9(1), 15–32. <https://doi.org/10.1007/s13238-017-0408-4>
- Liu, Y., Fang, Y., Zhou, Y., Zandi, E., Lee, C. L., Joo, K. I., & Wang, P. (2013). Site-specific modification of adeno-associated viruses via a genetically engineered aldehyde tag. *Small (Weinheim an der Bergstrasse, Germany)*, 9(3), 421–429. <https://doi.org/10.1002/smll.201201661>
- Lusby, E., Fife, K. H., & Berns, K. I. (1980). Nucleotide sequence of the inverted terminal repetition in adeno-associated virus DNA. *Journal of virology*, 34(2), 402–409. <https://doi.org/10.1128/JVI.34.2.402-409.1980>
- Maheshri, N., Koerber, J. T., Kaspar, B. K., & Schaffer, D. V. (2006). Directed evolution of adeno-associated virus yields enhanced gene delivery vectors. *Nature biotechnology*, 24(2), 198–204. <https://doi.org/10.1038/nbt1182>
- Mallender, W. D., & Voss, E. W., Jr (1994). Construction, expression, and activity of a bivalent bispecific single-chain antibody. *The Journal of biological chemistry*, 269(1), 199–206.

- Mathew, S., Scanlan, M. J., Mohan Raj, B. K., Murty, V. V., Garin-Chesa, P., Old, L. J., Rettig, W. J., & Chaganti, R. S. (1995). The gene for fibroblast activation protein alpha (FAP), a putative cell surface-bound serine protease expressed in cancer stroma and wound healing, maps to chromosome band 2q23. *Genomics*, 25(1), 335–337. [https://doi.org/10.1016/0888-7543\(95\)80157-h](https://doi.org/10.1016/0888-7543(95)80157-h)
- Matsushita, T., Elliger, S., Elliger, C., Podsakoff, G., Villarreal, L., Kurtzman, G. J., Iwaki, Y., & Colosi, P. (1998). Adeno-associated virus vectors can be efficiently produced without helper virus. *Gene therapy*, 5(7), 938–945. <https://doi.org/10.1038/sj.gt.3300680>
- McCarty D. M. (2008). Self-complementary AAV vectors; advances and applications. *Molecular therapy : the journal of the American Society of Gene Therapy*, 16(10), 1648–1656. <https://doi.org/10.1038/mt.2008.171>
- McCarty, D. M., Fu, H., Monahan, P. E., Toulson, C. E., Naik, P., & Samulski, R. J. (2003). Adeno-associated virus terminal repeat (TR) mutant generates self-complementary vectors to overcome the rate-limiting step to transduction in vivo. *Gene therapy*, 10(26), 2112–2118. <https://doi.org/10.1038/sj.gt.3302134>
- McCarty, D. M., Young, S. M., Jr, & Samulski, R. J. (2004). Integration of adeno-associated virus (AAV) and recombinant AAV vectors. *Annual review of genetics*, 38, 819–845. <https://doi.org/10.1146/annurev.genet.37.110801.143717>
- Merchant, A. M., Zhu, Z., Yuan, J. Q., Goddard, A., Adams, C. W., Presta, L. G., & Carter, P. (1998). An efficient route to human bispecific IgG. *Nature biotechnology*, 16(7), 677–681. <https://doi.org/10.1038/nbt0798-677>
- Mersmann, M., Schmidt, A., Rippmann, J. F., Wüest, T., Brocks, B., Rettig, W. J., Garin-Chesa, P., Pfizenmaier, K., & Moosmayer, D. (2001). Human antibody derivatives against the fibroblast activation protein for tumor stroma targeting of carcinomas. *International journal of cancer*, 92(2), 240–248. [https://doi.org/10.1002/1097-0215\(200102\)9999:9999<::aid-ijc1170>3.0.co;2-u](https://doi.org/10.1002/1097-0215(200102)9999:9999<::aid-ijc1170>3.0.co;2-u)
- Mezzadra, R., Sun, C., Jae, L. T., Gomez-Eerland, R., de Vries, E., Wu, W., Logtenberg, M., Slagter, M., Rozeman, E. A., Hofland, I., Broeks, A., Horlings, H. M., Wessels, L., Blank, C. U., Xiao, Y., Heck, A., Borst, J., Brummelkamp, T. R., & Schumacher, T. (2017). Identification of CMTM6 and CMTM4 as PD-L1 protein regulators. *Nature*, 549(7670), 106–110. <https://doi.org/10.1038/nature23669>
- Michelfelder, S., Kohlschütter, J., Skorupa, A., Pfenning, S., Müller, O., Kleinschmidt, J. A., & Trepel, M. (2009). Successful expansion but not complete restriction of tropism of adeno-associated virus by in vivo biopanning of random virus display peptide libraries. *PloS one*, 4(4), e5122. <https://doi.org/10.1371/journal.pone.0005122>

- Michelfelder, S., & Trepel, M. (2009). Adeno-associated viral vectors and their redirection to cell-type specific receptors. *Advances in genetics*, 67, 29–60. [https://doi.org/10.1016/S0065-2660\(09\)67002-4](https://doi.org/10.1016/S0065-2660(09)67002-4)
- Michelfelder, S., Varadi, K., Raupp, C., Hunger, A., Körbelin, J., Pahrman, C., Schrepfer, S., Müller, O. J., Kleinschmidt, J. A., & Trepel, M. (2011). Peptide ligands incorporated into the threefold spike capsid domain to re-direct gene transduction of AAV8 and AAV9 in vivo. *PloS one*, 6(8), e23101. <https://doi.org/10.1371/journal.pone.0023101>
- Milner, J. M., Kevorkian, L., Young, D. A., Jones, D., Wait, R., Donell, S. T., Barksby, E., Patterson, A. M., Middleton, J., Cravatt, B. F., Clark, I. M., Rowan, A. D., & Cawston, T. E. (2006). Fibroblast activation protein alpha is expressed by chondrocytes following a pro-inflammatory stimulus and is elevated in osteoarthritis. *Arthritis research & therapy*, 8(1), R23. <https://doi.org/10.1186/ar1877>
- Milstein, C., & Cuello, A. C. (1983). Hybrid hybridomas and their use in immunohistochemistry. *Nature*, 305(5934), 537–540. <https://doi.org/10.1038/305537a0>
- Mingozi, F., Chen, Y., Edmonson, S. C., Zhou, S., Thurlings, R. M., Tak, P. P., High, K. A., & Vervoordeldonk, M. J. (2013). Prevalence and pharmacological modulation of humoral immunity to AAV vectors in gene transfer to synovial tissue. *Gene therapy*, 20(4), 417–424. <https://doi.org/10.1038/gt.2012.55>
- Mingozi F, High KA (2017) Overcoming the Host Immune Response to Adeno-Associated Virus Gene Delivery Vectors: The Race Between Clearance, Tolerance, Neutralization, and Escape. *Ann Rev Virol* 4:511–534. <https://doi.org/10.1146/annurev-virology-101416-041936>
- Misra, R. M., Bajaj, M. S., & Kale, V. P. (2012). Vasculogenic mimicry of HT1080 tumour cells in vivo: critical role of HIF-1 α -neuropilin-1 axis. *PloS one*, 7(11), e50153. <https://doi.org/10.1371/journal.pone.0050153>
- Mitchell, A. M., Nicolson, S. C., Warischalk, J. K., & Samulski, R. J. (2010). AAV's anatomy: roadmap for optimizing vectors for translational success. *Current gene therapy*, 10(5), 319–340. <https://doi.org/10.2174/156652310793180706>
- Mitchell, A. M., & Samulski, R. J. (2013). Mechanistic insights into the enhancement of adeno-associated virus transduction by proteasome inhibitors. *Journal of virology*, 87(23), 13035–13041. <https://doi.org/10.1128/JVI.01826-13>
- Moore, G. L., Bautista, C., Pong, E., Nguyen, D. H., Jacinto, J., Eivazi, A., Muchhal, U. S., Karki, S., Chu, S. Y., & Lazar, G. A. (2011). A novel bispecific antibody format enables simultaneous bivalent and monovalent co-engagement of distinct target antigens. *mAbs*, 3(6), 546–557. <https://doi.org/10.4161/mabs.3.6.18123>
- Moretti, P., Skegro, D., Ollier, R., Wassmann, P., Aebischer, C., Laurent, T., Schmid-Printz, M., Giovannini, R., Blein, S., Bertschinger, M. (2013) BEAT® the bispecific challenge: a novel and efficient platform for the expression of bispecific IgGs. *BMC Proc* 7, O9 (2013). <https://doi.org/10.1186/1753-6561-7-S6-O9>

- Moskalenko, M., Chen, L., van Roey, M., Donahue, B. A., Snyder, R. O., McArthur, J. G., & Patel, S. D. (2000). Epitope mapping of human anti-adenovirus type 2 neutralizing antibodies: implications for gene therapy and virus structure. *Journal of virology*, 74(4), 1761–1766. <https://doi.org/10.1128/jvi.74.4.1761-1766.2000>
- Müller, O. J., Kaul, F., Weitzman, M. D., Pasqualini, R., Arap, W., Kleinschmidt, J. A., & Trepel, M. (2003). Random peptide libraries displayed on adenovirus to select for targeted gene therapy vectors. *Nature biotechnology*, 21(9), 1040–1046. <https://doi.org/10.1038/nbt856>
- Münch, R. C., Muth, A., Muik, A., Friedel, T., Schmatz, J., Dreier, B., Trkola, A., Plückthun, A., Büning, H., & Buchholz, C. J. (2015). Off-target-free gene delivery by affinity-purified receptor-targeted viral vectors. *Nature communications*, 6, 6246. <https://doi.org/10.1038/ncomms7246>
- Mulisch, M., Welsch, U., (2015) *Romeis - Mikroskopische Technik*. Spektrum München, Wien, Baltimore, pp. 172-257
- Murphy, K., Travers, P., Walport, M. (2009) *Janeway Immunologie*. Spektrum Heidelberg, pp. 141 – 152
- Muzyczka N. (1992). Use of adenovirus as a general transduction vector for mammalian cells. *Current topics in microbiology and immunology*, 158, 97–129. https://doi.org/10.1007/978-3-642-75608-5_5
- Nakai, H., Storm, T. A., & Kay, M. A. (2000). Recruitment of single-stranded recombinant adenovirus vector genomes and intermolecular recombination are responsible for stable transduction of liver in vivo. *Journal of virology*, 74(20), 9451–9463. <https://doi.org/10.1128/jvi.74.20.9451-9463.2000>
- Nam, H. J., Lane, M. D., Padron, E., Gurda, B., McKenna, R., Kohlbrenner, E., Aslanidi, G., Byrne, B., Muzyczka, N., Zolotukhin, S., & Agbandje-McKenna, M. (2007). Structure of adenovirus serotype 8, a gene therapy vector. *Journal of virology*, 81(22), 12260–12271. <https://doi.org/10.1128/JVI.01304-07>
- Nonnenmacher, M., & Weber, T. (2012). Intracellular transport of recombinant adenovirus vectors. *Gene therapy*, 19(6), 649–658. <https://doi.org/10.1038/gt.2012.6>
- Nyakatura, E. K., Soare, A. Y., & Lai, J. R. (2017). Bispecific antibodies for viral immunotherapy. *Human vaccines & immunotherapeutics*, 13(4), 836–842. <https://doi.org/10.1080/21645515.2016.1251536>
- Ogden, P. J., Kelsic, E. D., Sinai, S., & Church, G. M. (2019). Comprehensive AAV capsid fitness landscape reveals a viral gene and enables machine-guided design. *Science* (New York, N.Y.), 366(6469), 1139–1143. <https://doi.org/10.1126/science.aaw2900>

- Opie, S. R., Warrington, K. H., Jr, Agbandje-McKenna, M., Zolotukhin, S., & Muzyczka, N. (2003). Identification of amino acid residues in the capsid proteins of adeno-associated virus type 2 that contribute to heparan sulfate proteoglycan binding. *Journal of virology*, 77(12), 6995–7006. <https://doi.org/10.1128/jvi.77.12.6995-7006.2003>
- Pillay, S., Meyer, N. L., Puschnik, A. S., Davulcu, O., Diep, J., Ishikawa, Y., Jae, L. T., Wosen, J. E., Nagamine, C. M., Chapman, M. S., & Carette, J. E. (2016). An essential receptor for adeno-associated virus infection. *Nature*, 530(7588), 108–112. <https://doi.org/10.1038/nature16465>
- Padron, E., Bowman, V., Kaludov, N., Govindasamy, L., Levy, H., Nick, P., McKenna, R., Muzyczka, N., Chiorini, J. A., Baker, T. S., & Agbandje-McKenna, M. (2005). Structure of adeno-associated virus type 4. *Journal of virology*, 79(8), 5047–5058. <https://doi.org/10.1128/JVI.79.8.5047-5058.2005>
- Palomeque, J., Chemaly, E. R., Colosi, P., Wellman, J. A., Zhou, S., Del Monte, F., & Hajjar, R. J. (2007). Efficiency of eight different AAV serotypes in transducing rat myocardium in vivo. *Gene therapy*, 14(13), 989–997. <https://doi.org/10.1038/sj.gt.3302895>
- Park, H. K., Kim, M., Sung, M., Lee, S. E., Kim, Y. J., & Choi, Y. L. (2018). Status of programmed death-ligand 1 expression in sarcomas. *Journal of translational medicine*, 16(1), 303. <https://doi.org/10.1186/s12967-018-1658-5>
- Park, J. E., Lenter, M. C., Zimmermann, R. N., Garin-Chesa, P., Old, L. J., & Rettig, W. J. (1999). Fibroblast activation protein, a dual specificity serine protease expressed in reactive human tumor stromal fibroblasts. *The Journal of biological chemistry*, 274(51), 36505–36512. <https://doi.org/10.1074/jbc.274.51.36505>
- Patel, S. P., & Kurzrock, R. (2015). PD-L1 Expression as a Predictive Biomarker in Cancer Immunotherapy. *Molecular cancer therapeutics*, 14(4), 847–856. <https://doi.org/10.1158/1535-7163.MCT-14-0983>
- Pauling, L. (1940) A Theory of the Structure and Process of Formation of Antibodies *. *J Am Chem Soc* 62:2643–2657. <https://doi.org/10.1021/ja01867a018>
- Ponnazhagan, S., Mahendra, G., Kumar, S., Thompson, J. A., & Castillas, M., Jr (2002). Conjugate-based targeting of recombinant adeno-associated virus type 2 vectors by using avidin-linked ligands. *Journal of virology*, 76(24), 12900–12907. <https://doi.org/10.1128/jvi.76.24.12900-12907.2002>
- Porter R. R. (1959). The hydrolysis of rabbit γ -globulin and antibodies with crystalline papain. *The Biochemical journal*, 73(1), 119–126. <https://doi.org/10.1042/bj0730119>
- Qing, K., Mah, C., Hansen, J., Zhou, S., Dwarki, V., & Srivastava, A. (1999). Human fibroblast growth factor receptor 1 is a co-receptor for infection by adeno-associated virus 2. *Nature medicine*, 5(1), 71–77. <https://doi.org/10.1038/4758>

- Rabinowitz, J. E., Bowles, D. E., Faust, S. M., Ledford, J. G., Cunningham, S. E., & Samulski, R. J. (2004). Cross-dressing the virion: the transcapsidation of adeno-associated virus serotypes functionally defines subgroups. *Journal of virology*, 78(9), 4421–4432. <https://doi.org/10.1128/jvi.78.9.4421-4432.2004>
- Rettig, W. J., Garin-Chesa, P., Beresford, H. R., Oettgen, H. F., Melamed, M. R., & Old, L. J. (1988). Cell-surface glycoproteins of human sarcomas: differential expression in normal and malignant tissues and cultured cells. *Proceedings of the National Academy of Sciences of the United States of America*, 85(9), 3110–3114. <https://doi.org/10.1073/pnas.85.9.3110>
- Ridgway, J. B., Presta, L. G., & Carter, P. (1996). 'Knobs-into-holes' engineering of antibody CH3 domains for heavy chain heterodimerization. *Protein engineering*, 9(7), 617–621. <https://doi.org/10.1093/protein/9.7.617>
- Ried, M. U., Girod, A., Leike, K., Büning, H., & Hallek, M. (2002). Adeno-associated virus capsids displaying immunoglobulin-binding domains permit antibody-mediated vector retargeting to specific cell surface receptors. *Journal of virology*, 76(9), 4559–4566. <https://doi.org/10.1128/jvi.76.9.4559-4566.2002>
- Rose, J. A., Berns, K. I., Hoggan, M. D., & Koczot, F. J. (1969). Evidence for a single-stranded adenovirus-associated virus genome: formation of a DNA density hybrid on release of viral DNA. *Proceedings of the National Academy of Sciences of the United States of America*, 64(3), 863–869. <https://doi.org/10.1073/pnas.64.3.863>
- Rüger, R., Tansi, F. L., Rabenhold, M., Steiniger, F., Kontermann, R. E., Fahr, A., & Hilger, I. (2014). In vivo near-infrared fluorescence imaging of FAP-expressing tumors with activatable FAP-targeted, single-chain Fv-immunoliposomes. *Journal of controlled release : official journal of the Controlled Release Society*, 186, 1–10. <https://doi.org/10.1016/j.jconrel.2014.04.050>
- Ryman, J. T., & Meibohm, B. (2017). Pharmacokinetics of Monoclonal Antibodies. *CPT: pharmacometrics & systems pharmacology*, 6(9), 576–588. <https://doi.org/10.1002/psp4.12224>
- Salveti, A., Orève, S., Chadeuf, G., Favre, D., Cherel, Y., Champion-Arnaud, P., David-Ameline, J., & Moullier, P. (1998). Factors influencing recombinant adeno-associated virus production. *Human gene therapy*, 9(5), 695–706. <https://doi.org/10.1089/hum.1998.9.5-695>
- Samulski, R. J., Chang, L. S., & Shenk, T. (1989). Helper-free stocks of recombinant adeno-associated viruses: normal integration does not require viral gene expression. *Journal of virology*, 63(9), 3822–3828. <https://doi.org/10.1128/JVI.63.9.3822-3828.1989>
- Samulski, R. J., & Shenk, T. (1988). Adenovirus E1B 55-Mr polypeptide facilitates timely cytoplasmic accumulation of adeno-associated virus mRNAs. *Journal of virology*, 62(1), 206–210. <https://doi.org/10.1128/JVI.62.1.206-210.1988>

- Samulski, R. J., Zhu, X., Xiao, X., Brook, J. D., Housman, D. E., Epstein, N., & Hunter, L. A. (1991). Targeted integration of adeno-associated virus (AAV) into human chromosome 19. *The EMBO journal*, 10(12), 3941–3950.
- Sanlioglu, S., Benson, P. K., Yang, J., Atkinson, E. M., Reynolds, T., & Engelhardt, J. F. (2000). Endocytosis and nuclear trafficking of adeno-associated virus type 2 are controlled by *rac1* and phosphatidylinositol-3 kinase activation. *Journal of virology*, 74(19), 9184–9196. <https://doi.org/10.1128/jvi.74.19.9184-9196.2000>
- Schaefer, W., Völger, H. R., Lorenz, S., Imhof-Jung, S., Regula, J. T., Klein, C., & Mølhøj, M. (2016). Heavy and light chain pairing of bivalent quadroma and knobs-into-holes antibodies analyzed by UHR-ESI-QTOF mass spectrometry. *mAbs*, 8(1), 49–55. <https://doi.org/10.1080/19420862.2015.1111498>
- Schiele FL (2013) Structural And Biophysical Characterization Of Antibody:Antigen Complexes Of Therapeutic Relevance. Dissertation, Technische Universität München
- Schlehofer, J. R., Ehrbar, M., & zur Hausen, H. (1986). Vaccinia virus, herpes simplex virus, and carcinogens induce DNA amplification in a human cell line and support replication of a helpervirus dependent parvovirus. *Virology*, 152(1), 110–117. [https://doi.org/10.1016/0042-6822\(86\)90376-4](https://doi.org/10.1016/0042-6822(86)90376-4)
- Schnepp, B. C., Jensen, R. L., Chen, C. L., Johnson, P. R., & Clark, K. R. (2005). Characterization of adeno-associated virus genomes isolated from human tissues. *Journal of virology*, 79(23), 14793–14803. <https://doi.org/10.1128/JVI.79.23.14793-14803.2005>
- Scott, A. M., Wiseman, G., Welt, S., Adjei, A., Lee, F. T., Hopkins, W., Divgi, C. R., Hanson, L. H., Mitchell, P., Gansen, D. N., Larson, S. M., Ingle, J. N., Hoffman, E. W., Tanswell, P., Ritter, G., Cohen, L. S., Bette, P., Arvay, L., Amelsberg, A., Vlock, D., ... Old, L. J. (2003). A Phase I dose-escalation study of sibrutumab in patients with advanced or metastatic fibroblast activation protein-positive cancer. *Clinical cancer research : an official journal of the American Association for Cancer Research*, 9(5), 1639–1647.
- Seisenberger, G., Ried, M. U., Endress, T., Büning, H., Hallek, M., & Bräuchle, C. (2001). Real-time single-molecule imaging of the infection pathway of an adeno-associated virus. *Science (New York, N.Y.)*, 294(5548), 1929–1932. <https://doi.org/10.1126/science.1064103>
- Snyder, R. O., Miao, C. H., Patijn, G. A., Spratt, S. K., Danos, O., Nagy, D., Gown, A. M., Winther, B., Meuse, L., Cohen, L. K., Thompson, A. R., & Kay, M. A. (1997). Persistent and therapeutic concentrations of human factor IX in mice after hepatic gene transfer of recombinant AAV vectors. *Nature genetics*, 16(3), 270–276. <https://doi.org/10.1038/ng0797-270>
- Sonntag, F., Schmidt, K., & Kleinschmidt, J. A. (2010). A viral assembly factor promotes AAV2 capsid formation in the nucleolus. *Proceedings of the National Academy of Sciences of the United States of America*, 107(22), 10220–10225. <https://doi.org/10.1073/pnas.1001673107>

- Srivastava, A., Lusby, E. W., & Berns, K. I. (1983). Nucleotide sequence and organization of the adeno-associated virus 2 genome. *Journal of virology*, 45(2), 555–564. <https://doi.org/10.1128/JVI.45.2.555-564.1983>
- Stein, S., Weber, J., Nusser-Stein, S., Pahla, J., Zhang, H. E., Mohammed, S. A., Oppi, S., Gaul, D. S., Paneni, F., Tailleux, A., Staels, B., von Meyenn, F., Ruschitzka, F., Gorrell, M. D., Lüscher, T. F., & Matter, C. M. (2021). Deletion of fibroblast activation protein provides atheroprotection. *Cardiovascular research*, 117(4), 1060–1069. <https://doi.org/10.1093/cvr/cvaa142>
- Stemmer W. P. (1994). DNA shuffling by random fragmentation and reassembly: in vitro recombination for molecular evolution. *Proceedings of the National Academy of Sciences of the United States of America*, 91(22), 10747–10751. <https://doi.org/10.1073/pnas.91.22.10747>
- Strobel, B., Miller, F. D., Rist, W., & Lamla, T. (2015). Comparative Analysis of Cesium Chloride- and Iodixanol-Based Purification of Recombinant Adeno-Associated Viral Vectors for Preclinical Applications. *Human gene therapy methods*, 26(4), 147–157. <https://doi.org/10.1089/hgtb.2015.051>
- Strop, P., Ho, W. H., Boustany, L. M., Abdiche, Y. N., Lindquist, K. C., Farias, S. E., Rickert, M., Appah, C. T., Pascua, E., Radcliffe, T., Sutton, J., Chaparro-Riggers, J., Chen, W., Casas, M. G., Chin, S. M., Wong, O. K., Liu, S. H., Vergara, G., Shelton, D., Rajpal, A., Pons, J. (2012). Generating bispecific human IgG1 and IgG2 antibodies from any antibody pair. *Journal of molecular biology*, 420(3), 204–219. <https://doi.org/10.1016/j.jmb.2012.04.020>
- Summerford, C., Bartlett, J. S., & Samulski, R. J. (1999). AlphaVbeta5 integrin: a co-receptor for adeno-associated virus type 2 infection. *Nature medicine*, 5(1), 78–82. <https://doi.org/10.1038/4768>
- Summerford, C., & Samulski, R. J. (1998). Membrane-associated heparan sulfate proteoglycan is a receptor for adeno-associated virus type 2 virions. *Journal of virology*, 72(2), 1438–1445. <https://doi.org/10.1128/JVI.72.2.1438-1445.1998>
- Tahtis, K., Lee, F. T., Wheatley, J. M., Garin-Chesa, P., Park, J. E., Smyth, F. E., Obata, Y., Stockert, E., Hall, C. M., Old, L. J., Rettig, W. J., & Scott, A. M. (2003). Expression and targeting of human fibroblast activation protein in a human skin/severe combined immunodeficient mouse breast cancer xenograft model. *Molecular cancer therapeutics*, 2(8), 729–737.
- Teruya, K., Kusumoto, Y., Eto, H., Nakamichi, N., & Shirahata, S. (2019). Selective Suppression of Cell Growth and Programmed Cell Death-Ligand 1 Expression in HT1080 Fibrosarcoma Cells by Low Molecular Weight Fucoidan Extract. *Marine drugs*, 17(7), 421. <https://doi.org/10.3390/md17070421>

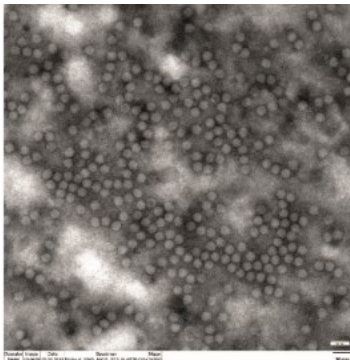
- Tratschin, J. D., Miller, I. L., & Carter, B. J. (1984a). Genetic analysis of adeno-associated virus: properties of deletion mutants constructed in vitro and evidence for an adeno-associated virus replication function. *Journal of virology*, 51(3), 611–619. <https://doi.org/10.1128/JVI.51.3.611-619.1984>
- Tratschin, J. D., West, M. H., Sandbank, T., & Carter, B. J. (1984b). A human parvovirus, adeno-associated virus, as a eucaryotic vector: transient expression and encapsidation of the procaryotic gene for chloramphenicol acetyltransferase. *Molecular and cellular biology*, 4(10), 2072–2081. <https://doi.org/10.1128/mcb.4.10.2072-2081.1984>
- Trepel, M., Grifman, M., Weitzman, M. D., & Pasqualini, R. (2000). Molecular adaptors for vascular-targeted adenoviral gene delivery. *Human gene therapy*, 11(14), 1971–1981. <https://doi.org/10.1089/10430340050143408>
- Trepel, M., Körbelin, J., Spies, E., Heckmann, M. B., Hunger, A., Fehse, B., Katus, H. A., Kleinschmidt, J. A., Müller, O. J., & Michelfelder, S. (2015). Treatment of multifocal breast cancer by systemic delivery of dual-targeted adeno-associated viral vectors. *Gene therapy*, 22(10), 840–847. <https://doi.org/10.1038/gt.2015.52>
- van der Neut Kolfshoten, M., Schuurman, J., Losen, M., Bleeker, W. K., Martínez-Martínez, P., Vermeulen, E., den Bleker, T. H., Wiegman, L., Vink, T., Aarden, L. A., De Baets, M. H., van de Winkel, J. G., Aalberse, R. C., & Parren, P. W. (2007). Anti-inflammatory activity of human IgG4 antibodies by dynamic Fab arm exchange. *Science (New York, N.Y.)*, 317(5844), 1554–1557. <https://doi.org/10.1126/science.1144603>
- van Sriel, A. B., van Ojik, H. H., & van De Winkel, J. G. (2000). Immunotherapeutic perspective for bispecific antibodies. *Immunology today*, 21(8), 391–397. [https://doi.org/10.1016/s0167-5699\(00\)01659-5](https://doi.org/10.1016/s0167-5699(00)01659-5)
- Vihinen-Ranta, M., Wang, D., Weichert, W. S., & Parrish, C. R. (2002). The VP1 N-terminal sequence of canine parvovirus affects nuclear transport of capsids and efficient cell infection. *Journal of virology*, 76(4), 1884–1891. <https://doi.org/10.1128/jvi.76.4.1884-1891.2002>
- Von Kreudenstein, T. S., Escobar-Carbrera, E., Lario, P. I., D'Angelo, I., Brault, K., Kelly, J., Durocher, Y., Baardsnes, J., Woods, R. J., Xie, M. H., Girod, P. A., Suits, M. D., Boulanger, M. J., Poon, D. K., Ng, G. Y., & Dixit, S. B. (2013). Improving biophysical properties of a bispecific antibody scaffold to aid developability: quality by molecular design. *mAbs*, 5(5), 646–654. <https://doi.org/10.4161/mabs.25632>
- Walz, C., Deprez, A., Dupressoir, T., Dürst, M., Rabreau, M., & Schlehofer, J. R. (1997). Interaction of human papillomavirus type 16 and adeno-associated virus type 2 co-infecting human cervical epithelium. *The Journal of general virology*, 78 (Pt 6), 1441–1452. <https://doi.org/10.1099/0022-1317-78-6-1441>
- Wang, X., Mathieu, M., & Brezski, R. J. (2018). IgG Fc engineering to modulate antibody effector functions. *Protein & cell*, 9(1), 63–73. <https://doi.org/10.1007/s13238-017-0473-8>

- Weinreich, M., & Frishman, W. H. (2014). Antihyperlipidemic therapies targeting PCSK9. *Cardiology in review*, 22(3), 140–146. <https://doi.org/10.1097/CRD.000000000000014>
- Welt, S., Divgi, C. R., Scott, A. M., Garin-Chesa, P., Finn, R. D., Graham, M., Carswell, E. A., Cohen, A., Larson, S. M., & Old, L. J. (1994). Antibody targeting in metastatic colon cancer: a phase I study of monoclonal antibody F19 against a cell-surface protein of reactive tumor stromal fibroblasts. *Journal of clinical oncology : official journal of the American Society of Clinical Oncology*, 12(6), 1193–1203. <https://doi.org/10.1200/JCO.1994.12.6.1193>
- Wehrhan, F., Stockmann, P., Nkenke, E., Schlegel, K. A., Guentsch, A., Wehrhan, T., Neukam, F. W., & Amann, K. (2011). Differential impairment of vascularization and angiogenesis in bisphosphonate-associated osteonecrosis of the jaw-related mucoperiosteal tissue. *Oral surgery, oral medicine, oral pathology, oral radiology, and endodontics*, 112(2), 216–221. <https://doi.org/10.1016/j.tripleo.2011.02.028>
- Weng, C., Dong, H., Chen, G., Zhai, Y., Bai, R., Hu, H., Lu, L., & Xu, Z. (2012). miR-409-3p inhibits HT1080 cell proliferation, vascularization and metastasis by targeting angiogenin. *Cancer letters*, 323(2), 171–179. <https://doi.org/10.1016/j.canlet.2012.04.010>
- West, M. H., Trempe, J. P., Tratschin, J. D., & Carter, B. J. (1987). Gene expression in adeno-associated virus vectors: the effects of chimeric mRNA structure, helper virus, and adenovirus VA1 RNA. *Virology*, 160(1), 38–47. [https://doi.org/10.1016/0042-6822\(87\)90041-9](https://doi.org/10.1016/0042-6822(87)90041-9)
- Wilson, J. M., & Flotte, T. R. (2020). Moving Forward After Two Deaths in a Gene Therapy Trial of Myotubular Myopathy. *Human gene therapy*, 31(13-14), 695–696. <https://doi.org/10.1089/hum.2020.182>
- Wistuba, A., Kern, A., Weger, S., Grimm, D., & Kleinschmidt, J. A. (1997). Subcellular compartmentalization of adeno-associated virus type 2 assembly. *Journal of virology*, 71(2), 1341–1352. <https://doi.org/10.1128/JVI.71.2.1341-1352.1997>
- Wistuba, A., Weger, S., Kern, A., & Kleinschmidt, J. A. (1995). Intermediates of adeno-associated virus type 2 assembly: identification of soluble complexes containing Rep and Cap proteins. *Journal of virology*, 69(9), 5311–5319. <https://doi.org/10.1128/JVI.69.9.5311-5319.1995>
- Wobus, C. E., Hügler-Dörr, B., Girod, A., Petersen, G., Hallek, M., & Kleinschmidt, J. A. (2000). Monoclonal antibodies against the adeno-associated virus type 2 (AAV-2) capsid: epitope mapping and identification of capsid domains involved in AAV-2-cell interaction and neutralization of AAV-2 infection. *Journal of virology*, 74(19), 9281–9293. <https://doi.org/10.1128/jvi.74.19.9281-9293.2000>
- Xiao, W., Berta, S. C., Lu, M. M., Moscioni, A. D., Tazelaar, J., & Wilson, J. M. (1998a). Adeno-associated virus as a vector for liver-directed gene therapy. *Journal of virology*, 72(12), 10222–10226. <https://doi.org/10.1128/JVI.72.12.10222-10226.1998>

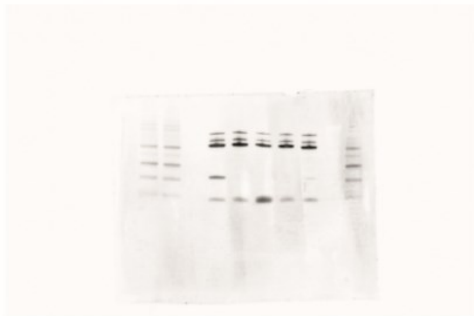
- Xiao, X., Li, J., McCown, T. J., & Samulski, R. J. (1997). Gene transfer by adeno-associated virus vectors into the central nervous system. *Experimental neurology*, 144(1), 113–124. <https://doi.org/10.1006/exnr.1996.6396>
- Xiao, X., Li, J., & Samulski, R. J. (1996). Efficient long-term gene transfer into muscle tissue of immunocompetent mice by adeno-associated virus vector. *Journal of virology*, 70(11), 8098–8108. <https://doi.org/10.1128/JVI.70.11.8098-8108.1996>
- Xiao, X., Li, J., & Samulski, R. J. (1998b). Production of high-titer recombinant adeno-associated virus vectors in the absence of helper adenovirus. *Journal of virology*, 72(3), 2224–2232. <https://doi.org/10.1128/JVI.72.3.2224-2232.1998>
- Xie, Q., Bu, W., Bhatia, S., Hare, J., Somasundaram, T., Azzi, A., & Chapman, M. S. (2002). The atomic structure of adeno-associated virus (AAV-2), a vector for human gene therapy. *Proceedings of the National Academy of Sciences of the United States of America*, 99(16), 10405–10410. <https://doi.org/10.1073/pnas.162250899>
- Xu, D., Alegre, M. L., Varga, S. S., Rothermel, A. L., Collins, A. M., Pulito, V. L., Hanna, L. S., Dolan, K. P., Parren, P. W., Bluestone, J. A., Jolliffe, L. K., & Zivin, R. A. (2000). In vitro characterization of five humanized OKT3 effector function variant antibodies. *Cellular immunology*, 200(1), 16–26. <https://doi.org/10.1006/cimm.2000.1617>
- Yang, L., Jiang, J., Drouin, L. M., Agbandje-McKenna, M., Chen, C., Qiao, C., Pu, D., Hu, X., Wang, D. Z., Li, J., & Xiao, X. (2009). A myocardium tropic adeno-associated virus (AAV) evolved by DNA shuffling and in vivo selection. *Proceedings of the National Academy of Sciences of the United States of America*, 106(10), 3946–3951. <https://doi.org/10.1073/pnas.0813207106>
- Zhang, F., Aguilera, J., Beaudet, J. M., Xie, Q., Lerch, T. F., Davulcu, O., Colón, W., Chapman, M. S., & Linhardt, R. J. (2013). Characterization of interactions between heparin/glycosaminoglycan and adeno-associated virus. *Biochemistry*, 52(36), 6275–6285. <https://doi.org/10.1021/bi4008676>
- Zhang, L., Rossi, A., Lange, L., Meumann, N., Koitzsch, U., Christie, K., Nesbit, M. A., Moore, C., Hacker, U. T., Morgan, M., Hoffmann, D., Zengel, J., Carette, J. E., Schambach, A., Salvetti, A., Odenthal, M., & Büning, H. (2019). Capsid Engineering Overcomes Barriers Toward Adeno-Associated Virus Vector-Mediated Transduction of Endothelial Cells. *Human gene therapy*, 30(10), 1284–1296. <https://doi.org/10.1089/hum.2019.027>
- Zhong, L., Li, W., Yang, Z., Qing, K., Tan, M., Hansen, J., Li, Y., Chen, L., Chan, R. J., Bischof, D., Maina, N., Weigel-Kelley, K. A., Zhao, W., Larsen, S. H., Yoder, M. C., Shou, W., & Srivastava, A. (2004). Impaired nuclear transport and uncoating limit recombinant adeno-associated virus 2 vector-mediated transduction of primary murine hematopoietic cells. *Human gene therapy*, 15(12), 1207–1218. <https://doi.org/10.1089/hum.2004.15.1207>

7 Appendix

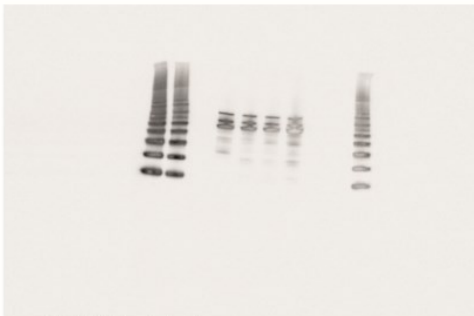
S1



S2

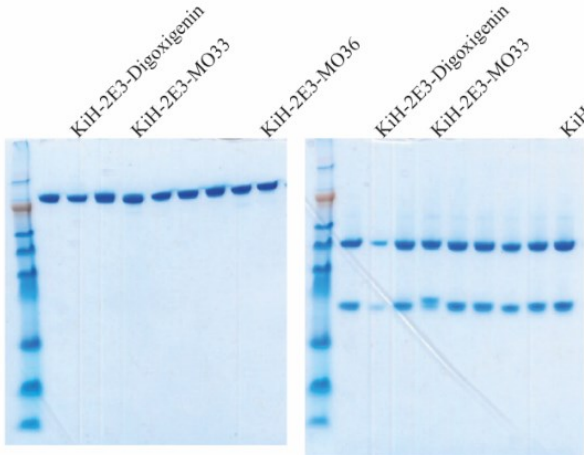


anti-VP staining



anti-2E3 staining

S3



S4

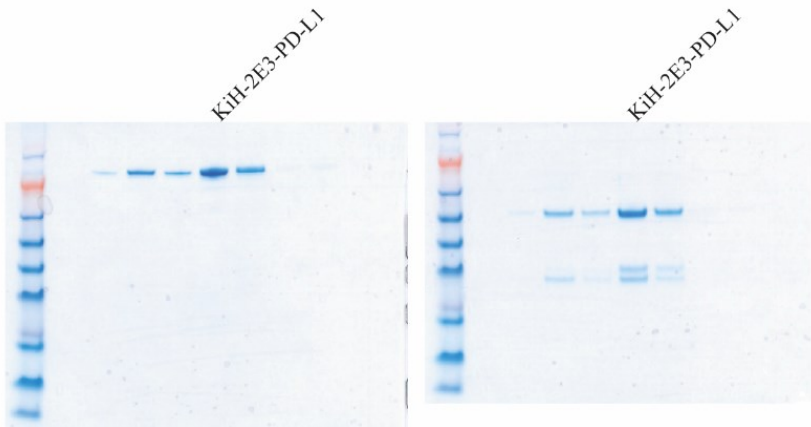


Figure 27: Supplemental uncropped full-size images (Kuklik et al. 2021) **S1)** EM image of negative stained rAAV-2E3.v6, scale bar 50 μm . **S2)** Western blot stainings of reduced rAAV-2E3 and AAV2 viral variants incubated with B1 anti-VP antibody (left) and anti-2E3 antibody (right). **S3)** SDS PAGE of native (left) or reduced (right) bispecific antibodies after SEC purification: KiH-2E3-Digoxigenin, KiH-2E3-MO33 and KiH-MO36. Labeled lanes indicate antibody fractions that were used in further experiments. **S4)** SDS PAGE of native (left) or reduced (right) KiH-2E3-PD-L1 antibody. Labeled lanes indicate antibody fractions used in further experiments.

8 Acknowledgements

The content has been removed for data privacy protection.

9 Declaration

I hereby declare that I wrote the present dissertation with the topic:

Development of a novel capsid modified AAV vector platform enabling retargeting by modular bispecific antibody binding

independently and used no other aids than those cited. In each individual case, I have clearly identified the source of the passages that are taken word for word or paraphrased from other works.

I also hereby declare that I have carried out my scientific work according to the principles of good scientific practice in accordance with the current „Satzung der Universität Ulm zur Sicherung guter wissenschaftlicher Praxis“ [Rules of the University of Ulm for Assuring Good Scientific Practice].

Juliane Kuklik